Erasmus MC
Universitair Medisch Centrum Rotterdam

Thoraxcentre

The 17th European Symposium on Ultrasound Contrast Imaging

- An ICUS Conference -

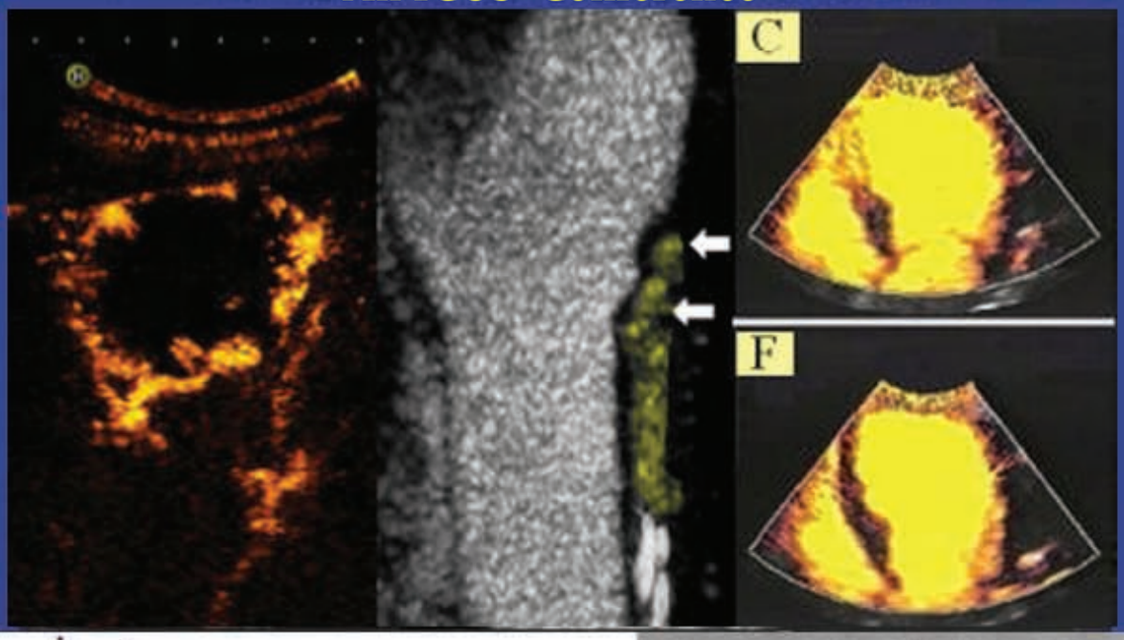

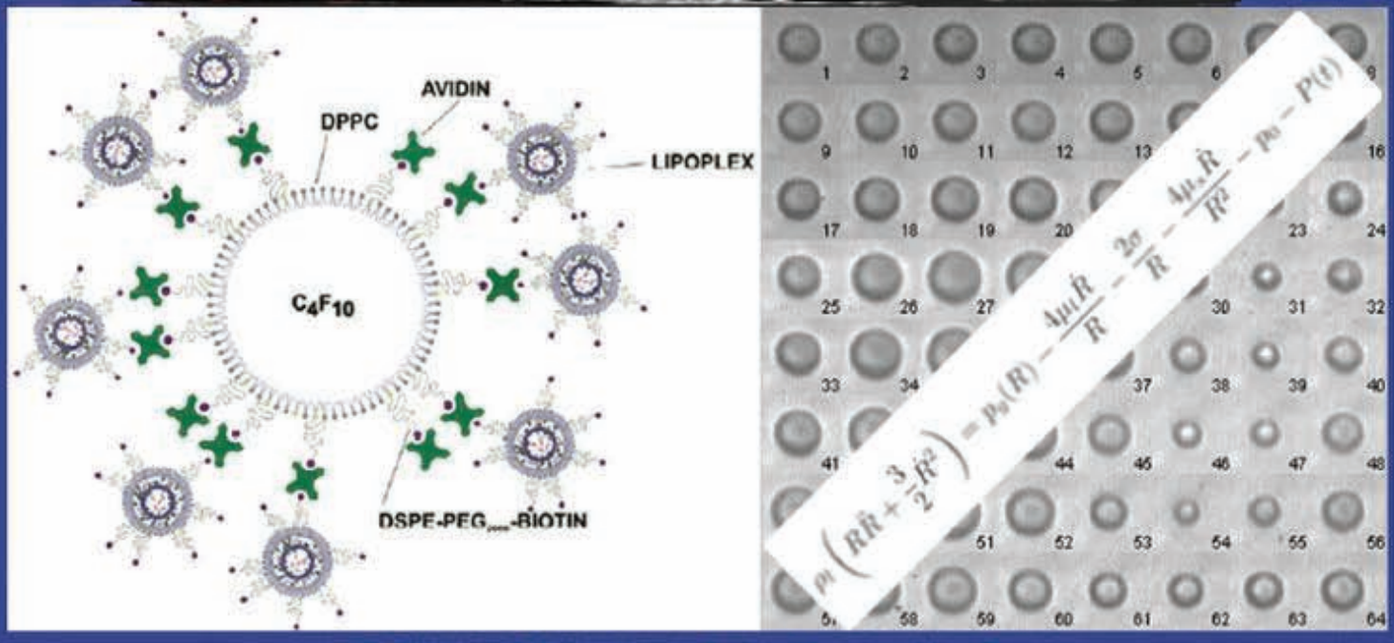

Abstract book

January, 19-20 2012, Rotterdam, The Netherlands

Organized by Folkert ten Cate, Nico de Jong, Arend Schinkel, Edward Leen

Erasmus MC Rotterdam - Imperial College London

17th EUROPEAN SYMPOSIUM ON ULTRASOUND CONTRAST IMAGING
19-20 JANUARY 2012, Rotterdam, The Netherlands

WEDNESDAY, 18 January 2012

18.00 - 20.00 Registration - Welcome Drinks ..... World Trade Center – Town Hall Room

THURSDAY, 19 January 2012

Oral program

World Trade Center – Oscar Auditorium

08.00 – 09.00 Registration ..... World Trade Center – Town Hall Room

09.00 – 09.05 Introduction and opening ..... *Folkert ten Cate*

09.05 – 10.35 PERFUSION IMAGING ..... *Chairperson: Jeff Powers / Mark Monaghan*

10.35 – 11.05 Intermission

11.05 – 12.35 RADIOLOGY ..... *Chairpersons: David Cosgrove / Mike Averkiou*

12.35 – 14.00 LUNCH in main hall (first floor)

12.35 – 14.00 Oscar Auditorium: Parallel Company presentation of Bracco: Vuebox™ a new quantification tool - From qualitative to quantitative analysis of linear data *(lunch boxes are provided during this presentation)*

14.00 – 15.30 THERAPY ..... *Chairpersons: Folkert ten Cate / Michel Versluis*

15.30 – 16.00 Intermission

16.00 – 16.45 THERAPY - continuation ..... *Chairpersons: Folkert ten Cate / Michel Versluis*

16.45 – 17.30 COEUR Round Table discussion ..... *Chairperson:Tom Porter / Edward Leen*

Mark Monaghan — King's College Hospital
Francois Tranquart — Bracco Suisse SA
Jeff Powers — Philips Ultrasound
Wilko Wilkening — Siemens
Joshua Rychak — Targeson

18.30 – 22.30 SOCIAL EVENT (Incl. Dinner buffet) .....

17th EUROPEAN SYMPOSIUM ON ULTRASOUND CONTRAST IMAGING
19-20 JANUARY 2012, Rotterdam, The Netherlands

FRIDAY, 20 January 2012

07.30 - 08.00 Registration

Poster sessions

World Trade Center – Oscar Auditorium

07.30 - 09.00 MODERATED POSTER SESSION A ..... *Moderator: Folkert ten Cate*

07.30 - 09.00 MODERATED POSTER SESSION B ..... *Moderator: Nico de Jong*

07.30 - 09.00 GENERAL POSTER SESSION C

17th EUROPEAN SYMPOSIUM ON ULTRASOUND CONTRAST IMAGING
19-20 JANUARY 2012, Rotterdam, The Netherlands

FRIDAY, 20 January 2012

Oral program

World Trade Center – Oscar Auditorium

MCE perfusion for detection of CAD. The PHOENIX trial: protocol design and inter-reader variability

P. Colonna[1], F.J. ten Cate[2], H. Becher[3]

[1]Policlinico Hospital, Department of Cardiology, Bari, Italy
[2]Erasmus Medical Center, Thoraxcenter, Department of Cardiology, Rotterdam, the Netherlands
[3]Mazankowski Alberta Heart Institute, Edmonton, Canada

Aim

The ongoing Phoenix trial evaluates the accuracy of myocardial perfusion stress echo during infusion of SonoVue echocontrast in detecting significant coronary artery disease, in comparison to ECG-gated SPECT. Prior studies indicate the difficulty of blinded echo readers to read perfusion images with high consistency and accuracy.

The main importance for a stress test, like the stress MCE perfusion for detection of CAD, is to have a high sensitivity, in order to select patients who need to undergo coronary angiography, not missing patients with CAD and higher risk of ischemia. Similar consideration has to be done for negative predictive value. Similarly interesting, but surely less important, is to have a high value of specificity and positive predictive value of the test.

We aimed to evaluate the effect of training with conjunct reading roundtables in improving inter-reader agreement and accuracy to detect significant coronary artery disease (CAD).

Methods

Training between the 3 official blinded readers of the Phoenix trial was held in 2 conjunct reading roundtables, each of them with images of myocardial perfusion obtained with Sonovue (in real time and triggered mode) from 50 patients suspected for CAD, different from those included in the Phoenix trial. During the roundtables the 3 blinded readers trained establishing common criteria for detection of perfusion defects and for definition of contrast artefacts. Testing and training sessions were independent.

In the 3 testing sessions the three blinded readers evaluated myocardial perfusion in the different coronary distribution of patients, dividing the patients in those with presence (41) or absence (26) of significant (>70% stenosis) CAD.

The inter-reader agreement and the accuracy for CAD detection was evaluated for the pre-training session, after the first (Post 1) and after the second training roundtable (Post 2 session).

Results

Overall (2 over 3) inter-reader agreement and accuracy in CAD detection improved from pre-training (62 % and 69 %, respectively) to post-training 1 (74 % and 75 %, respectively) and post 2 session (88 % and 87 %, respectively). Mean changes in overall agreement and accuracy post-training2 to pre-training were 26.5 % (p=0.001) and 18.3 % (p=0.021), respectively. Individual readers values are depicted in the figure.

Conclusion

These data suggest that appropriate training increases inter-reader agreement and accuracy for CAD detection.

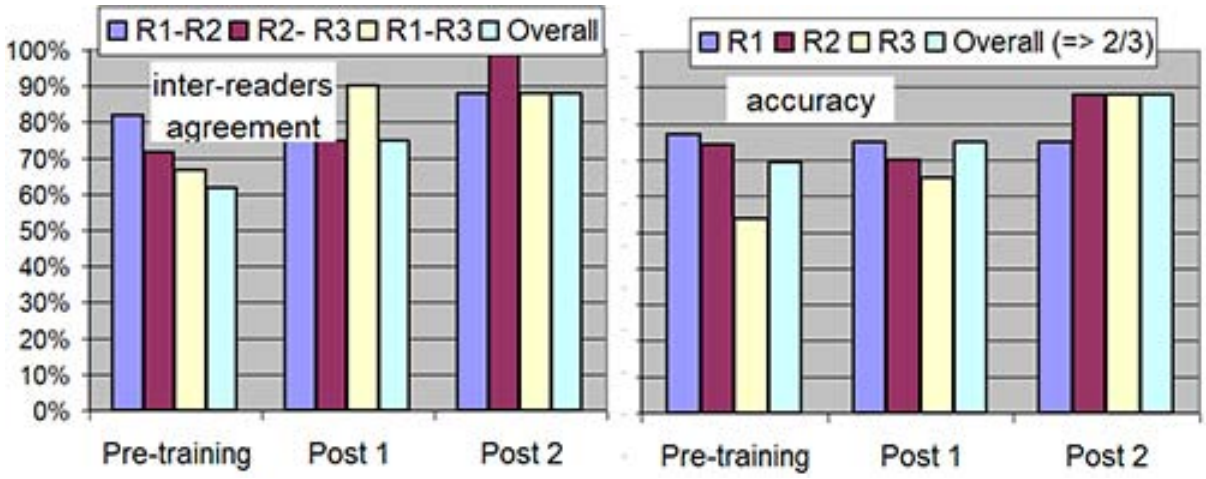

Does subclinical atherosclerosis burden identify the increased risk of cardiovascular disease mortality amongst UK Indian Asians versus European whites? Role of contrast enhanced carotid ultrasonography

Professor Roxy Senior, Consultant Cardiologist

Royal Brompton Hospital, London, United Kingdom

Indian Asians in the United Kingdom have over 50% higher risk of cardiovascular disease (CVD) death compared with native European whites. The mechanism underlying excess mortality in the former group is unclear. Subclinical atherosclerosis detected in carotid arteries by ultrasound is an established prognosticator for major CVD events. Recently, characteristics of carotid plaque in terms of detection of neo-vascularisation by contrast-enhanced ultrasound has been shown to predict CVD events beyond that predicted by unenhanced ultrasound. The paper will discuss the role of contrast enhanced carotid ultrasound for detecting differences in plaque neo-revascularisation between Indian Asians versus European white and its possible role in outcome prediction.

Perfluorocarbon nanodroplets for extravascular contrast

Nikita Reznik[1], Ross Williams[3], Naomi Matsuura[3], Erik Gelderblom[2], Peter N. Burns[1,3]

[1]University of Toronto, Canada
[2]University of Twente, Enschede, the Netherlands
[3]Sunnybrook Research Institute, Toronto, Canada

Although the fact that microbubbles stay within the vasculature offers a number of advantages to contrast ultrasound imaging, there are some situations where the pattern of extravasation of a diffusible tracer has important clinical relevance. One example if the use of Gd-DPTA with MRI to detect breast cancer by increased leakage of the agent through angiogenic vascular endothelium; another is the 'late' enhancement of myocardium with contrast MRI, where the extravasation of contrast is used to characterise muscle viability. Both of these clinical areas are ones in which ultrasound would have interesting potential were it to avail itself of a diffusible agent.

We and others have been developing nano- (or more accurately, submicron-) droplets of perfluorocarbon (PFC) around the 200-400nm diameter range, which makes them selectively diffusible through angiogenic vascular endothelium and, due to the so-called 'enhanced permeability and retention' (EPR) effect, able to accumulate in solid tumours (1). Detection of the droplets is then accomplished by exposure to an externally applied ultrasound field, which 'activates' the droplets into bubbles. If the bubbles are of an appropriate size and adequate stability, they can then be detected using familiar nonlinear ultrasound imaging methods which rely on bubble resonance. The key to this process is a droplet formulation that enables vaporisation of the liquid at low - and preferably diagnostic - acoustic energy levels. This is accomplished by using a PFC with a boiling point at or below that of blood temperature, so that the droplets are superheated *in vivo*. A number of different formulations have been made to date, including perfluorohexane, perfluoropentane and perfluorobutane; these are being studied by various groups for applications which include high-intensity focused ultrasound therapy sensitisation (2, 3), embolotherapy by bubble-induced vessel occlusion (4) and drug delivery (5).

We have been using droplets of dodecafluoropentane (DDFP) coated with fluorosurfactant (Zonyl FSP), with diameter of 415 ± 20 nm. We have shown that these can be converted *in vitro* to produce bubbles which are stable for hundreds of milliseconds, during which they can produce second harmonic echoes which can be detected by pulse inversion imaging (6). We have also shown that droplets injected intravenously in a model of hepatocellular carcinoma (HEP-3B) initiated in SCID mice. After 4 hours of accumulation and after clearance from the circulation, phase conversion was achieved with 10 MHz

ultrasound at Pneg= 5.5MPa. The converted droplets were then imaged in the tumour with low MI amplitude modulation contrast imaging at 40MHz.

While results to date appear promising, several aspects of the mechanism of this procedure remain to be explained. First, while subharmonic emission is detectable when the droplets are vaporised, the threshold of peak negative acoustic pressure for conversion of the droplets goes down with increasing frequency, which is the opposite to what one would expect for a cavitation dominated process. Second, it is not clear whether the surfactant coating of the droplet contributes to the shell of the resulting bubble and hence plays an important role in its stability. These two questions are currently under investigation using combined acoustic and optical approaches, including the labelling of the surfactant material with a fluorescent marker and high speed imaging with the Brandaris system.

References

1. Campbell RB. Tumor physiology and delivery of nanopharmaceuticals. Anticancer Agents Med Chem. 2006 Nov;6(6):503-12
2. Kawabata K, Yoshizawa A, Asami R, Azuma T, Yoshikawa H, Watanabe H, et al., editors. Site-Specific Contrast Imaging with Locally Induced Microbubbles from Liquid Precursors. IEEE UFFC Ultrasonics Symposium; 2006: IEEE
3. Zhang P, Porter T. An in vitro Study of a Phase-Shift Nanoemulsion: A Potential Nucleation Agent for Bubble-Enhanced HIFU Tumor Ablation. Ultrasound in Medicine & Biology. 2010
4. Lo AH, Kripfgans OD, Carson PL, Rothman ED, Fowlkes JB. Acoustic droplet vaporization threshold: effects of pulse duration and contrast agent. Ultrasonics, Ferroelectrics and Frequency Control, IEEE Transactions on. 2007;54(5):933-46
5. Rapoport N, Nam KH, Gupta R, Gao Z, Mohan P, Payne A, et al. Ultrasound-mediated tumor imaging and nanotherapy using drug loaded, block copolymer stabilized perfluorocarbon nanoemulsions. Journal of Controlled Release. 2011
6. Reznik N, Williams R, Burns PN. Investigation of Vaporized Submicron Perfluorocarbon Droplets as an Ultrasound Contrast Agent. Ultrasound in Medicine & Biology. 2011;37(8):1271-9

Targeted microbubble prostate cancer imaging with BR55

Hessel Wijkstra[1], Martijn Smeenge[1], Jean de la Rosette[1], Sibylle Pochon[2], Isabelle Tardy-Cantalupi[2], Francois Tranquart[2]

[1]AMC University Hospital, Amsterdam, the Netherlands
[2]Bracco Research, Geneva, Switzerland

Prostate cancer (PCa) is the number one cancer in men in the Western world. In 2011 it is expected that 29% of all new cancer cases in men (excludes e.g. skin cancer) will be prostate cancer. This makes it the #1 cancer in males. In estimated deaths it is the #2 cancer in men, accounting for 11% of all cancer related deaths.

For e.g. breast cancer detection, imaging techniques are available which enable large-scale, image-based, screening programs. However, for prostate cancer, no imaging technique currently exists, which can accurately diagnose and stage this malignancy, and the final diagnosis nowadays is always made with the help of large number of systematic biopsies.

The growth of new capillary vessels from existing vessel (Angiogenesis) is a crucial process during e.g. development and wound healing. Furthermore, it is essential for the growth of solid tumors beyond a size of approximately 2 mm. The Vascular Endothelial Growth Factor Receptor 2 (VEGF-R2) plays a major role in this process. VEGF-R2 expression has been linked to the progression and aggressiveness of prostate cancer.

Recently, a VEGF-R2 targeted microbubble (BR55) was introduced as an ultrasound contrast agent for molecular imaging of tumor angiogenesis. It was designed without potentially immunogenic proteins like streptavidin or antibodies, and therefore could make clinical application of ultrasound molecular imaging in humans possible. Promising results in in-vitro as well as in-vivo animal experiments have been published [1,2].

This presentation deals with the first application of BR55 in humans.

In a phase 0 study, 12 patients scheduled for a radical prostatectomy in the AMC University Hospital, Amsterdam, the Netherlands were included after approval of the ethics committee and after signed informed consent of the patients.

A iU22 (Philips) scanner and a C8-4V transrectal probe were used for imaging. After a bolus injection of BR55, imaging was performed at a low MI and a low frame-rate to minimize possible bubble destruction. The inflow of contrast was recorded, and after that at regular times (op to 15 minutes) short periods of imaging was used to examine the binding of bubbles.

After the radical prostatectomy the excised prostate was cut in 4 mm slices, and the histopathology was correlated to the imaging results. VEGF-R2 and CD31 staining of cancerous lesions were determined to correlate VEGF-R2 expression and Micro Vessel Density with the binding of BR55 bubbles.

We demonstrated that BR55 binds to VEGF-R2 receptors in humans. In the presentation, the results are presented including image processing techniques to differentiate between ‘circulating’ and ‘bound’ bubbles. It will be shown that in potential BR55 can improve prostate cancer detection and localization.

An advantage of targeted bubbles is that after binding, for several minutes, the whole prostate can be scanned for attached microbubbles, and thus enough time is available for e.g. targeted biopsies. This implies that with one injection of contrast, the whole prostate can be imaged with 2D contrast-specific imaging. It is further hypothesized that more aggressive and faster-growing tumors have an increased VEGFR-2 expression, and this in potential could make grading based on imaging possible. Since focal therapy and active surveillance are increasingly used, molecular ultrasound imaging with targeted microbubbles could play a role in selecting patients for the most appropriate treatment.

References

1. Pochon S, Tardy I, Bussat P, Bettinger T, Brochot J, von Schneider WM, Passantino L (2010) BR55: a lipopeptide-based VEGFR2-targeted ultrasound contrast agent for molecular imaging of angiogenesis. Invest Radiol 45:89–95
2. Tardy I, Pochon S, Theraulaz M, Emmel P, Passantino L, Tran- quart F, Schneider M (2010) Ultrasound molecular imaging of VEGFR2 in a rat prostate tumor model using BR55. Invest Radiol 45:573–578

The effect of acoustic radiation force on the binding efficiency of BR55 VEGFR2-specific contrast-agent microbubbles

Peter Frinking[1], Isabelle Tardy[1], Martine Théraulaz[1], Marcel Arditi[1], Jeffry Powers[2], Sibylle Pochon[1], François Tranquart[1]

[1]Bracco Suisse S.A., Geneva Research Center and Manufacturing Site, Plan-les-Ouates / Geneva, Switzerland
[2]Philips Medical Systems Inc., Bothell, WA, USA

Target-specific contrast agents are showing great potential in ultrasound molecular imaging applications; ligand-bearing microbubbles can be targeted to specific receptors, delineating pathologies which would otherwise be difficult to detect. The binding efficiency of such microbubbles is, however, determined by an effective interaction between the ligands present on the bubbles and target receptors expressed on the vascular endothelium. This interaction depends on local agent concentration and physiological factors such as receptor density, vessel diameter and wall shear rate. Acoustic Radiation Force (ARF) has been suggested to improve bubble binding by pushing the bubbles towards the endothelium of the vessel wall. However, nonspecific binding in healthy tissue may also be promoted by radiation force and could reduce binding specificity. In this work, the effect of radiation force on binding efficiency and specificity of BR55 microbubbles (Bracco Suisse S.A., Geneva, Switzerland) was investigated.

BR55 VEGFR2-specific microbubbles were injected in 38 Copenhagen rats in which adenocarcinoma cells (G Dunning R-3327) were implanted in one lobe of the ventral prostate. An iU22 (Philips Medical Systems Inc., Bothell, WA) ultrasound system was modified by implementing high duty-cycle 3.5-MHz center frequency ARF bursts in a scanning configuration. This enabled comparing the effects of ARF on binding in tumor and healthy tissue effectively in the same field of view. Bubble binding was established by measuring late-phase enhancement in Amplitude Modulation (AM) contrast-specific imaging mode (4 MHz, 150 kPa) 10 min after agent injection when the unbound bubbles were cleared from the circulation. Optimal experimental conditions, such as agent concentration ($0.4x10^8$-$1.6x10^8$ bubbles/kg), acoustic pressure amplitude (26-51 kPa) and duty-cycle (20-95%) of the ARF bursts, were evaluated in their ability to enhance binding in tumor without significantly increasing binding in healthy tissue.

Using the optimal conditions (0.8x108 bubbles/kg, 38 kPa peak-negative pressure, 95% duty cycle), ARF-assisted binding of BR55 in tumor improved significantly by a factor of 7.0 compared to binding without ARF (Wilcoxon signed rank test, $P < 0.0001$), but it had little effect on its binding in healthy tissue (ARF-to-No ARF ratio of 2.0). To assess the effect of ARF on a non-targeted phospholipid blood pool agent having a similar mean diameter in number, BR38 (Bracco) was used as a control ($0.5x10^8$ bubbles/kg). ARF slightly increased binding of BR38 in tumor (ARF-to-No ARF ratio of 1.9), but binding did not differ significantly between tumor and healthy tissue (Wilcoxon signed rank test, $P = 0.2395$). Moreover, binding of BR38 was similar to that of BR55 in healthy tissue (Kruskal-Wallis test, $P = 0.4391$).

The results of this study demonstrate that a significant improvement in binding efficiency of BR55 targeted microbubbles is obtained by using ARF, and it confirms their high specificity for targeting VEGFR2 present at sites of active angiogenesis on the tumoral endothelium. Therefore, it is believed that ultrasound molecular imaging using target-specific contrast-agent microbubbles should preferably be performed in combination with ARF.

Contrast-enhanced ultrasound of intraplaque neovascularisation

Arend F.L. Schinkel, G. Luit ten Kate, Stijn C. van den Oord

Contrast-enhanced ultrasound (CEUS) provides real-time in-vivo visualization of intraplaque neovascularization. There is growing evidence that intraplaque neovascularization of carotid plaques is associated with plaque bleeding and plaque growth which may eventually lead to plaque rupture. Rupture of an atherosclerotic plaque may cause clinical events such as stroke and myocardial infarction. Identification of patients at risk for plaque rupture using CEUS may help to improve risk reducing strategies.

To evaluate the use of CEUS for assessment of intraplaque neovascularization an animal model of atherosclerosis was used. After induction of atherosclerosis in the animal model, plaque formation and the development of intraplaque neovascularization was followed using CEUS. Finally histology was obtained, and a clear correlation between CEUS findings and histological evidence of intraplaque neovascularization was observed.

Subsequently a study comparing carotid CEUS and histology in patients scheduled for carotid endarterectomy was started. Before surgery carotid CEUS of the atherosclerotic plaque is performed and the imaging results will be compared with histology of the plaque. To optimize the comparison between CEUS and histology, plaques are removed in toto during surgery and a standardized specimen cutting protocol was developed.

To evaluate the prognostic implications of intraplaque neovascularization assessed by CEUS for the occurrence of cardiovascular events a follow-up study was started. Patients with >=1 cardiovascular risk factors are asked to participate in this prospective study. Biomedical engineers and clinicians work closely together in this project to further improve the current CEUS technique and develop methods for quantification of intraplaque neovascularization.

Ultrasound guided therapy for liver disease

Professor Edward Leen, MD, FRCR.Chair of Radiology
Imaging Lead – Biomedical Research centre
Clinical Lead for Interventional Ablative Therapy Service
Imperial College London /Imperial College NHS Trust, Hammersmith Hospital Campus, London, UK

Liver metastases and hepatocellular carcinomas (HCCs) are two of the most common causes of cancer deaths in the world. Local ablative therapy is a well recognized, effective and minimally invasive means of treating these focal malignant hepatic tumours. There had been numerous different techniques developed over the last 3 decades namely cryoablation, microwave ablation and radiofrequency ablation (RFA), which is currently the most popular method used in the western world. However they are mostly thermal based methods, which are limited by the heat sink effect when the tumour is adjacent to a major blood vessel. Hence novel non-thermal based method such as irreversible electroporation (IRE) has been developed. These procedures are all performed under image guidance and CT and US are most commonly used. In this lecture, different ablative methods will be described and in particular the novel IRE technique where preliminary clinical results and as well as microbubble imaging findings will be discussed. With respect to current and future ablative practice, the use of US in combination with microbubble contrast agents in staging, guidance, monitoring of response and follow-up will be highlighted.

Can US with contrast enhanced ultrasound (CEUS) replace nonenhanced CT (NECT) in those with contraindication to intravenous CT contrast agents?

Stephanie R. Wilson

University of Calgary, Canada

Introduction

CT scan is routinely performed without IV contrast in those with contraindication to its use on the basis of poor renal function or prior allergy. We hypothesize that US performed with selective use of microbubble contrast agents allows for superior clinical performance without use of ionizing radiation and with no risk of nephrotoxicity.

Materials and methods

This study has approval of our IRB and all patients provided signed informed consent. As possible, consecutive patients booked for NECT were recruited to undergo US, and, as indicated, also CEUS, just prior to their CT scan. CEUS was performed on all patients who showed pathology which might benefit from additional vascular information.

Blind review of all CT and US examinations was performed to determine all positive observations. The CT and matching US scans were not interpreted consecutively. In cases with solid organ pathology, both the identification and the characterization of the pathology were assessed.

Results

160 of a planned 200 subjects have been recruited. All patients have both NECT and US. 117/170 also had CEUS performed with Definity (Lantheus, Bellrica MA) if focal pathology was noted in a solid organ or the retroperitoneum. 78 patients had CEUS of the liver, 72 with focal liver masses and 6 with no mass. All liver masses were characterized and identified on CEUS. Of the 72 abnormal livers, CT variously showed no mass (n=32), or a mass which could not be confidently characterized (n=40). 35 renal masses were identified and shown on CEUS to be vascular or avascular. Although 30 of them were shown on CT, they were not confidently characterized in any. Masses in the spleen, pancreas, bowel, and gallbladder comprise the remaining cases with CEUS, with similar superior result to NECT. A malignant bladder mass was shown only on US with CEUS in a 35 year old male who had gross hematuria and a nonenhanced CT scan performed with a renal colic protocol. Two patients, both with prior renal malignancy presented with acute flank pain and renal failure. NECT showed an indeterminate retroperitoneal mass in each, characterized correctly by CEUS as a hematoma in one and a recurrent massive enhancing tumor in the other.

NECT was superior to US in showing the extent of disease in 5 large patients, all with a BMI greater than 30, 4 with retroperitoneal adenopathy and 1 with a mesenteric calcified mass.

Conclusion

US performed with the option of CEUS to study identified focal organ pathology is superior to NECT and is recommended in selected populations. If retroperitoneal adenopathy is considered possible or likely, NECT may be superior in very large patients.

*Work in progress.

*This investigator initiated study is partially sponsored by a research grant from Lantheus Medical Imaging.

Contrast-enhanced ultrasound is a high diagnostic and cost-effective alternative to MRI in focal liver lesions

P. Taimr[1], R. Zaim[2], R. de Knegt[1], R. de Man[1], C.A. Uyl–de Groot[2], H.L.A. Janssen[1]

[1]Department of Gastroenterology and Hepatology, Erasmus MC University Hospital, Rotterdam, the Netherlands
[2]The Institute for Medical Technology Assessment, Department of Health Policy and Management, Erasmus University Rotterdam, the Netherlands

Aim

Primary: to compare diagnostic efficacy of contrast-enhanced ultrasound (CEUS) to magnetic resonance imaging (MRI) to differentiate benign from malignant focal liver lesions (FLL). Secondary: to evaluate cost-effectiveness of the application of contrast enhanced ultrasound (CEUS) as a diagnostic imaging technique in the front-line characterization of FLL in the Netherlands.

Methods

We performed CEUS (Sonovue, Bracco, Italy) in 170 patients with FLL, the majority of the patients were non-cirrhotic, which matches common clinical practice. The reference standard of the study comprised of imaging results, histology examinations and imaging results interpreted by experienced clinicians/radiologists blinded to the results of other investigations. Data collection was performed at the single-patient level (bottom up approach) and the patients were used as their own control. The volume of the cost items was obtained from the hospital database and patient files. The base year was 2010.

Results

CEUS was able to identify benign from malignant focal liver lesions with a sensitivity of 96.9% and specificity of 92.3%. The overall diagnostic accuracy was 94,0%. For correct tumor subgroup characterization the results were 85,8% for benign and 86,4% for malignant.

The incremental per patient cost advantage of -€452 was predicted for CEUS strategy. It was further estimated that -€160 was a cost advantage for diagnostic phase and -€292 was a cost advantage for treatment phase. CEUS testing strategy achieved slightly higher LYs (life years) for lower total per patient costs. Life expectancy in the form of the years saved or gained was the effectiveness endpoint of the study.

In order to identify model drivers and examine key areas of uncertainty, one-way deterministic sensitivity analyses were performed. Resource use and unit costs data were tested by varying the costs by +30% and -30% from the mean. The most influential variable found was the sensitivity of CEUS.

Probabilistic sensitivity analysis was performed by using Monte Carlo Simulation. Analysis was based on 100,000 simulations. CEUS was likely to be cost-saving in 89.99% of the simulations.

Conclusion

Our results confirm that CEUS is a high diagnostic accuracy imaging method and a cost-effective alternative compared to the traditional diagnostic procedures and should be considered as one of “the first step” options in the front-line characterization of focal liver lesions in the Netherlands. Further research should explore the role of CEUS in different clinical applications.

New developments in prostate cancer localization by contrast ultrasound dispersion imaging

Massimo Mischi[1], Maarten Kuenen[1,2], Tamerlan Saidov[1], Stefan Schalk[1], Wout Scheepens[3], Hessel Wijkstra[1,2]

[1]Department of Electrical Engineering, Eindhoven University of Technology, Eindhoven, the Netherlands
[2]Department of Urology, Academic Medical Center University of Amsterdam, Amsterdam, the Netherlands
[3]Department of Urology, Catharina Hospital, Eindhoven, the Netherlands

Background

In the United States, prostate cancer (PCa) accounts for 29% and 11% of all cancer diagnoses and deaths in men, respectively [1]. Although efficient focal therapies are available, their applicability is hampered by a lack of imaging solutions. Despite their invasiveness and poor spatial accuracy, systematic biopsies remain the most reliable option for PCa localization. Contrast-enhanced ultrasound imaging has recently opened new possibilities for PCa localization. Based on a proven correlation between cancer aggressiveness and angiogenesis [2, 3], several imaging methods have been proposed that are based on blood-perfusion assessment. However, possibly due to the complex hemodynamic effects produced by angiogenesis [4, 5], no method has yet generated reliable results. We have recently proposed contrast-ultrasound dispersion imaging (CUDI) as a new alternative method for PCa localization [6]. Different from perfusion, whose relation with angiogenesis is affected by opposing effects [4, 5], the intravascular dispersion of ultrasound contrast agents is directly influenced by angiogenic changes in the microvascular architecture.

Methodology

CUDI is performed after an intravenous injection of a 2.4-mL SonoVue® (Bracco, Milan) bolus. The bolus passage through the prostate is imaged by an iU22 ultrasound scanner (Philips Healthcare, Bothell) equipped with a C8-4v (more recently C10-3v) transrectal probe. Power modulation imaging at low mechanical index (MI = 0.06) is adopted to increase contrast sensitivity and avoid contrast destruction. After data linearization, an indicator dilution curve (IDC) is obtained at each video pixel. Linearization is obtained in two steps. First the relation between contrast concentration and acoustic intensity is established by in vitro measurements similar to those proposed in [7]. The gray map is then estimated by software Q-Lab® (Philips Healthcare, Bothell) as shown in [8].

Local dispersion can be estimated by IDC modeling based on a convective dispersion model. To this end, a modified Local Density Random Walk model is fitted to IDCs measured at each pixel [8]. An alternative approach, making use of the full spatiotemporal information, consists of the estimation of the “similarity” between neighbor IDCs [9]. Similarity is defined as the spectral coherence in a suitable predefined bandwidth. By this approach, no model fitting is required. An analytical relation between these two alternative dispersion estimates can be demonstrated.

The analysis of spatial similarity is influenced by the image resolution, which is anisotropic and depth-dependent. Therefore, a spatial pre-filter is proposed in order to regularize the image resolution and enable a similarity estimation that is not affected by resolution inhomogeneity and anisotropy. The proposed pre-filter performs a local Wiener deconvolution [7] that restores details up to the pixel resolution. Gaussian low-pass filtering in space is then performed in order to improve signal-to-noise ratio and enable accurate coherence analysis.

Preliminary validation of both methods was performed in five patients referred for a radical prostatectomy at the Academic Medical Center, University of Amsterdam (the Netherlands). The results obtained by ultrasound imaging were compared with those obtained by histopathological analysis. This task is complicated by misalignment between histology slices and ultrasound imaging planes, and by prostate deformations in the ultrasound image, due to insertion of the transrectal ultrasound probe, as well as in the histology, due to fixation processes. To overcome these problems, a 3D ultrasound image of the prostate is reconstructed based on two 2D imaging sweeps, longitudinal and lateral. Also a 3D reconstruction of the histology results, including cancer position, is realized by integration and interpolation of 4-mm prostate slices. A combination of rigid and elastic registration is then applied for 3D mapping of the histology on the ultrasound surface. The deformation of the inner volume is estimated on the basis of the surface deformation, without need for additional landmarks.

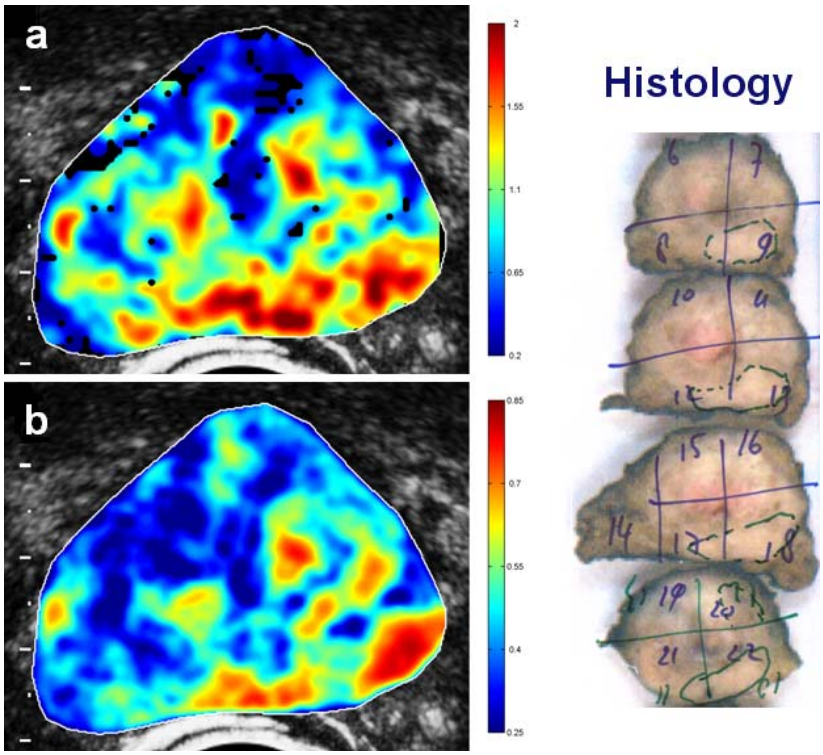

Figure 1. Dispersion maps by IDC fitting (a) and by coherence analysis (b), respectively. On the right, the corresponding histological analysis is shown.

Results

In all patients, the dispersion images showed a good agreement on a pixel basis with the histology. The resulting average area of the receiver operating characteristic (ROC) curve was 0.84 (sensitivity 78.5% and specificity 79.5%) and 0.86 (sensitivity 75.6% and specificity 87.1%) for the dispersion estimates by IDC fitting and coherence analysis, respectively. These results were superior to those obtained by perfusion measurements, such as IDC mean transit time, wash-in time, and area under the curve. Figure 1 shows an example of dispersion maps obtained by both analysis methods.

Conclusions

Our preliminary results evidence the promising value of CUDI for PCa localization and motivate towards extensive validation to optimize and compare the method with other techniques. To this end, CUDI is being tested with different equipment, such as the ultrasound scanner Hi Vision Preirus (Hitachi Medical Systems, Wellingborough) equipped with a V53W transrectal probe. As CUDI aims at characterization of the microvascular architecture, more accurate validation requires immunohistological analysis of the excised prostate for assessment of microvascular density and architecture. Additional measurements with animal models are also ongoing for accurate validation of the relation between estimated dispersion and microvascular architecture. Once fully validated, CUDI can possibly support both targeting of biopsy and focal-therapy.

References

1. American Cancer Society. Cancer facts & figures 2011, 2011
2. J. Folkman, “Tumor angiogenesis: Therapeutic implications,” N. Engl. J. Med., vol. 285, pp. 1182-1186, 1971
3. M.K. Brawer, “Quantitative microvessel density. A staging and prognostic marker for human prostatic carcinoma,” Cancer, vol. 78, no. 2, pp. 345-349, 1996
4. D. Cosgrove, “Angiogenesis imaging - ultrasound,” The British Journal of Radiology, vol. 76, pp. S43–S49, 2003
5. N. Elie, A. Kaliski, P. P´eronneau, P. Opolon, A. Roche, and N. Lassau, “Methodology for quantifying interactions between perfusion evaluated by DCE-US and hypoxia throughout tumor growth,” Ultrasound in Med. and Biol., vol. 33, no. 4, pp. 549-560, 2007
6. M. Smeenge, M. Mischi, M.P. Laguna Pes, J.J.M.C.H. de la Rosette, and H. Wijkstra, “Novel contrast-enhanced ultrasound imaging in prostate cancer,” World J. Urology, vol. 29, no. 5, pp. 581-587, 2011
7. M. Mischi, “Contrast echocardiography for cardiac quantifications,” Ph.D. dissertation, Eindhoven University of Technology, 2004, available at http://www.sps.ele.tue.nl/members/M.Mischi/
8. M. P. J. Kuenen, M. Mischi, and H. Wijkstra, “Contrast-ultrasound diffusion imaging for localization of prostate cancer,” IEEE Trans. Medical Imaging, vol. 30, no. 8, pp. 1493-1502, 2011
9. M.P.J. Kuenen, M. Mischi, and H. Wijkstra, “Coherence-based contrast ultrasound diffusion imaging for prostate cancer detection,” IEEE Proc. on IUS, San Diego (CA), Oct. 11-14, 2010, pp. 1936-1939

Therapeutic use of bubbles in brain tumours

Nathan McDannold, Ph.D.

Brigham & Women's Hospital, Harvard Medical School, Boston, MA, USA

The diagnosis for many brain tumor patients is grim and new treatment options are desperately needed. One of the main limitations in developing new treatments for brain tumors is the difficulty in delivering drugs to the brain. The blood-brain barrier (BBB), a physical and functional barrier present in the brain vasculature, prevents most agents from reaching the brain. A decade ago we found that low-energy ultrasound bursts, when combined with a microbubble-based ultrasound contrast agent, can induce a temporary disruption of the blood-brain barrier (BBB) with little or no other evident effects. This technique, when combined with focused ultrasound systems that can effectively focus ultrasound through the human skull has a huge potential as a completely noninvasive means for targeted drug delivery to infiltrating cancer cells that are protected by the BBB. It has also been shown that the ultrasound bursts increase delivery to tumors that lack a BBB.

We recently completed initial tests of the method in nonhuman primates using a clinical MR-guided focused ultrasound system (ExAblate 4000, InSightec). We have found that BBB disruption can be achieved repeatedly in nonhuman primates without evidence of tissue damage or functional deficits. Furthermore, the disruption has been found to only occur at targeted locations in the brain. Example images showing MRI contrast agent penetration to volumes in the putamen and visual cortex are shown below.

In another recently completed study, we tested whether combining BBB disruption with trastuzumab (Herceptin), an antibody-based drug for HER2-positive breast cancer that often fails with brain metastases, can improve outcomes in nude rats implanted with human breast cancer cells. Tests in the breast cancer brain metastases model have shown improvement in tumor growth rate, with tumors in 4/10 animals in the Herceptin/BBB disruption group disappearing. This result was not achieved in the control groups.

These and other similar studies, while still ongoing, are encouraging and supportive of preparing for initial human tests of this technique. We think that brain metastases may be good initial candidates for this technique, as effective drugs often already exist for extracranial disease.

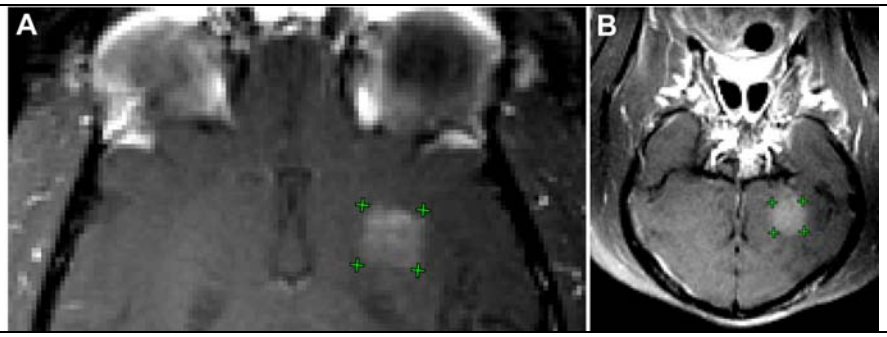

Fig 1. Contrast-enhanced MRI of showing localized volumetric BBBD in the putamen and in a rhesus macaque using a clinical MR-guided focused ultrasound device capable of transcranial sonication. The focal point was steered dynamically to 9 locations in a 3×3 square pattern during sonication to target a volume. The corners of the targeted volume are shown in the axial image (left). A contiguous region of BBBD was observed, without any evident effects in the beam path or the skull (right). .

Effectiveness of ultrasound and microbubbles in acute myocardial infarction on thrombus resolution and no-reflow

Otto Kamp, MD, PhD, FESC

Amsterdam, the Netherlands

Research has been shown that (diagnostic) ultrasound in the presence of microbubbles enhance thrombolysis, the so-called sonothrombolysis. Although the exact working mechanisms remain to be elucidated, it is known that destruction of microbubbles and local application of ultrasound leads to several (bio)effects resulting in enhanced thrombolysis. Especially, cavitation which produces mechanical effect and bio-effects is an important underlying mechanism.

Animal studies in the setting of acute myocardial infarction confirmed the therapeutic potential of diagnostic ultrasound in the presence of microbubbles and the first in human study is underway.
The aforementioned animal studies also observed that, despite the absence of epicardial coronary recanalization, the myocardial perfusion in the area at risk did improve, indicating microvascular adaptation. It is hypothesized that this might be due to a positive effect of ultrasound in the presence of microbubbles on the disbalance between nitric oxide and superoxide production and a decrease of inflammatory response. However, the exact mechanism remains unclear.

On the other hand, concerns have been risen, that inertial cavitation may have harmful effects as well, although they seem to be limited. Nevertheless, local destruction of microbubbles under influence of ultrasound might have a favorable effect on the no-reflow phenomenon.
Therefore, our present research is directed to explore the potential clinical application of (diagnostic) ultrasound in patients with acute myocardial infarction and the no-reflow phenomenon after primary PCI.

Key references

1. Lepper W, Hoffmann R, **Kamp O**, Franke A, de Cock CC, Kühl HP, Sieswerda GT, Dahl J, Janssens U, Voci P, Visser CA, Hanrath P. Assessment of myocardial reperfusion by intravenous myocardial contrast echocardiography and coronary flow reserve after primary percutaneous transluminal coronary angioplasty [correction of angiography] in patients with acute myocardial infarction. Circulation. 2000 May 23;101(20):2368-74. Erratum in: Circulation 2000 Jul 25;102(4):482
2. **Kamp O**, Lepper W, Vanoverschelde JL, Aeschbacher BC, Rovai D, Assayag P, Voci P, Kloster Y, Distante A, Visser CA. Serial evaluation of perfusion defects in patients with a first acute myocardial infarction referred for primary PTCA using intravenous myocardial contrast echocardiography. Eur Heart J. 2001 Aug;22(16):1485-95
3. Dijkmans PA, Juffermans LJ, Musters RJ, van Wamel A, ten Cate FJ, van Gilst W, Visser CA, de Jong N, **Kamp O**. Microbubbles and ultrasound: from diagnosis to therapy. Eur J Echocardiogr. 2004 Aug;5(4):245-56. Review

4. Dijkmans PA, Knaapen P, Sieswerda GT, Aiazian E, Visser CA, Lammertsma AA, Visser FC, **Kamp O**. Quantification of myocardial perfusion using intravenous myocardial contrast echocardiography in healthy volunteers: comparison with positron emission tomography. J Am Soc Echocardiogr. 2006 Mar;19(3):285-93
5. Juffermans LJ, Dijkmans PA, Musters RJ, Visser CA, **Kamp O**. Transient permeabilization of cell membranes by ultrasound-exposed microbubbles is related to formation of hydrogen peroxide. Am J Physiol Heart Circ Physiol. 2006 Oct;291(4):H1595-601. Epub 2006 Apr 21
6. Dijkmans PA, Senior R, Becher H, Porter TR, Wei K, Visser CA, **Kamp O**. Myocardial contrast echocardiography evolving as a clinically feasible technique for accurate, rapid, and safe assessment of myocardial perfusion: the evidence so far. *J Am Coll Cardiol* 2006 December 5;48(11):2168-2177
7. Slikkerveer J, Dijkmans PA, Sieswerda GT, Doevendans PA, van Dijk AP, Verheugt FW, Porter TR, **Kamp O**. Ultrasound enhanced prehospital thrombolysis using microbubbles infusion in patients with acute ST elevation myocardial infarction: Rationale and design of the Sonolysis study. Trials 2008;9:72
8. Meijering BD, Juffermans LJ, van Wamel A., Henning RH, Zuhorn IS, Emmer M, Versteilen AM, Paulus WJ, van Gilst WH, Kooiman K, de Jong N., Musters RJ, Deelman LE, Kamp O. Ultrasound and microbubble-targeted delivery of macromolecules is regulated by induction of endocytosis and pore formation. Circ Res 2009 March 13;104(5):679-687
9. Slikkerveer J, Xie F, Kamp O, Gao S, Unger EC, Matsunaga T, Lof J, Porter TR. Improvement in myocardial blood volume and ultimate infarct size despite persistent epicardial occlusion using three-dimensional transthoracic ultrasound and intravenous non-targeted microbubbles. Eur Heart J 2010;31 (suppl 1):873-1071
10. Slikkerveer J, Kleijn SA, Appelman Y, Porter TR, Veen G, van Rossum AC, Kamp O. Ultrasound enhanced prehospital thrombolysis using microbubbles infusion in patients with acute ST elevation myocardial infarction: pilot of the Sonolysis study. Ultrasound in Med & Biol 2012 in press

What's new in carotid vasa vasorum imaging?

Steven B. Feinstein, M.D., FACC, FESC
Professor of Medicine, Section of Cardiology

Rush University Medical Center, Chicago, Illinois

Overview

Contrast –enhanced, ultrasound imaging (CEUS) provides unparalleled, spatial and temporal resolution of the heterogeneous patterns of microvascular blood flow and blood volumes. The diagnostic applications of CEUS include interrogation of the vascular system, atherosclerotic plaques. The current and future applications of diagnosis and therapy will be discussed.

Topics to be included in the review:

- Discuss the role of non-traditional CV imaging for CV prevention
- Review of the pathophysiology of the vulnerable plaque intra-plaque angiogenesis and role of CEUS
- Update on USA FDA clinical trials of CEUS for carotid vascular imaging
- Review of current status of 3D/4D carotid plaque imaging
- Highlight intra-plaque chemistry and therapy

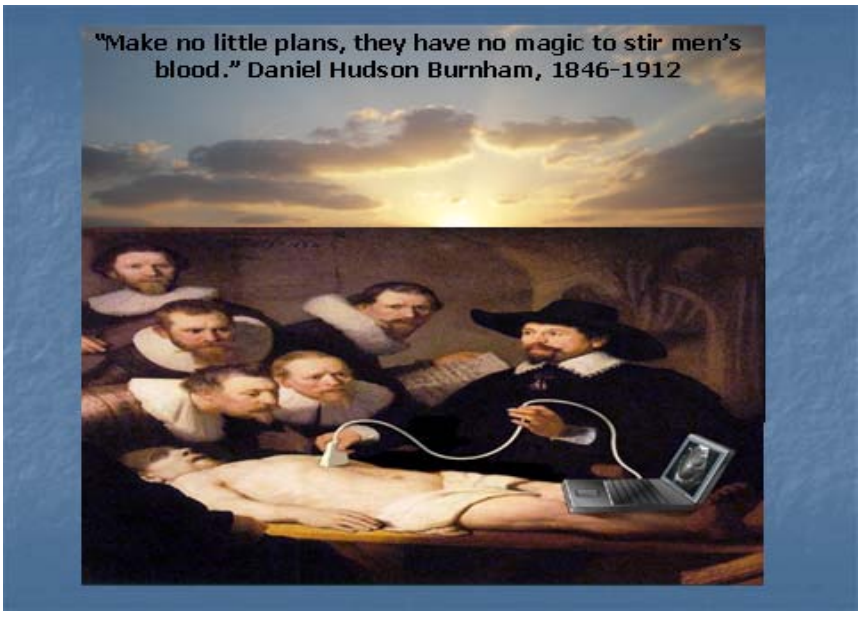

Long term stem cell tracking *in vivo* using contrast ultrasound

Flordeliza S. Villanueva, Huili Fu, Xucai Chen, Xiaoping Leng, Stephen Thorne, Jianjun Wang

Center for Ultrasound Molecular Imaging and Therapeutics
University of Pittsburgh, PA, USA

Background

Human mesenchymal stem cell (hMSC) therapy is promising for cardiac repair. Clinical translation requires a method to track serially the cell migration and distribution *in vivo*. We have previously shown that polylactide microbubbles (MB) are internalized by hMSC, persist in the cytoplasm, and allow ultrasound (US) imaging of intramuscularly injected stem cells in mice, but only up to 4 hr at 37°C. We sought to design a more durable MB for prolonged US cell tracking and validated our method against *in vivo* bioluminescence imaging (BLI).

Methods

Polymer MBs with a polycarprolactone and albumin double layer shell filled with nitrogen gas were synthesized. MB acoustic activity was measured in a water tank (Contrast Pulse Sequencing, 7 MHz) after synthesis (Day 0) and 7 day storage at 37°C. Cultured hMSCs expressing luciferase gene were incubated with MB. MB uptake was studied by confocal microscopy. MB-hMSC complexes or control hMSCs were lifted, washed, and re-suspended for *in vitro* US imaging or *in vivo* injection into nude mouse thigh muscle (0.5–1.0 $x10^6$ cells). Mice had serial US and concurrent BLI up to 7 days post INJ.

Results

In vitro videointensity (VI) of MB alone (27±1 dB, Day 0) was stable up to 7 days at 37°C ($p=0.50$). MB internalization occurred in 67% hMSC and did not impair cell viability by trypan blue exclusion. *In vitro* VI of MB-hMSC on Day 0 (17±1 dB, n=3) was higher than hMSC alone (0±0 dB, n=2, $p<0.01$), unchanged at Day 1 (15±2 dB, $p=0.18$), and decreased but was still easily seen at Day 7 post-labeling (9±1 dB, $p<0.05$). Mouse thigh US enhancement was visualized for MB-hMSC (n=8) but not for hMSC-only (n=4) immediately post injection (0 hr) (7±3 dB vs 0±0 dB, $p<0.01$). MB-hMSCs were still seen by US at 2 days, but VI was decreased ($p< 0.05$ vs. 0 hr). In the mice receiving 10^6 MB-hMSC, US signal persisted up to 7 days. BLI showed hMSC luminescence co-localizing with the thigh muscle US signal.

Conclusion

hMSCs labeled with a new polymer MB can be serially detected *in vivo* by US over a time period relevant to clinical cell therapy. US imaging of MB-hMSC identifies viable hMSC as confirmed by concurrent BLI, offers non-invasive serial *in vivo* tracking of hMSC fate, and may facilitate implementation of cell therapy strategies. Optimization of MB formulation and dose to further extend US persistence *in vivo* should be possible.

Ultrasound imaging of inflammation using leukocyte-inspired microbubbles

***Thierry Bettinger*, Philippe Bussat, Isabelle Tardy, Sibylle Pochon, Jean-Marc Hyvelin, Patricia Emmel, Sylvie Henrioud, Nathalie Biolluz, Michel Schneider, Francois Tranquart**

Bracco Suisse SA, Geneva, Switzerland

Objectives

Contrast-enhanced ultrasound molecular imaging is increasingly used in pre-clinical studies to measure the expression of vascular markers. In this context, a new ultrasound contrast agent functionalized with a recombinant P-selectin glycoprotein ligand-1 analog (PSGL-Ig) was developed ($MB_{PSGL-Ig}$). This agent was assayed in vitro and in vivo to evaluate its binding performance and potential to image expression of inflammatory markers E-selectin and P-selectin. Performance of this newly developed agent was compared to that of antibody (MB_{Ab}) or sialyl Lewis X (MB_{sLe^x}) containing microbubbles.

Materials and Methods

The targeted ultrasound contrast agents were prepared by functionalizing streptavidin-containing microbubbles with biotin-conjugated ligands. First, in vitro experiments were performed to measure adhesion efficiency of these microbubbles constructs under static or flow conditions conditions (114 s^{-1}) on cell monolayer (HUVEC and bEnd.5 cells) or coatings of E-selectin or P-selectin of various animal species, respectively. Secondly, molecular imaging studies using a Siemens Sequoia ultrasound scanner (CPS mode, 15L8 probe, 7 MHz, MI of 0.25) were performed in a rat inflammatory model, 24 h after an intra-muscular injection of lipopolysaccharide (LPS) in the hind limb. Finally, immunohistochemistry staining on inflamed muscle of rat was performed to assess expression of the E-selectin and P-selectin.

Results

Microbubbles functionalized with PSGL-Ig ($MB_{PSGL-Ig}$) displayed firm in vitro binding on coatings of both recombinant E-selectin or P-selectin, with an efficiency similar to microbubbles modified with antibody (MB_{Ab}). Lower binding capacity was measured with sLe^x microbubbles (MB_{sLe^x}), resulting from a marked rolling behaviour under flow conditions. $MB_{PSGL-Ig}$ were able to interact specifically with E-selectin and P-selectin at the surface of TNFα-stimulated mouse bEnd.5 endothelial cells (Figure 2).

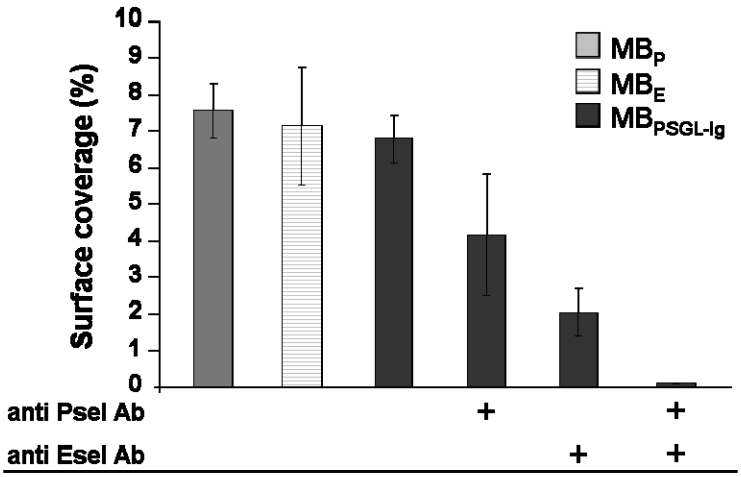

Figure 2: Adhesion of microbubbles to inflamed mouse brain endothelioma cells (bEnd.5) under static conditions. Microbubbles were conjugated either to rPSGL-Ig ($MB_{PSGL-Ig}$) or to anti P-selectin mAb (MB_P) (anti mouse P-selectin) or to anti E-selectin polyclonal Ab (MB_E) (anti rat E-selectin). Binding specificity was assessed by incubating bEnd.5 cells with a mixture of $MB_{PSGL-Ig}$ and anti mouse P-selectin antibody or anti rat E-selectin antibody or mixture of both. n=5.

Ten minutes after microbubbles injection, strong echo signal was measured with $MB_{PSGL-Ig}$ in the inflamed muscle, whereas in the contra lateral muscle only background level was detected (Figure 3).

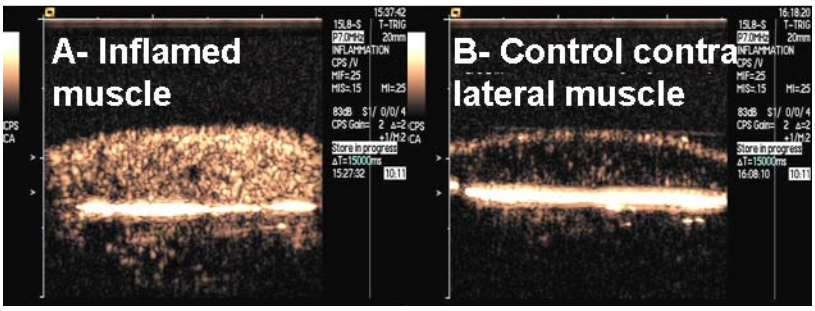

Figure 3: Contrast enhanced ultrasound of microbubbles adhesion 24 h after i.m. of LPS in the rat hind limb. $MB_{PSGL-Ig}$ in the inflamed (A) and control contra-lateral muscle (B) 10 min after MB injection.

This signal obtained with $MB_{PSGL\text{-}Ig}$ in the inflamed muscle was 20-fold higher compared to control microbubbles (MB_C) (Figure 4). Moreover, the in vivo adhesion of $MB_{PSGL\text{-}Ig}$ was 2 and 7-fold higher compared to E-selectin or P-selectin specific microbubbles, respectively. Very poor binding was measured for microbubbles comprising sialyl Lewis X (MB_{sLe^x}), in agreement with the in vitro results.

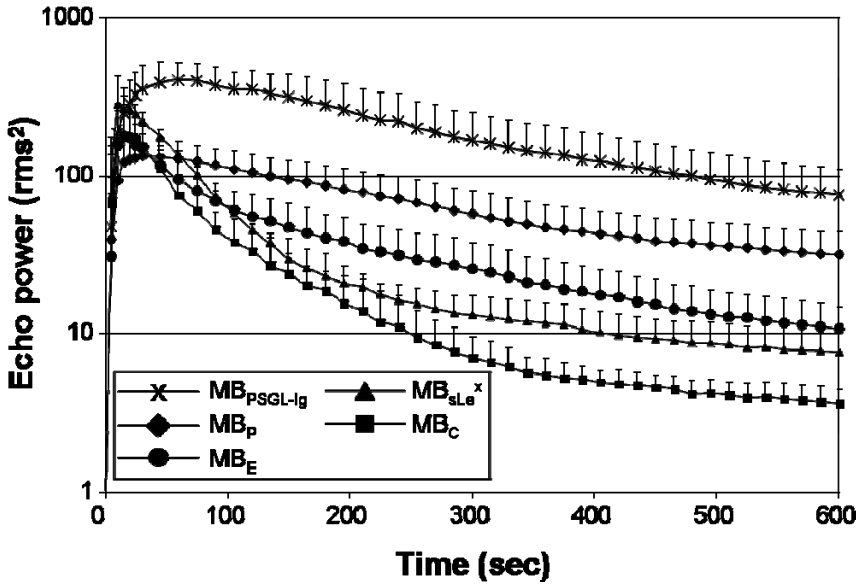

Figure 4: Mean time intensity curves of $MB_{PSGL\text{-}Ig}$ (n=7), MB_P (n=12), MB_E (n=4), MB_{sLe^x} (n=3), MB_C (n=4) in the inflamed muscle of rats 24 h after the onset of inflammation.

Immunohistochemistry revealed a temporal co-expression of E-selectin and P-selectin in the vascular bed of inflamed rat muscle, 24 h after LPS injection.

Conclusion

The molecular imaging study demonstrates that $MB_{PSGL\text{-}Ig}$ provide imaging signal higher than those measured with antibody or sLe^x-containing microbubbles. These results suggest that $MB_{PSGL\text{-}Ig}$ is a powerful dual-targeted agent to image the expression of both E-selectin and P-selectin in the context of an inflammatory process.

From contrast to cancer immunotherapy: exploring sonoporation-induced mRNA transfection of dendritic cells

***Heleen Dewitte*, Marie-Luce De Temmerman, Bart Lucas, Stefaan C. De Smedt, Joanna Rejman, Ine Lentacker**

Ghent Research Group on Nanomedicine, Department of Pharmaceutical Sciences, Ghent University, Harelbekestraat 72, 9000 Ghent, Belgium

Introduction and aim

For many years, microbubbles have been safely used as ultrasound contrast agents. More recently, they sparked interest as drug and gene delivery agents, by using ultrasound-induced pore formation upon microbubble implosion to our advantage. This sonoporation-based gene delivery paved the way for many new and exciting microbubble applications and cellular targets. One of these is the current investigation of mRNA-lipoplex loaded microbubbles for transfection of dendritic cells (DCs).

The discovery of DCs as key players in triggering immune responses not only provided Ralph Steinman with a Nobel Prize in 2011, it also initiated a novel immunotherapeutic approach: Dendritic Cell Vaccination[1]. DCs form a bridge between the innate and adaptive immunity by continuously sampling antigens, processing them and presenting them to T cells. If an antigen is recognized as non-self (e.g. tumor-derived), antigen-specific T cells will become activated to selectively target and destroy the cancer cells. In DC vaccination, the immune triggering is enforced by loading DCs with tumor associated antigens (TAAs) in such a way that it will lead to an efficient antitumor cytotoxic T cell response[2]. A particularly suitable way of doing this, is to use mRNA sequences encoding TAAs. This way, the DCs themselves can produce the TAAs and are thus capable of presenting multiple antigenic determinants to the patient's immune cells.

In this research, we aim to use sonoporation as a physical adjuvant to load DCs with mRNA. A graphic illustration of this application can be found in **figure 1**.

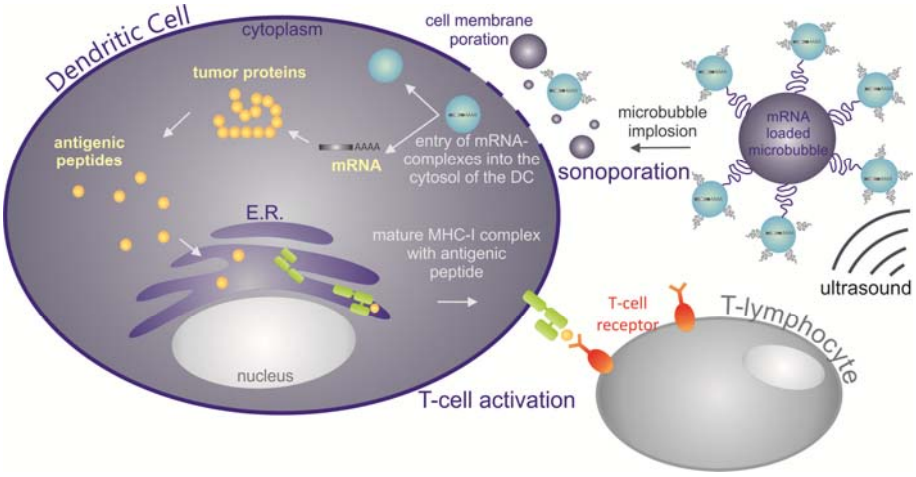

Figure 1. Overview of sonoporation-mediated mRNA transfection of DCs for immunotherapy

Results

It is known that DCs are quite resistant to transfection, and require a physical cell membrane disruption to provide direct access of the nucleic acids to the cytoplasm. To address this problem, we intended to use sonoporation and therefore designed a lipid microbubble that can be loaded with mRNA lipoplexes via avidin-biotin interactions. By using reporter mRNA (mLuc and mEGFP), we could measure the transfection efficiency after addition of the mRNA-lipoplex loaded microbubbles to bone marrow-derived DCs and ultrasound application (Sonitron2000, 2 W/cm², 1 MHz, 20% duty cycle). This approach proved to significantly enhance transfection efficiency compared to free mRNA-lipoplexes. A fast-onset protein expression (30 min after ultrasound application, **figure 2**) was detectable in up to 24% of the DCs. Importantly, this approach does not compromise cell viability, as 84% of DCs are capable of repairing the cell membrane damage within 24 h after treatment with mRNA-lipoplex loaded microbubbles and ultrasound[3].

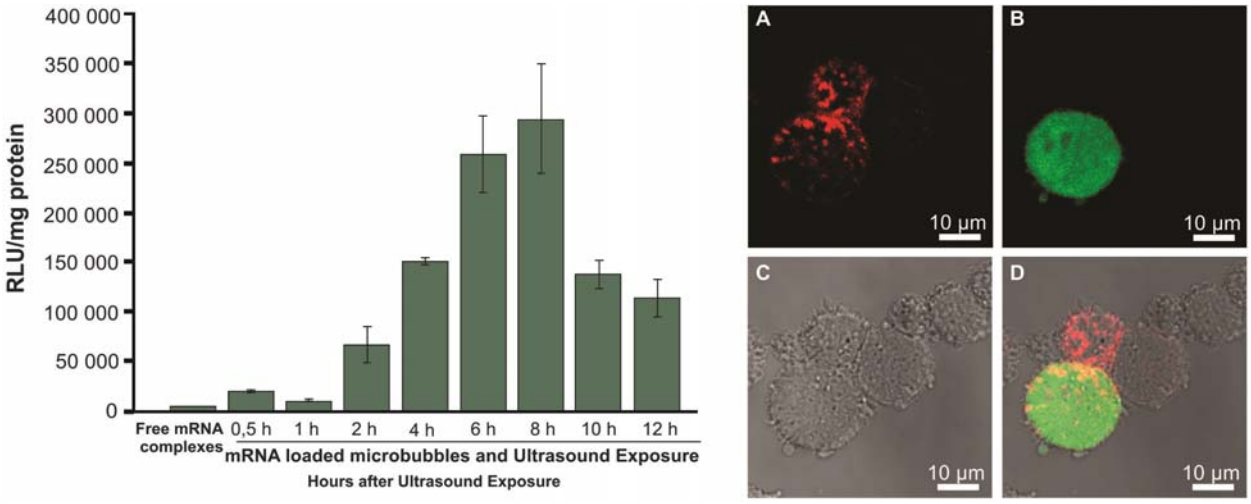

Figure 2. Transfection efficiency of mRNA-lipoplex loaded microbubbles and ultrasound. Luciferase expression kinetics (left) and confocal images of mEGFP transfected DCs (right, DCs are stained for CD11c in red and green fluorescence is due to EGFP)

During the process of maturation, DCs undergo phenotypical changes that shift their function from antigen-sampling cells to antigen-presenting cells. Therefore, it is important to assess the influence of the transfection procedure on the maturation status of the DCs. For this, the expression of the maturation markers CD40 and CD86 on the surface on the DCs was determined by flow cytometry. The results showed that, compared to untreated DCs, there was a minor increase in expression of these markers after transfection with mRNA-lipoplex loaded microbubbles and ultrasound. Notably, complete maturation of the transfected DCs was still possible by addition of bacterial lipopolysaccharide, indicating that the normal DC functions are not compromised by the transfection procedure. Finally, we investigated whether there is a difference in transfection efficiency for immature or mature DCs, as several reports on mRNA electroporation of DCs proved that mature DCs are more susceptible to taking up the mRNA.

However, as shown in **figure 3**, for sonoporation, the contrary is true and mRNA-loading proved to be largely hampered after maturation of DCs.

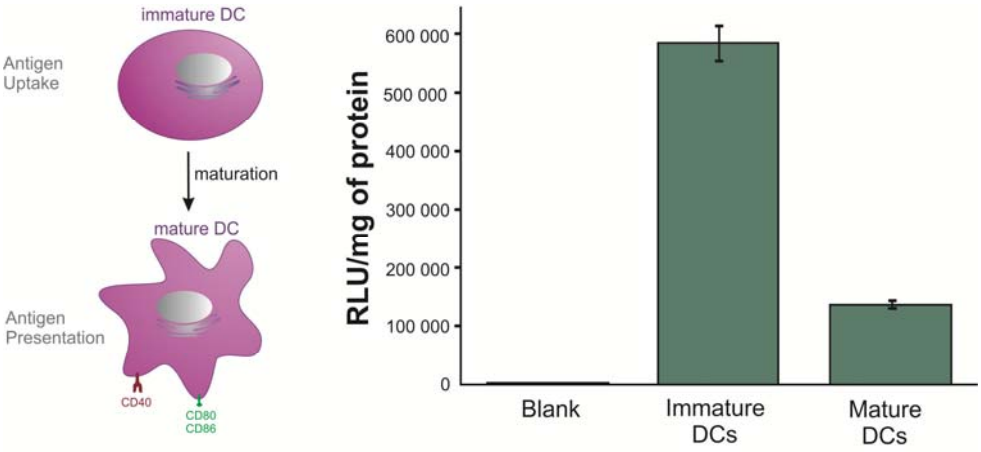

Figure 3. Maturation of DCs. Schematic representation of the maturation process in DCs (left) and the differences in transfection efficiency in immature and mature DCs using mLuc-lipoplex loaded microbubbles and ultrasound.

Conclusions

mRNA-lipoplex loaded microbubbles can be used as an efficient ultrasound-triggered tool for transfection of DCs without compromising cell viability or DC maturation capacities. The main advantage of this technique is the *in vivo* possibilities it holds; Immediate *in vivo* transfection of intranodally present DCs could circumvent current *ex vivo* procedures, making DC vaccination less expensive and time-consuming.

References

1. J. Banchereau, R. M. Steinman, Nature 1998, 392, 245-252
2. E. Gilboa, Immunity 1999, 11, 263-270
3. M.-L. De Temmerman, H. Dewitte, R. E. Vandenbroucke, B. Lucas, C. Libert, J. Demeester, S. C. De Smedt, I. Lentacker, J. Rejman, Biomaterials 2011, 32, 9128-9135

Acknowledgements
Heleen Dewitte is a doctoral fellow of the Institute for the Promotion of Innovation through Science and Technology in Flanders, Belgium (IWT-Vlaanderen). Ine Lentacker is a postdoctoral fellow of the Research Foundation Flanders, Belgium (FWO-Vlaanderen).

Molecular and functional ultrasound assessment of antiangiogenic therapy with BR55

I. Tardy, J.M. Hyvelin, S. Pochon, M. Theraulaz, A. Helbert, M. Arditi and F. Tranquart

Bracco Suisse SA, Geneva Research Center and Manufacturing Site, CH-1228 Plan-Les-Ouates, Geneva, Switzerland

Purpose

Efficacy of anticancer therapies is commonly evaluated by measuring direct effects on the tumor by use of the Response Evaluation Criteria In Solid Tumors (RECIST). However, with the advent of anti-angiogenic chemotherapy, vascular changes might occur initially without tumor size reduction, which can cast doubt on the sensitivity of RECIST criteria. Tumoral vascular growth is triggered by different pro-angiogenic factors. Molecular imaging of these markers could predict the response to anti-angiogenic treatment at an early stage. Ultrasound molecular imaging (US-MI), combined with quantification software is a promising non-invasive imaging method that allows assessment of both tumor perfusion and molecular marker expression. BR55 is an ultrasound contrast agent designed for molecular imaging of human VEGFR2 (KDR). BR55 is functionalized with a heterodimer peptide that binds to KDR with high affinity. We tested the hypothesis that performing US-MI with BR55 might be more predictive of anti-angiogenic treatment efficacy than changes in tumor perfusion and/or tumor volume.

Methods and Materials

Spontaneous rat mammary tumor model (N-nitroso-N-methylurea treatment) and rat prostate tumor model (orthotopic implantation of G - Dunning R-3327 cells) were used. When tumor cross-sectional areas reached 0.4 cm^2 (prostate tumor) or 1.5 cm^2 (mammary tumor), animals received an anti-angiogenic treatment (sunitinib, LC-Laboratories, Woburn MA). Tumor response was monitored by US-MI over a 10-day period. Contrast enhancement was quantified (from DICOM files) using a software package developed in-house. Time intensity curves generated from linearized data were used to determine perfusion estimates during the initial wash-in phase. Targeted contrast enhancement due to bound BR55 microbubbles was assessed 10 minutes after BR55 injection. Perfusion parameters were measured in a scan plane across the largest section of the tumor, whereas BR55 binding was assessed by sweeping through the entire tumor (in 1mm steps), 10 min after injection, in order to evaluate global KDR expression.

Results and Conclusion

In both animal models, sunitinib treatment resulted in an earlier and more pronounced decrease in BR55 binding than reduction in tumor volume. Furthermore, decreased BR55 binding was larger and more consistent throughout the treatment course than perfusion changes These data suggest that molecular imaging with BR55 of the specific angiogenesis marker KDR, will likely prove useful in humans for an early and accurate assessment of tumor response to specific treatment.

Financial interest Statement: All authors are employees of Bracco Suisse SA, part of the Bracco Group.

Thursday, January 19, 2012

Social Event

Grillcafé Bar Bowling "DOK 99"
Straatweg 99 Rotterdam

Buffet: around 7.30 pm

Coaches will be leaving from the World Trade Center at 18:00, from Hilton at 18.15 and will be back in Hilton around 22:30

Advances in microbubble delivery of apoA-I DNA for the therapeutic elevation of HDL

Jason Castle, Biologist

GE Global Research

Apolipoprotein A-I (apoA-I) is the predominant protein component of high-density lipoprotein (HDL) in plasma, and in animal models, increasing apoA-I in transgenic animals or infusing recombinant HDL (rHDL) promotes prominent regression of atherosclerosis and enhanced macrophage-specific reverse cholesterol transport. Additionally, elevated LDL and low HDL remain independent risk factors for cardiac disease. Furthermore, patients with a genetic incapability of producing significant levels of HDL (hypoalphalipoproteinemia) demonstrate a debilitating disease prone to early cardiac disease and ultimately death. Although well described, the pharmaceutical intervention of HDL has yet remained allusive.

Here, we report on the first animal study to consider HDL regulation through the targeted delivery of apoA-I DNA. Utilizing ultrasound mediated targeted drug delivery; the plasmid is transported to the liver via intravenous injection of diagnostic microbubble (Optison). Upon perfusion, acoustic energy is directed to the liver (GEHC Vivid *i* system) for site-selective cavitation of the microbubbles. This facilitates the delivery of apoA-I DNA to the hepatic intracellular environment. To date we have demonstrated a study response rate as high as 93%, with rats averaging a 32% increase in HDL level 24 hours post-procedure. This success has been enabled by accounting for the subtle factors pertaining to vessel size, microbubble density and acoustic sequencing.

Ultimately, this delivery platform may allow therapeutic intervention in many challenging diseases whereby drugs may need a greater therapeutic index or where the delivered drug is of a genetic material composition.

Microbubble-loaded red blood cells to produce acoustically active ghosts

Ali H. Dhanaliwala[1,3], Alexander L. Klibanov[2], John A. Hossack[1]

[1]Department of Biomedical Engineering, University of Virginia, Charlottesville, USA
[2]Department of Cardiovascular Medicine, University of Virginia, Charlottesville, USA
[3]Cardiovascular Research Center, University of Virginia, Charlottesville, USA

Introduction & Background

The most common ultrasound contrast agents are microbubbles: 1 - 10 μm diameter gas bubbles stabilized by a shell coating. Microbubbles are FDA approved to enhance detection of cardiac wall motion abnormalities, but have also been shown to improve Doppler velocity and tissue perfusion imaging. In addition, microbubbles continue to be investigated for molecular targeting and as drug delivery vehicles. Even though current generation microbubbles utilize lipid, protein, or polymer shells and low solubility gasses, *in vivo* half life is still limited to several minutes as a result of gas core dissolution and filtration by the lungs and the reticuloendothelial system.

Red blood cells are similar in size to microbubbles and are an intriguing alternative ultrasound contrast agent. When lysed then resealed, red blood cells exchange their cytoplasm for the contents of the surrounding solution. In the process, hemoglobin is lost and the cells are renamed ghosts. If the surrounding solution contains a drug, red blood cell ghosts become drug delivery vehicles with a large payload capacity and a long circulation time. While red blood cell ghosts share similar properties to microbubbles – similar diameters, freely traverse the vasculature, and are inherently biocompatible – they possess low backscatter at clinical ultrasound frequencies (6-15 MHz) making them ineffective as contrast agents. To combine the advantages of microbubbles (acoustic contrast) with red blood cells (inherent biocompatibility and longevity), we have developed a method to load microbubbles into red blood cell ghosts, thus producing acoustically active red blood cells that can be used as ultrasound contrast agents

Methods

Acoustically active red blood cell ghosts were produced by loading microbubbles into red blood cells using a modified hypo-osmotic method. Briefly, fresh canine or bovine blood was collected in EDTA containing tubes to prevent clotting. The whole blood was then washed three times in an isotonic solution. The resulting packed red blood cells were incubated in a hypotonic lysis solution containing microbubbles. The microbubble shell was composed of phosphatidylcholine, polyethylene glycol stearate and a trace amount of the fluorescent marker DiI while the gas core was perfluorobutane. After lysis, the solution was brought back to isotonicity and incubated at 37 °C to enhance membrane

resealing. Finally, the resulting microbubble-loaded red blood cell ghosts (MB-ghosts) were washed to remove all unencapsulated microbubbles and stored in an isotonic solution. The MB-ghosts were imaged using phase contrast and fluorescence microscopy. Acoustic properties were determined by insonating MB-ghosts with a 2.25 MHz focused single element piston transducer. Plain microbubbles, empty red blood cell ghosts, and whole blood were insonated, at equivalent concentrations, as controls.

Results

Composite fluorescence (outlining microbubbles) with phase contrast (outlining red blood cell ghosts) images showed the successful loading of microbubbles into red blood cell ghosts (Fig 1a-d). Four types of MB-ghosts could be classified: 1) red blood cell ghosts with microbubbles attached to the outer membrane 2) red blood cell ghosts with microbubbles attached to the inner membrane 3) red blood cell ghosts with microbubbles wholly in the cytoplasm and 4) empty red blood cell ghosts. Acoustically, the MB-ghosts signal was 8.3 dB larger than empty red blood cells but 4.4 dB lower than plain microbubbles (Fig 1e).

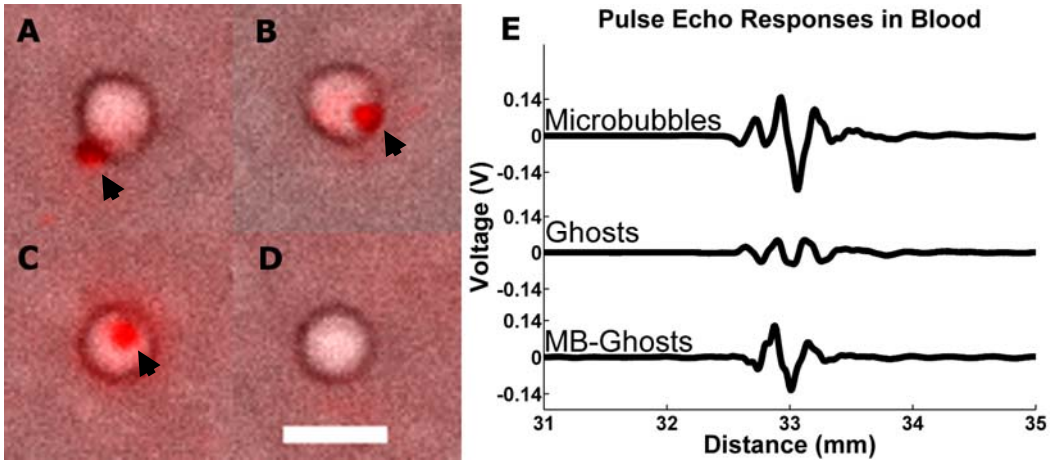

Figure 1: Composite fluorescence (microbubbles) and phase contrast (red blood cell ghosts) images showing microbubbles (arrowhead) attached to the (A) outer leaflet, (B) inner leaflet, and (C) freely contained within the cytoplasm, of a red blood cell ghost. (D) An empty red blood cell ghost. Scale bar = 10 µm. (E) Acoustic signal from plain microbubbles, empty red blood cell ghosts, and MB-ghosts diluted in whole blood. MB-ghosts have an 8.3 dB increase in signal over empty red blood cells alone.

Discussion & Conclusion

The lower acoustic signal of MB-ghosts compared to plain microbubbles is likely due to two main factors. First, the loading efficiency of microbubbles into red blood cell ghosts is low and there is no efficient method for separating empty ghosts from MB-ghosts. As a result, while red blood cell ghosts can be concentration-matched to plain microbubbles, the two are unlikely to have the same number of acoustically active particles. Second, the red blood cell ghost membrane may dampen the microbubble oscillations resulting in a reduced acoustic signal.

We have shown proof of concept for acoustically active red blood cell ghosts, a promising new ultrasound contrast agent. By shielding microbubbles inside a red blood cell, acoustic contrast is maintained while potentially increasing the biocompatibility and circulation time of the microbubble. As a result, MB-ghosts have the potential to allow longitudinal imaging using the same contrast agents and to extend ultrasound contrast agents beyond simple vasculature opacification.

Ultrasound-assisted doxorubicin delivery using doxorubicin-liposomes loaded microbubbles

Jean-Michel Escoffre[1,2], Anthony Novell[1,2], Bart Geers[3], Ine Lentacker[3], Ayache Bouakaz[1,2]

[1]Université François Rabelais de Tours, UMR-S930 and ERL3106, Tours, France
[2]Inserm, U 930, Tours, France
[3]Laboratory of General Biochemistry and Physical Pharmacy, Department of Pharmaceutics, Ghent University, Ghent, Belgium

Rationale and aim

Doxorubicin (Dox) is a potent chemotherapeutic whose severe side effects limit its application. Microbubble-assisted ultrasound has become a promising strategy for non-invasive local drug delivery to increase the drug concentration locally and to reduce systemic side effects. Bart et al. designed doxorubicin-loaded microbubbles through a covalent binding of doxorubicin-containing liposomes to the lipid shell of microbubbles (Dox-LPS MB)[1]. The aim of this study is to evaluate the effectiveness of administration of these smart microbubbles combined with ultrasound in human U-87MG glioblastoma cells.

Material & Methods

Dox-loaded liposomes containing DSPE-PEG-maleimide and C_4F_{10} gas were added to vials containing: DPPC and DSPE-PEG-SPDP dissolved in a glycerin:propyleneglycol:H_20 mixture and were mechanically activated using a Capmix™ device. This activation generates C_4F_{10} lipid-shelled MBs loaded with liposomes. The liposomes become coupled to the MBs' surface through covalent thiol-maleimide linkages. Experiments were carried out with free Dox or Dox-LPS MBs (final concentration of Dox, 3 µg/mL) on a cell suspension of U-87MG cell line. Ultrasound waves were transmitted at 1 MHz frequency with a pulse repetition period of 100 µs, 40 cycles per pulse and for 30 s at 600 kPa^2. 48h later, doxorubicin uptake and cell viability were respectively evaluated by flow cytometry and MTT assay. Doxorubicin release from Dox-LPS or Dox-LPS MB was performed by spectrofluorimetry at the experimental conditions previously described (Positive control: Treatment of Dox-LPS and Dox-LPS MB with 10% v/v Triton X-100 in OptiMEM-1% FCS; Negative control: Incubation of Dox-LPS and Dox-LPS MB in OptiMEM-1% FCS).

Results

Using Dox alone, the cell viability was 67±1% at 48h (Figure 1A). The combination of ultrasound at 600 kPa and Dox-LPS MB induced a 4-fold decrease of cell viability compared to the incubation of Dox-LPS MB alone at 48h after treatment (Figure 1A).

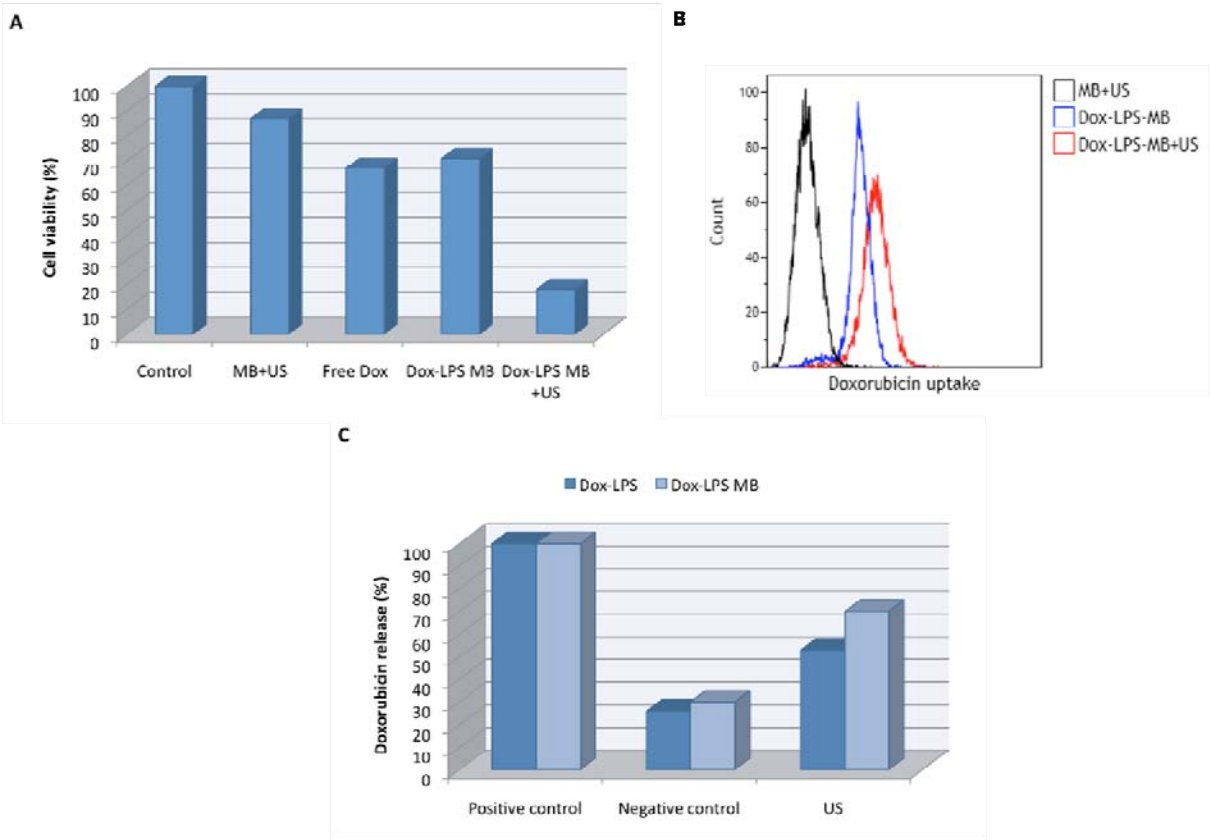

Figure 1: A. Enhancement of Doxorubicin-induced cell death by ultrasound combined with Dox-LPS MB. B. Improvement of doxorubicin uptake into U-87 MG cells after Dox-LPS MB-assisted ultrasound. C. Enhancement of doxorubicin release from Dox-LPS and Dox-LPS after insonation.

The therapeutic efficiency of this approach was correlated to the doxorubicin uptake into the human U-87MG glioblastoma cells (Figure 1B). To understand the mechanism involved in the doxorubicin delivery, the doxorubicin release from Dox-LPS and Dox-LPS MB after ultrasound treatment was investigated (Figure 1C). The application of ultrasound at 600 kPa induced a 2- and 2.5-fold increased doxorubicin release from Dox-LPS or Dox-LPS MB, respectively, compared to the negative control.

Conclusions

The conclusions drawn from this *in-vitro* study show the potential of this strategy for a controlled, efficient, and safe drug delivery. Indeed, the encapsulation of doxorubicin into liposomes and the ultrasound-triggered delivery would allow a reduction of the therapeutic dose and the side effects of doxorubicin. The interaction of ultrasound with microbubbles would induce the membrane permeabilization, the doxorubicin release from Dox-LPS MB and uptake into the human U-87MG glioblastoma cells.

Acknowledgement
Project funded in part by the EU FP7 Project SONODRUGS (NMP4-LA-2008-213706).

Reference

1. Geers B, Lentacker I, Sanders NN, Demeester J, Meairs S, De Smedt SC (2011) Self-assembled liposome-loaded microbubbles: The missing link for safe and efficient ultrasound triggered drug-delivery. J. Control. Release, 152:249-256
2. Escoffre JM, Piron J, Novell A, Bouakaz A (2011) Doxorubicin delivery into tumor cells with ultrasound and microbubbles. Mol. Pharm., 8:799-806

Targeted liposome-loaded microbubbles to detect and selectively destroy metastasis cells

***Bart Geers*[1], *Mareike Mühlmeister*[3], *Olivier de Wever*[2], *Klaus Tiemann*[3], *Marc Bracke*[2], *Stefaan de Smedt*[1], *Ine Lentacker*[1]**

[1]*Ghent Research Group on Nanomedicines, Lab of General Biochemistry and Physical Pharmacy, Faculty of Pharmaceutical Sciences, Ghent University, Harelbekestraat 72, 9000 Gent, Belgium*
[2]*Laboratory of Experimental Cancer Research, Faculty of Medicine, Ghent University, De Pintelaan 185, 9000 Gent, Belgium*
[3]*Department of Cardiology and Angiology, University Hospital Münster, Albert-Schweitzer-Campus 1, 48149 Münster, Germany*

Introduction

One of the main problems in cancer treatment is disease-relapse through metastasic colonization, which is the cause of most cancer deaths. Liposome-loaded microbubbles have a known potential for ultrasound-triggerable drug-delivery to cancer cells [1] in vitro. Hence, we wanted to design a liposome-loaded microbubble that was able to sensitively and specifically detect circulating tumor cells, that express an antigen specific for a circulating metastasis cell (N-Cadherin)[2]. Microbubbles were loaded with liposome-antibody conjugates that are able to interact with the surface of the microbubbles via thiol-maleimide bonds (Figure 1A). These microbubbles can selectively bind N-Cadherin expressing tumor cells and subsequent insonation would allow us to selectively deliver therapeutic molecules into these cells (Figure 1B).

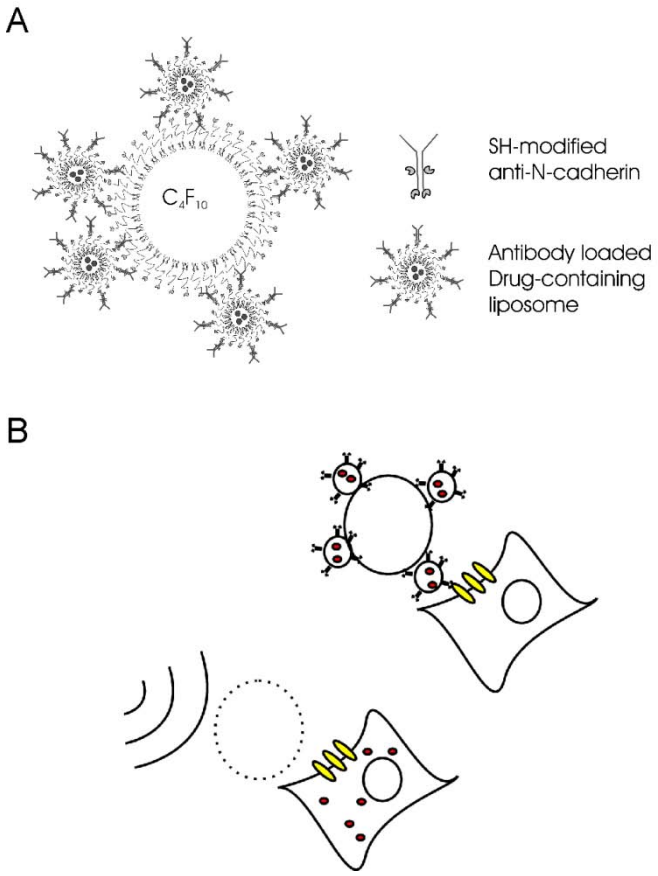

Figure 1: (A) schematic depiction of the microbubble design used in this study. Anti-N-cadherin antibodies are Thiol(SH)-modified and loaded on Maleimide-containing liposomes. Via the method described by Geers et al. these "targeted-liposomes" can be loaded on the microbubbles' surface via a one step process. (B) The aim of the study is to selectively bind the liposome-loaded microbubbles to cells expressing N-cadherin. Insonation would hence allow us to selectively destroy N-cadherin positive metastasis cells.

Materials and Methods

C_4F_{10} microbubbles with a lipid coating containing 5 mol% of DSPE-PEG-SPDP and 95mol% of DPPC were prepared. N-Cadherin-targeted liposomes were prepared using SH-modified anti-N-Cadherin antibodies. These antibody modified liposomes were covalently linked to the lipid microbubbles via a maleimide linker. We've visualized antibody and liposome loading with a Nikon EZC1 confocal microscope. Quantification of microbubble properties, sensitivity and specificity was measured with Flow Cytometry (BD Facscalibur, Beckton Dickinson, Erembodegem, Belgium).

Results

We've showed loading of a microbubble with an antibody and a liposome at the same time with confocal microscopy. We've quantified the relation between antibody-loading and the number of antibodies loaded on the surface of the bubbles. The sensitivity of the binding of the DiD-labeled targeted liposome-loaded microbubbles to N-Cadhrin expressing HMB-2 cells, that were aspecifically labeled with the Cell Tracker® dye, was analyzed with flow cytometry. We could clearly observe an

increased number of events positive for both red and green fluorescence. This clearly indicates that a sensitive binging of targeted liposome-loaded microbubbles to N-cadherin expressing HMB2 cells was feasible. Specificity of this binding in a more complex mixture of N-cadherin expressing HMB-2 cells and non-N-Cadherin expressing H1299 lung epithelium cells was also quantified with flow cytometry.

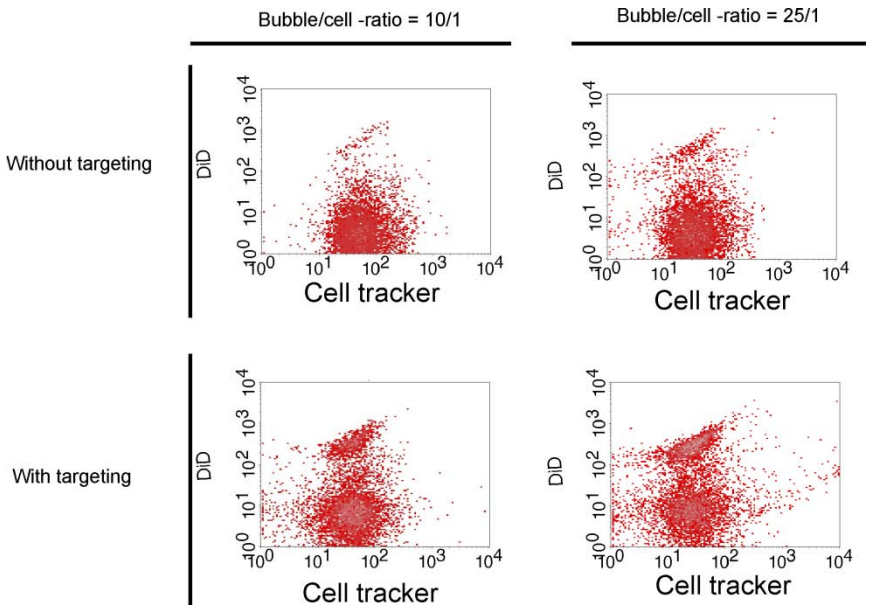

Figure 2: Flow cytometry measurements with red fluorescent DiD-labeled liposome-loaded microbubbles and HMB2 cells labeled with the aspecific green-fluorescent Cell Tracker® dye. The graphs clearly show an increased number of events positive for both red and green fluorescence upon targeting, indicating a sensitive detection of the HMB2 cells by the targeted liposome-loaded microbubbles.

Acknowledgements
This work was funded by the FWO-flanders research project (G.0187.11) and is also part of the EU FP7 collaborative project Sonodrugs (NMP4-LA-2008-213706). Ine Lentacker is a post-doctoral fellow of the Fund for Scientific Research Flanders (FWO-Vlaanderen).

References

1. Geers, B.; Lentacker, I.; Sanders, N. N.; Demeester, J.; Meairs, S.; De Smedt, S. C. Self-assembled liposome-loaded microbubbles: The missing link for safe and efficient ultrasound triggered drug-delivery. *J. Control Release* **2011**, 152, 249-56
2. De Wever. O.; Derycke, L.; Hendrix, A.; De, M. G.; Godeau, F.; Depypere, H.; Bracke, M. Soluble cadherins as cancer biomarkers. *Clin. Exp. Metastasis* **2007,** *24* (8), 685-697

Single-chain vegf-carrying microbubbles as a molecular imaging agent for tumor vasculature targeting: effect of ligand surface density and receptor expression in vitro and in vivo on the bubble targeting efficacy

Z. Du[1], J. Rychak[2], D. Smith[2], J. Backer[3], M. Backer[3], A. Klibanov[1]

[1]Cardiovascular Division, University of Virginia, Charlottesville VA 22908; USA
[2]Targeson Inc., San Diego CA, [3]Sibtech Inc, Brookfield CT, USA

Introduction

Use of targeted microbubbles as molecular imaging ultrasound contrast agent has been suggested more than a decade ago, tested first in vitro [1] and eventually in vivo [2]. There is a variety of microbubble formulations currently, suitable for vascular endothelium biomarker detection, mostly for inflammation marker imaging [2,3] and imaging of angiogenesis markers, such as $\alpha_V\beta_3$ [4] or VEGF Receptor 2, targeted with synthetic peptide derivatives [5], or with a single-chain VEGF [6]. The latter molecule is among the favorable markers for the detection of tumor vasculature; however, optimization of ligand surface on the microbubble surface has not yet been described in detail until now. It would be desirable to minimize the amount of expensive ligand on the surface of microbubbles, yet at the same time obtain effective contrast accumulation in the tumor vasculature. Here, we present a systematic effort of such optimization of microbubble targeting in vitro and in vivo.

Methods

Microbubbles were prepared from decafluorobutane gas and stabilized with a monolayer shell of phosphatidylcholine, PEG stearate and maleimide-PEG-phosphatidylethanolamine. Single-chain VEGF (scVEGF) was designed as a fusion protein with an external adapter sequence. A thiol residue was generated by a selective reduction process from a terminal cysteine residue on the adapter sequence. The disulfide bonds necessary for the proper conformation of VEGF were left intact. Thiol-VEGF at a wide range of concentrations was incubated with maleimide bubbles, and resulting reaction mixture was subjected to flotation to separate unreacted ligand from the microbubbles. Microbubble product was stored in stoppered vials under decafluorobutane atmosphere. Amount of scVEGF on the microbubble surface was assessed with VEGF-specific immunoassay. Control bubbles did not have scVEGF attached. Microbubble targeting in vitro was evaluated in a parallel plate flow chamber assay, using 35mm Petri dishes coated with VEGFR2-IgG fusion protein as a target.

In vivo microbubble targeting was assessed by ultrasound imaging in two murine subcutaneous tumor models: MC38 murine colon adenocarcinoma or PC3 human prostate cancer cells were grown subcutaneously in the hind legs of mice. Microbubbles were injected intravenously to mice under isoflurane anesthesia; bubble influx in the tumor mass was monitored by Sequoia 512 ultrasound imaging system with 15L8 probe, operated in CPS mode at low MI. Accumulation of microbubbles in the target tissue, along with microbubble clearance from the bloodstream was monitored up to 10 min; targeted microbubbles were then destroyed to evaluate the residual level of circulating bubbles and to confirm the negligible signal from the tissue background. Image analysis was performed for the selected (tumor) region of interest with ACQ software on the scanner. VEGFR2 expression in the target tumor tissue was checked histologically, after animals were euthanized. Excised tumor tissue samples were fixed in formalin, embedded in the paraffin blocks, thin sections cut and stained with anti-VEGFR2 antibody-peroxidase complex and DAB substrate.

Results

Thiol-scVEGF was attached to the shell of maleimide-carrying microbubbles with the surface density dependent on the amount of added protein. Initial protein concentration in the samples was varied within a 500-fold range; resulting scVEGF surface density varied from ~2000 to ~14 molecules/um^2 of microbubble surface. At highest initial protein load, coupling saturation was observed, i.e., coupling was less efficient and more ligand was lost unproductively. In the in vitro flow chamber binding study, adherence of targeted microbubbles to the layer of VEGFR2 on the polystyrene dish was observed by video microscopy. Targeting was significantly higher than control only for the samples that carried ~200 or more scVEGF molecules per um^2 of the bubble surface. For the samples with lower load of the targeting ligand, microbubble adhesion to the dish was not statistically significant when compared with ligand-free control bubbles.

In vivo testing of microbubble targeting was performed first in MC38 colon adenocarcinoma murine hindleg subcutaneous tumor model. Microbubble influx into the tumor could be observed in real time following intravenous bolus. In some instances, especially for larger tumors, central non-perfused necrotic core was present, surrounded by active vasculature. Targeted microbubbles (Targeson formulations VS-01-032) were marking the tumor as observed by ultrasound contrast imaging. Control bubbles lacking the surface scVEGF were not adherent. Statistical significance of targeted microbubble specific adhesion over control bubbles was established for all the bubble ligand surface density preparations. Adhesion of bubbles in the contralateral leg (non-tumor) muscle region was minimal. By histology, VEGFR2 expression in MC38 tumor tissue was significant.

scVEGF-microbubble targeting was also tested by ultrasound imaging in another murine subcutaneous tumor model, based on a slow-growing PC3 human prostate cancer cell line. Moderate microbubble targeting in the tumor ROI was observed for the samples with higher ligand load, although targeting was statistically significant when compared with control bubbles. By histology, VEGFR2 expression in PC3 tumor tissue was significantly less than in MC38 tumor.

Conclusions

Attachment of targeting ligands, such as scVEGF, to microbubble surface via thiol-maleimide coupling can be optimized to attain reasonable coupling yield while maintaining significant ligand bubble surface density, useful in the in vitro and in vivo targeting. Targeted microbubbles adhere to VEGFR2 in vitro (in a parallel plate flow chamber system) and in vivo (in MC38 and PC3 tumors), marking tumor vasculature for ultrasound molecular imaging applications.

References

1. Klibanov AL, Hughes MS, Marsh JN, Hall CS, Miller JG, Wible JH, Brandenburger GH. Targeting of ultrasound contrast material. An in vitro feasibility study. Acta Radiol Suppl. 1997;S412:113-120
2. Lindner JR, Song J, Christiansen J, Klibanov AL, Xu F, Ley K. Ultrasound assessment of inflammation and renal tissue injury with microbubbles targeted to P-selectin. Circulation. 2001;104(17):2107-2112
3. Weller GE, Lu E, Csikari MM, Klibanov AL, Fischer D, Wagner WR, Villanueva FS. Ultrasound imaging of acute cardiac transplant rejection with microbubbles targeted to intercellular adhesion molecule-1. Circulation. 2003;108:218-224
4. Anderson CR, Hu X, Zhang H, Tlaxca J, Declèves AE, Houghtaling R, Sharma K, Lawrence M, Ferrara KW, Rychak JJ. Ultrasound molecular imaging of tumor angiogenesis with an integrin targeted microbubble contrast agent. Invest Radiol. 2011;46:215-224
5. Pochon S, Tardy I, Bussat P, Bettinger T, Brochot J, von Wronski M, Passantino L, Schneider M. BR55: a lipopeptide-based VEGFR2-targeted ultrasound contrast agent for molecular imaging of angiogenesis. Invest Radiol. 2010;45:89-95
6. Anderson CR, Rychak JJ, Backer M, Backer J, Ley K, Klibanov AL. scVEGF microbubble ultrasound contrast agents: a novel probe for ultrasound molecular imaging of tumor angiogenesis. Invest Radiol. 2010;45:579-585

Contrast ultrasound for myocardial no-reflow: a new therapy?

Jonathan Leeman, Jong S. Kim, Francois Yu, Xucai Chen, Kang Kim, Flordeliza Villanueva, John Pacella

Background

Ultrasound (US) mediated microbubble (MB) destruction facilitates thrombolysis of the infarct related epicardial coronary artery in acute myocardial infarction (AMI). After reperfused AMI, epicardialrecanalization often does not restore adequate microvascular perfusion ("no-reflow"), which is associated with microvasculararthromboemboli and worse clinical outcomes. We tested the hypothesis that US mediated MB destruction can also achieve microvascular clot lysis. Because the physiologic and fluid dynamic conditions in the microvasculature are distinct from that in epicardial arteries, we specifically sought to define the acoustic requirements for effective microvascularsonothrombolysis using a novel in vitro open loop model of thrombotic microvascular occlusion.

Methods

A phantom vessel (i.d. 4mm) containing an intraluminal mesh with 40 µm pores was used to simulate a microvascular bed. Upstream pressure (mmHg) measured with a fluid filled transducer was used as an index of thrombus burden. To model microembolization, microthrombi were injected and entrapped in the mesh, increasing resistance and hence upstream pressure. A saline suspension of lipid MBs (2 x 107 MB/ml) was infused at a flow rate of 1.5 ml/min. US was delivered from a focused single element transducer driven by a pulse generator and a power amplifier at 1 MHz, with varying pulse length (100 - 5000 cycles) and peak to peak pressure (0.23 - 1.5 MPa). The pulses were applied for 20 minutes at a repetition rate of 0.33 Hz (duty cycle <0.16%) to allow MB replenishment between pulses.

Results

Upstream pressure decreased progressively during US delivery, indicating decreased thrombus burden, but efficacy varied as a function of the US parameters. More rapid and complete lysis occurred with increasing acoustic pressure at a fixed pulse length of 5000 cycles (Figure 1A), and increasing pulse length at a fixed acoustic pressure of 1.5 MPa (Figure 1B).

Conclusion

Our in vitro model offers a platform for evaluating the US parameters that provide optimal microvascularthrombolysis. Our studies suggest that clot lysis is most effective with the use of US applied at higher acoustic pressure and longer pulse length. The mechanism for the incremental lytic efficacy of longer pulse lengths even at high acoustic pressure requires further study.

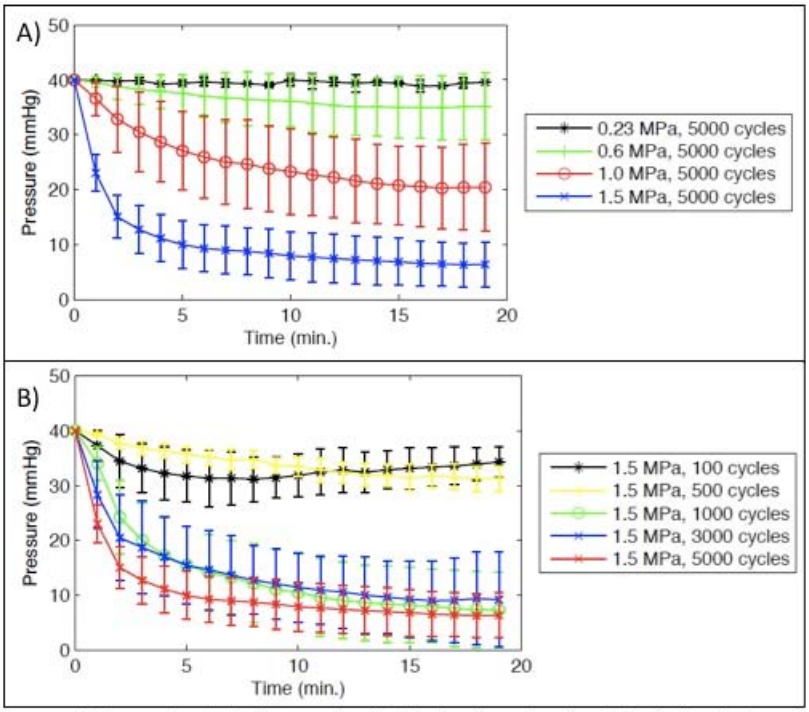

Figure 1. Efficacy of contrast ultrasound mediated microthrombus dissolution. Lytic effect improved significantly with increasing peak to peak pressure (A, p<.01, ANOVA) and increasing pulse length (B, p<.01, ANOVA). An 84% decrease in upstream pressure was achieved at 1.5 MPa and a pulse length of 5000 cycles. A statistically significant difference in pressure change was observed between 500 cycles and 1000 cycles at 1.5 MPa (B, p<.01, ANOVA). n ≥ 2 for all samples.

Contrast-enhanced carotid ultrasound for detecting subclinical atherosclerosis

S.C.H. van den Oord, G.L. ten Kate, Z. Akkus, G. Renaud, E.J.G. Sijbrands, F.J. ten Cate, A. van der Lugt, J.G. Bosch, N. de Jong, A.F.W. van der Steen, A.F.L. Schinkel

Purpose

Current risk-assessment for cardiovascular diseases might be improved by the incorporation of imaging techniques that could detect subclinical atherosclerosis. Because standard carotid ultrasound is not sufficiently sensitive to detect subclinical atherosclerosis, it was tested in combination with contrast-enhanced ultrasound (CEUS).

Materials and Methods

The study protocol was approved by the local ethics committee, and all participants provided informed consent before the ultrasound examination. Carotid intima-media thickness (CIMT) measurement, standard ultrasound, and CEUS were performed in 100 patients with ≥1 risk factor for atherosclerosis. Ultrasound clips obtained with standard ultrasound and CEUS were reviewed by 2 independent observers, who measured CIMT and scored them for the presence of atherosclerotic plaques. The presence of subclinical atherosclerosis was compared between groups using McNemar's test.

Results

Twenty-one patients (21%) had a CIMT value above their age-corrected threshold and were considered to have subclinical atherosclerosis. Standard carotid ultrasound helped identify atherosclerotic plaques in 77 patients (77%); the addition of CEUS clips revealed plaques in 11 more (11%). The detection of patients with subclinical atherosclerosis was thus significantly improved by the incorporation of CEUS into the standard carotid ultrasound protocol ($p<0.01$).

Conclusion

These findings suggest that CEUS improves the detection of subclinical atherosclerosis in the carotid arteries. CEUS may thus add considerable clinical value to the tools currently used to assess risk in cardiovascular diseases.

Dose-dependent artefact in the far wall of the carotid artery with dynamic contrast enhanced ultrasound

Ankur Thapar[1], Joseph Shalhoub[1], Christophoros Mannaris[2], Alun H Davies[1], Michalakis Averkiou[2], Edward LS Leen[3]

[1]Academic Section of Vascular Surgery, Imperial College London, UK
[2]Department of Mechanical and Manufacturing Engineering, University of Cyprus, Nicosia, Cyprus
[3]Department of Experimental Medicine, Imperial College London, UK

Purpose

Dynamic contrast enhanced ultrasound (DCE-US) is an emerging technology to assess neovascularization in atherosclerosis. The aim of this study was to quantify a pseudo-enhancement phenomenon observed during the DCE-US of the carotid artery both *in-vitro* and *in-vivo*.

Materials and Methods

Ethical approval was obtained prior to commencing this prospective case series and each patient gave written informed consent to participate. 31 patients with 50-99% internal carotid artery stenosis underwent DCE-US imaging of the carotid bifurcation using 2 ml of intravenous SonoVue™. In the final 10 patients, an additional 1 ml bolus was administered after 15 minutes. Raw linear DICOM data was analysed offline. Regions of interest were drawn within the common carotid artery lumen and immediately adjacent to the lumen in the near and far wall adventitia. Peak intensity was measured. In addition, an *in vitro* experiment using a single channel flow phantom was performed. This in vitro apparatus consisted of an 8 mm diameter latex tube placed in a tissue-mimicking fluid. SonoVue™ concentrations of 0.02, 0.1, 0.5, 1, and 2 ‰ were pumped into the tube. Regions of interest were drawn in a similar fashion to the in vivo experiments and peak intensity measured. The Wilcoxon signed rank test and paired t-tests were used to compare the difference between the near and far wall intensities at each dose; a multiplication factor comparing near- and far wall intensity was derived.

Results

The far wall of the common carotid artery was significantly more echogenic than the near wall at 2ml contrast doses ($p<0.0001$, $n=31$), and the far wall intensity rose synchronously with that of the lumen. The intensity difference between near and far wall regions was significantly greater at 2 ml than 1 ml ($p=0.012$, $n=10$). *In vitro*, the phantom tubing demonstrated a similar pattern and magnitude of enhancement to that seen *in vivo*.

Conclusion

A dose-dependent, non-linear propagation artefact, which we term "pseudo-enhancement," occurs in the far wall adventitia of the carotid artery, which should not be mistaken as a marker of plaque vulnerability.

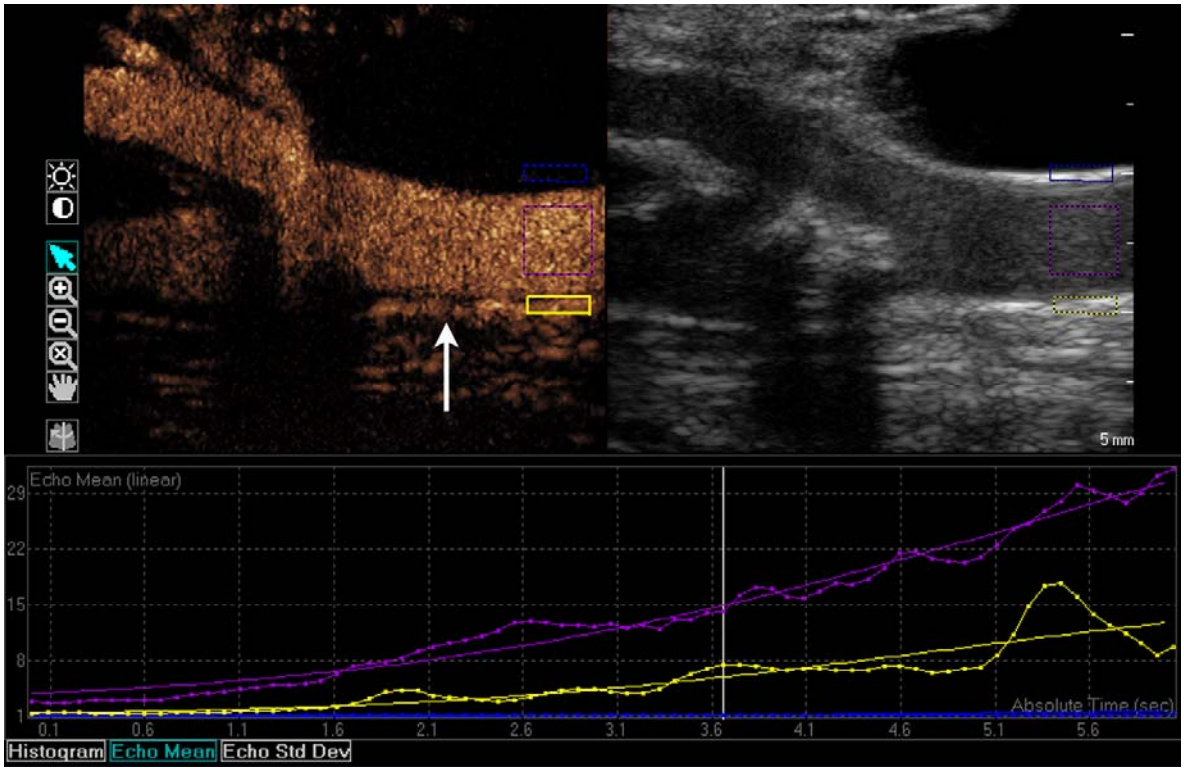

Figure 1 Longitudinal image of the left common carotid bifurcation in an asymptomatic 79 year old male with a 50% internal carotid artery stenosis. Quantification of intensity was performed using the dual-display mode with the contrast enhanced image to the left of the screen and the B-mode reference to the right. Adventitia is seen as an echogenic line on B-mode, aiding identification. Pseudo-enhancement mimicking neovascularization in the region of the far wall carotid adventitia is seen (white arrow). Plaque is seen as a filling defect in the internal carotid artery. Regions of interest have been drawn: blue (far wall adventitia); purple (common carotid lumen); and yellow (far wall adventitia). The time-intensity curves are shown below in linear units in the same colours as the regions of interest. The lumen and far wall adventitia intensity curves rise synchronously however the near fall does not follow this pattern.

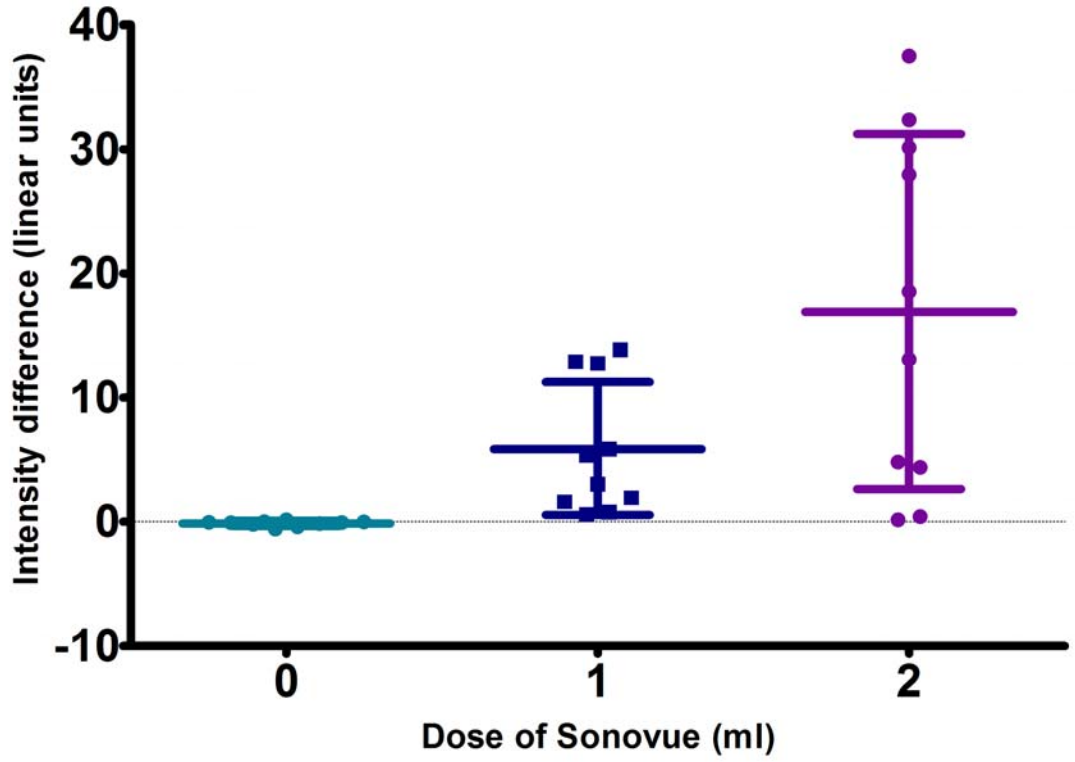

Figure 2 Graphical representation of the absolute mean difference between far and near wall peak intensity with increasing doses of contrast (error bars represent standard deviation).

Size dependant asymmetrical microbubble response

Jonathan Casey**, Charles Sennoga*, Meng-Xing Tang[+], Robert J. Eckersley

**Imaging Sciences Dept, Imperial College London, UK*
[+]Department of Bioengineering, Imperial College London, UK

Background and Motivation

Acoustically driven microbubbles are well documented as undergoing complex asymmetrical oscillations. In this work the effect of size and the resonant behaviour of the microbubbles on their asymmetrical response to acoustic stimulation were investigated.

Materials and Methods

Single bubble acoustics were performed on in house lipid shelled microbubbles, with radii in the range between 1.5 and 4 µm. The testing apparatus consisted of a pair of focussed transducers and a microscope objective lens co-focally aligned on a 200 µm capillary fibre. The microbubbles were insonated with a 10 cycle, 2 MHz pulse at 90 kPa peak negative pressure. Resultant pressure traces were analysed and the degree of asymmetry extracted. Using the method set out in [1] the measured pressure response was used to estimate the radial motion of the microbubble wall.

Results and Discussion

The figure below shows an index of asymmetry, calculated as the normalised ratio of the difference between positive and negative excursions, for both the pressure and estimated radial responses of the individual microbubbles. Under the experimental conditions used, the resonant size for a 2 MHz driving pulse was determined to be approximately 1.9 µm. The shape of both the pressure and radial response can be seen to be directly related to each other, size dependant in nature and strongly affected by resonance. The positive asymmetry in the pressure data demonstrates a positive pressure dominated response where as the negative radial response asymmetry demonstrates a compression dominated response. The size and resonance dependant nature of this response asymmetry could provide a method of indirectly detecting bubble resonance and could have potential when developing size and hence frequency specific imaging techniques.

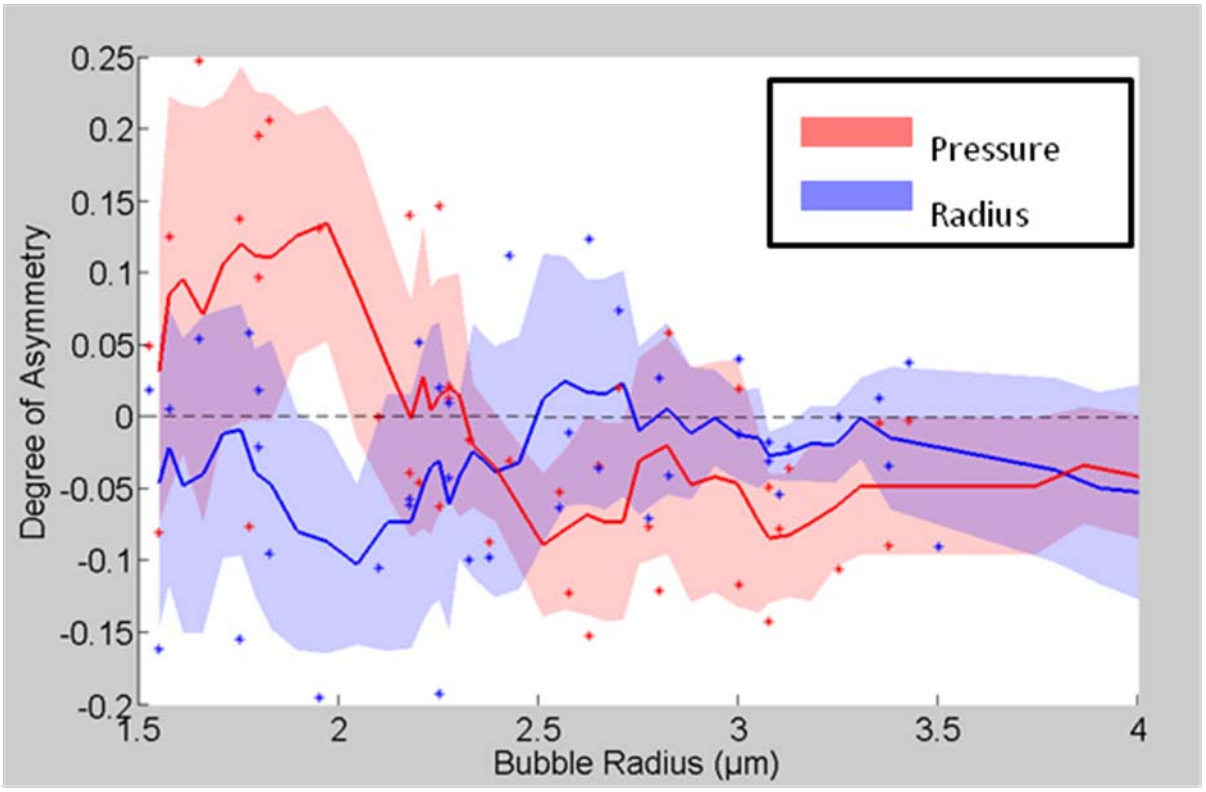

Response asymmetry as a function of microbubble radius. Discrete points are the raw data, solid line and shaded region represents the mean and standard deviation of a 5 point moving average window.

Reference

J. Sijl *et al*, "Simultaneous optical and acoustical recording of the dynamics of a single ultrasound contrast microbubble," *J Acoust Soc of Am*, 2009

Study of a generalised pulse-pair model for contrast imaging and nonlinear Doppler

Véronique Mahue[1], Jean Martial Mari[1,2], Robert J. Eckersley[3], Meng-Xing Tang[1]

[1]Department of Bioengineering, Imperial College London, Prince Consort Road, SW7 2AZ, London, UK
[2]Inserm, U1032, Lyon, F-69003, France; Université de Lyon, Lyon, F-69003, France
[3]Institute of Clinical Sciences, Imperial College London, Hammersmith Hospital, Du Cane Road, London W12 0NN, UK

A generalised nonlinear imaging and Doppler approach is tested in a simulation study, which is based on the construction of pulse pairs from linear combinations of an elementary pulse (Pulse Inversion, Amplitude Modulation and Pulse Subtraction being particular case of the general equation), under the assumption that an optimum pulse can be designed. The contrast from a single microbubble is obtained from simulations based on the modified Rayleigh-Plesset equation for a wide range of pulse combinations and the pulse sequences tested. These are compared with regards to criteria connected with technical and medical ultrasound imaging requirements.

Conclusion is that for a well characterised ultrasound system, and a particular clinical application, an appropriate choice of the contrast specific pulse sequence may be achieved in order to improve the sensitivity to a specific parameter of the imaging process. Furthermore, there is no ideal nonlinear sequence to be used by all scanners, but rather a dedicated pulse pair should be designed for each specific system. For example, results show that for deep tissue Doppler contrast imaging (e.g. imaging of the aorta or umbilical cords), using a Pulse-Inversion Amplitude-Modulation Pulse-Subtraction combination pulse-pair is likely to maximize the microbubble response at the fundamental frequency. This enables to decrease the influence of frequency dependent attenuation, in comparison to the transmission of a Pulse Inversion based pulse pair which is *3.8* times lower at the fundamental and responds essentially at the second harmonic. On another hand, when optimising the non linear response solely while minimizing the transmitted peak negative pressure, results underline the superiority of Pulse Inversion over other techniques by at least a factor of *1.13*. However an increased complexity of the pulse sequence tends to decrease the signal to noise ratio and an appropriate trade-off must be found between the sophistication of the pulse pair and its final efficiency. The proposed approach provides an objective quantifiable way to significantly improve the quality of medical perfusion imaging and provides pulse sequences which are Doppler compatible, which widens the imaging possibilities.

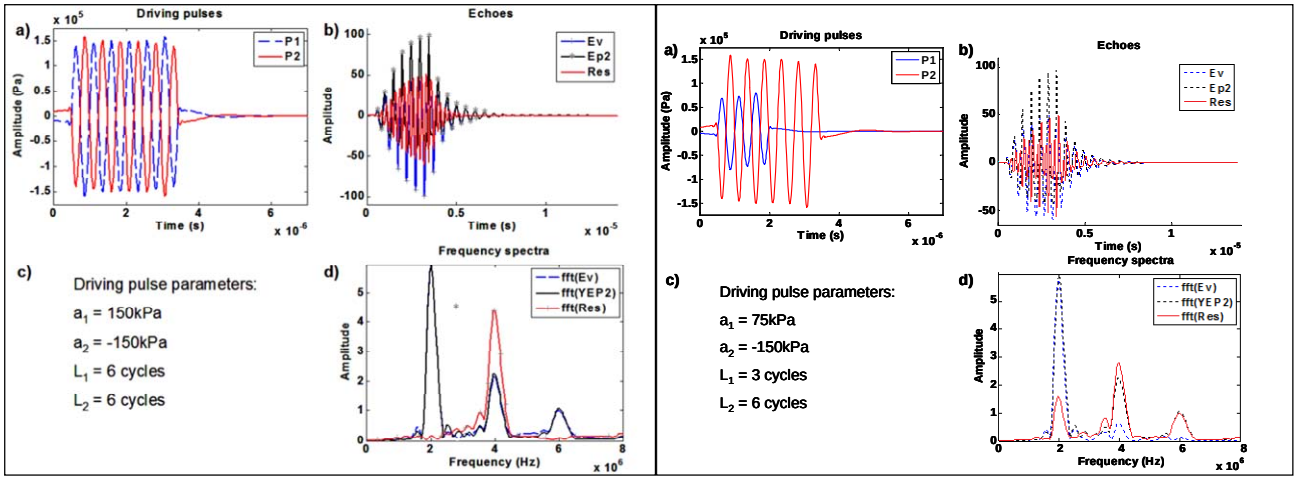

Figure 5: <u>Left</u>: PI pulse pair sequence example, a) driving pulses, b) echoes and residue, c) pulse parameters, d) Doppler spectra of the echoes and the residue; <u>Right</u>: PIAMPS pulse pair sequence example, a) driving pulses, b) echoes and residue, c) pulse parameters, d) Doppler spectra of the echoes and the residue. A proper parameterization of the model optimizes the response in the desired frequency band.

Ultrasound-induced temperature elevation for in-vitro controlled release of thermosensitive liposomes

Christophoros Mannaris[1], Jean-Michele Escoffre[2], Ayache Bouakaz[2], M. E Meyre[3], M. Germain[3], Michalakis Averkiou[1]

[1]Dept. of Mechanical and Manufacturing Engineering, University of Cyprus, Nicosia, Cyprus
[2]UMRS INSERM U930, CNRS ERL3106, Université François Rabelais-Tours, France
[3]Nanobiotix, Paris, France

Introduction

Drug loaded thermosensitive liposomes (TSL) release their payload with mild hyperthermia near their phase transition temperature (T_m = 43-45 °C) [1]. Focused ultrasound may be used to non-invasively induce local mild hyperthermia in a region of interest with high accuracy [2]. In combination, ultrasound induced temperature elevation for localized drug delivery using TSL shows potential in improving the efficacy of drug delivery in a lesion while at the same time reducing undesired side effects.

In spite of several reports for in-vivo drug delivery using ultrasound and TSL [3-5], reports for in-vitro work are scarce mainly due to the difficulty in finding an appropriate in-vitro experimental setup. One of the main problems often encountered is that cell culture media have a very low absorption coefficient and are thus unable to be heated with ultrasound. Finding a biocompatible medium with high absorption coefficient has not been possible thus far.

In the present work, an in-vitro method that allows activation of TSL using ultrasound is presented. A single element focused transducer is used to induce the required temperature elevation in Opti-MEM® cell culture medium via thermal conduction and activate drug loaded TSL. A significant release of doxorubicin from TSL is achieved.

Materials and methods

Experimental setup

Figure 1 shows a schematic of the experimental setup. A small volume sample holder containing Opti-MEM® cell culture medium and TSL solution was placed inside a plastic cuvette filled with 99% glycerol that has a high absorption coefficient (α=5.7 Np/m/MHz). Mylar acoustic windows on the cuvette and holder allowed ultrasound to propagate through thus avoiding heating of the plastic walls. A single element focused transducer (center frequency 1.1 MHz, 50 mm diameter and 50 mm focus) was used to heat up the glycerol in the cuvette. The Opti-MEM®/TSL solution in the sample holder reached

the required temperature for activation of the TSL via thermal conduction. The experiments were carried out in a 37°C water bath.

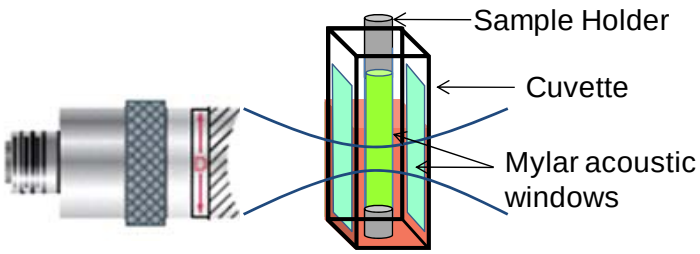

Figure 1: Schematic of experimental setup

Ultrasound Exposure

Detailed characterization of the ultrasound field was done in water using a 0.4 mm element membrane hydrophone (Precision Acoustics Ltd, Dorchester, UK). The acoustic field experienced by the TSL in the sample holder was also measured with the cuvette in place using a 0.5 mm needle hydrophone placed in the middle of the cuvette (the rear Mylar window was removed). Any diffraction effects due to the presence of the cuvette were negligible. The sample holder was placed at the focus of the transducer. Ultrasound was applied for 15 minutes at 1.1 MHz frequency, 45% duty cycle and 1.4 MPa peak negative pressure.

Activation protocol

Thermosensitive liposomes [DPPC:HSPC:Chol:DPPE-PEG (50:25:15:3)] from Nanobiotix were diluted in OptiMEM® to a concentration of 3 μg/mL. The experiments were separated in the following categories:

1. OptiMEM + US: To check if US exposure alters the parameters of the medium.
2. Negative control: Samples kept at room temperature (0% release).
3. Positive control: Samples in 45°C water bath for 15 minutes (100% release).
4. TSL + US (no heating): Same exposure conditions applied but without heating to check if US alone induces any release from TSL. This was done by replacing the glycerol in the cuvette with water. Since water has very low absorption, it does not heat up with US.
5. TSL + US + Heating: TSL activation experiment at p=1.4 MPa.
6. TSL + US + Heating*: TSL activation experiment at p=1.8 MPa.

Analysis of results

Analysis of the results was done using a 96-wells plate spectrofluorometer. The excitation wavelength, λ_{ex} was 485 nm and the emission wavelength, λ_{em} was 580 nm. Each category was repeated at least three times and the results are presented as mean ± standard deviation. The % release of doxorubicin was evaluated using equation 1 below [1]:

$$\% \, Release = \frac{I_{exp} - I_{neg}}{I_{pos} - I_{neg}} \qquad (1)$$

where, $I_{exp,}$ I_{neg} and I_{pos} are the fluorescence intensities of the experiment, negative control and positive control respectively.

Results

A theoretical model based on the Pennes' Bioheat equation was initially used to calculate the ultrasound parameters required for temperature elevation in glycerol under conditions for drug activation (5-8°C). Fine-wire (50μm) thermocouple readings were in close agreement with our theoretical predictions as shown in figure 2. A temperature elevation of 6-7°C was obtained in the sample holder within 6 minutes before reaching a plateau.

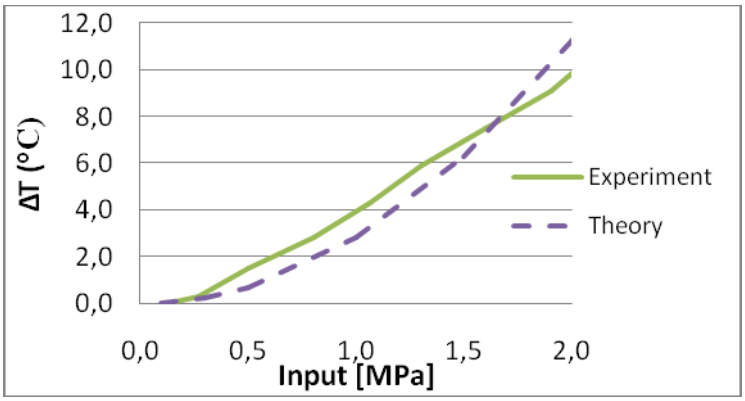

Figure 2: Comparison of experimental with predicted values for temperature elevation in glycerol as a function of input pressure (f=1.1 MHz, 45% DC)

The results for TSL activation and release are shown in Figures 3 and 4. Figure 3 shows the fluorescence measurements from each category whereas figure 4 shows the calculated % release [using equation (1)]. It is noted that ultrasound induced almost as much release as the positive control while further increasing the pressure (and temperature) does not show any added benefit. It is also noted that ultrasound does not affect the medium properties (OptiMEM = OptiMEM + US) and that US alone does not influence the TSL or cause any release (NEG Control = TSL + US).

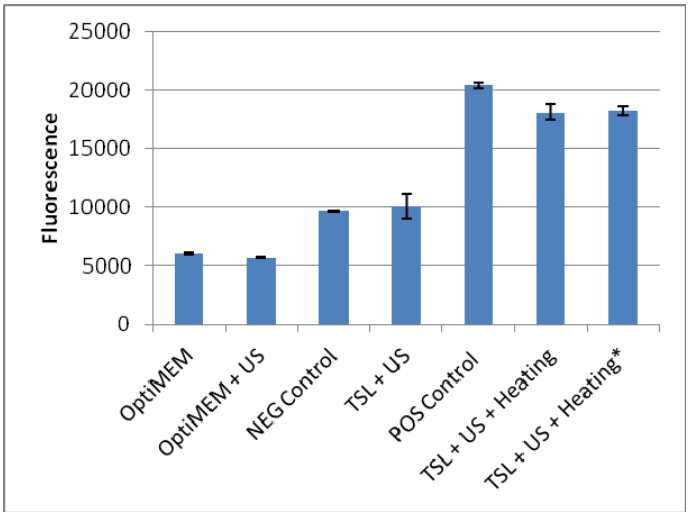

Figure 3: Fluorescence measurements of the different categories.

Discussion

An ultrasound method for in-vitro drug release from thermosensitive liposomes has been developed. Water-based cell culture media present difficulties in ultrasound heating but our method overcomes this issue. Temperature elevation of 5-8 degrees (needed for the activation of the TSL) is reached with focused ultrasound at 1.1 MHz and an 80% drug release was achieved with our method. Heating by thermal conduction approach mimics in-vivo conditions where ultrasound is used to induce hyperthermia in tissue and the TSL (in blood) would be heated by conduction.

Further improvements of the method will allow for faster and more uniform heating. A broader acoustic field (very low focussing gain or even unfocused sources) will result in larger treatment areas. The current setup may be used with cells in suspension; one possible modification is to allow testing of seeded cell cultrures (perhaps in OptiCell).

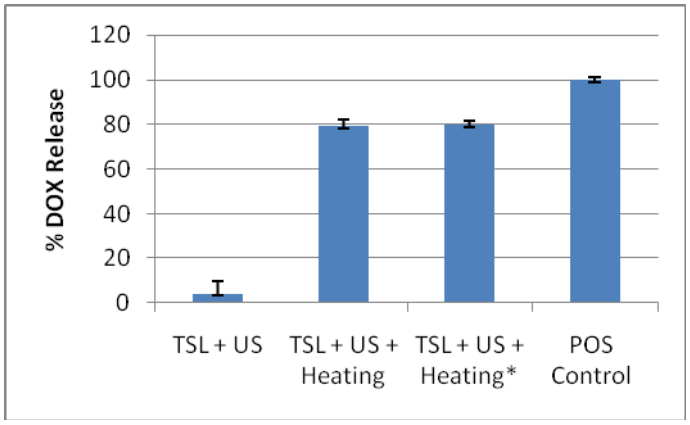

Figure 4: Induced doxorubicin % release from thermosensitive liposomes.

Acknowledgements
This project was funded by the EU Project SONODRUGS (NMP4-LA-2008-213706).

References

1. M. de Smet, *et al.*, "Temperature-sensitive liposomes for doxorubicin delivery under MRI guidance," *Journal of Controlled Release*, vol. 143, pp. 120-127, 2010
2. M. O. Köhler, *et al.*, "Volumetric HIFU ablation under 3D guidance of rapid MRI thermometry," *Medical Physics*, vol. 36, pp. 3521-3535, 2009
3. S. Dromi, *et al.*, "Pulsed-high intensity focused ultrasound and low temperature - Sensitive liposomes for enhanced targeted drug delivery and antitumor effect," *Clinical Cancer Research*, vol. 13, pp. 2722-2727, 2007
4. R. Staruch, *et al.*, "Localised drug release using MRI-controlled focused ultrasound hyperthermia," *International Journal of Hyperthermia*, vol. 27, pp. 156-171, 2011
5. A. Yudina, *et al.*, "Ultrasound-mediated intracellular drug delivery using microbubbles and temperature-sensitive liposomes," *Journal of Controlled Release*, vol. 155, pp. 442-448, 2011

Photoacoustics and contrast enhanced ultrasound for imaging of experimental murine tumours

Andrew Needles[1], John Sun[1], Melissa Yin[2], Andrew Heinmiller[1], Theresa McGrath[1], Dave Bates[1], Catherine Theodoropoulos[1], F. Stuart Foster[2]

[1]VisualSonics, Toronto, Canada
[2]Sunnybrook Health Sciences Centre, Toronto, Canada

Introduction

Contrast enhanced ultrasound (CEUS) relies of the detection of gas filled microbubbles *in vivo*. Photoacoustics (PA) is a new imaging modality capable of creating images from signals that are based on the optical absorption of imaging targets, yet detected with ultrasound. A recently developed high-frequency imaging system (VevoLAZR, VisualSonics) is capable of combining these two imaging modalities onto a common platform. In this study we compared the results obtained assessing tumour perfusion with CEUS against those obtained with PA using both endogenous and exogenous contrast.

Methods

A photoacoustic transducer with integrated fiber optics (LZ250, fc = 21 MHz, VisualSonics) was used for imaging two sets of tumor-bearing mice. In the first set of experiments, human metastatic breast cancer cells (231/LM2-4) were surgically implanted in the mammary fat pads of 4 control and 7 treated female nude SCID mice. The cells were allowed to grow for 10 days prior to initiation of experimental treatment, which consisted of either 4 consecutive daily gavage doses of 120mg/kg sunitinib, or control vehicle. Imaging was done prior to and after treatment. Tumor volume was quantified with 3D ultrasound imaging, using a linear stepper motor. Indices of relative blood volume and perfusion were quantified with CEUS during a 50uL ($2x10^9$/mL) intravenous bolus injection of microbubbles (MicroMarker, VisualSonics). Blood oxygen saturation, relative tissue oxygen saturation, and hemoglobin density were measured with photoacoustic imaging.

In the second set of experiments, a 50uL ($2x10^9$/mL) intravenous bolus injection of MicroMarker microbubbles was injected into mice bearing hind limb subcutaneous Lewis Lung carcinoma (LLC) tumors (n=3) to assess tumour perfusion. Subsequently, 150 μL of 1.5 mgAu/mL gold nanorods (Ntracker, Nanopartz) were injected intravenously. The extent of nanoparticle accumulation in the tumor was observed up to 3 hours later by quantifying photoacoustic signal intensity.

Results

Following treatment of the mammary tumours, we observed significant ($p<0.05$) suppression in tumor growth (-35%), decrease in blood volume (-91%), perfusion (-86%), relative tissue oxygen saturation (-60%), and hemoglobin density (-40%) in the sunitinib- relative to control-treated mice. When comparing pre- and post-treatment within the control group, there were increases in tumor volume (+120%), however, interestingly, there were also decreases in perfusion (-52%), blood volume (-22%) and relative tissue oxygen saturation (-31%). When comparing CEUS and PA data, there was a strong correlation between relative tissue oxygen saturation and perfusion ($R^2 = 0.722$), moderate correlation between relative tissue oxygenation and blood volume ($R^2 = 0.576$), and weaker correlation between blood volume and hemoglobin density ($R^2 = 0.294$).

In the case of the LLC tumours, an interesting observation was noted. Tumours that showed very little blood perfusion with CEUS, accumulated a more significant amount (3-4 times) of gold nanorods than those tumours that were more highly perfused. This suggests an inverse correlation between tumor perfusion measured with CEUS and uptake of gold nanorods detected with PA. It is hypothesized that this may be due to the leaky tumour vasculature or presence of non-functional vessels. More work is required to investigate this further.

Conclusions

This study demonstrates the ability of integrated PA and CEUS imaging to provide quantitative functional assessment of tumour models and their response to therapy. The potential for adding PA derived measures of oxygen saturation and hemoglobin density, along with nanoparticle detection to an ultrasound based platform represents a new development in preclinical imaging. The types of information provided by the two modalities appear to be complementary, however, the degree to which the correlations observed here translate to real prognostic value remain to be investigated. Nonetheless, these results suggest that the combination of PA imaging with CEUS for *in vivo* imaging of tumour development and response to therapy has a role to play in the future of preclinical cancer research.

Investigating retention of magnetic microbubbles in a flow phantom

Joshua Owen[1], Bin Zhou[2], Nicolas Hayotte[1], Meng-Xing Tang[2], Quentin Pankhurst[3], Robert Eckersley[4] , Eleanor Stride[1]

[1]Institute of Biomedical Engineering, University of Oxford, Oxford, UK
[2]Department of Bioengineering, Imperial College London, UK
[3]Davy-Faraday Research Laboratory, The Royal Institution of Great Britain, London, UK
[4]Imaging Sciences Department, Imperial College London, UK

Magnetic localisation ofmicrobubbles containing superparamagnetic nanoparticles has been proposed as an alternative or potentially complementary strategy to existing biochemical methods for targeted drug and gene delivery *in vivo.* Different types of magnetic microbubble have previously been synthesised and their efficacy as transfection agents tested *in vitro* and in *vivo*[1-3]. A key question for the development of this technique is the strength and gradient of the magnetic field required to retain magnetic microbubbles at a target site underphysiologically relevant flow conditions. The aim of this study was address this question.

Theoretical calculations were made to determine the range of vessel sizes, flow velocities, magnetic field strengths and gradients, bubble size and nanoparticle loading fractions under which retention could be achieved. The results indicated that there was a reasonably wide parameter spaceunder which retention should be possible,corresponding to clinically safe magnetic fields, bubble sizes, bubble composition and relevant flow rates.

A simple experimental flow phantom was constructed consisting of a 1cm diameter tubular vessel immersed in a water bath and positioned approximately 1 cm above a Halbach arrayof permanent magnetswhich provided a magnetic force of approximately 1 N/m^3 at thewall of the vessel. The vessel was perfused with magnetic microbubble suspensions of varying composition at a range of different flow rates. The bubbles were imaged at 2.5 MHz using a standard imagingprobe simultaneously acquiring B-mode and RF data. The actual flow rate in the vessel was determined through particle image velocimetry. Successful retention was confirmed for all microbubble suspensions tested (Fig. 1) at all but the highest flow rates.

Further examination under simultaneous optical and acoustic observation in a smaller vessel (200 µm diameter) under flow revealed that the bubbles formed short chains in the presence of a magnetic field which were then attracted towards the region of maximum force and retained (Fig. 2).

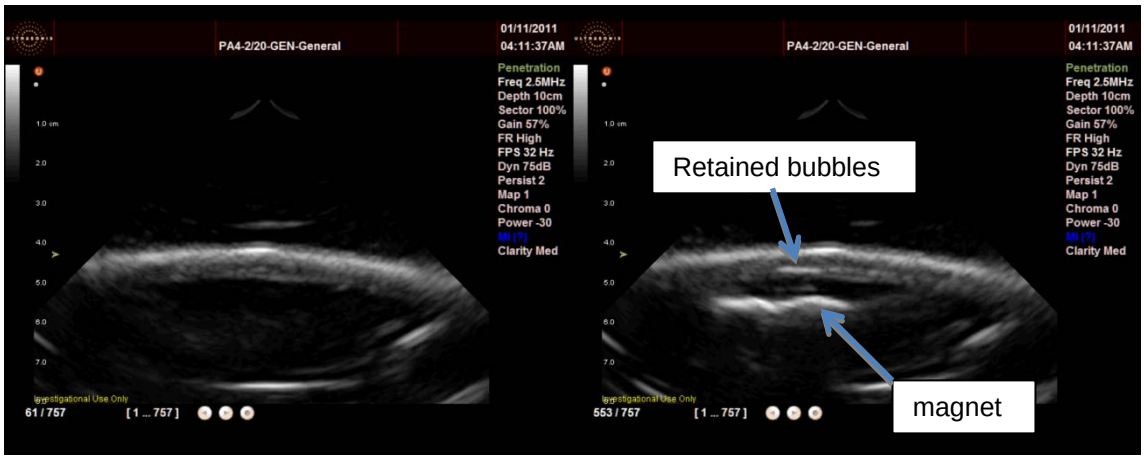

Figure 1: B-mode ultrasound images of magnetic microbubbles in a flow phantom before and after application of a magnetic field.

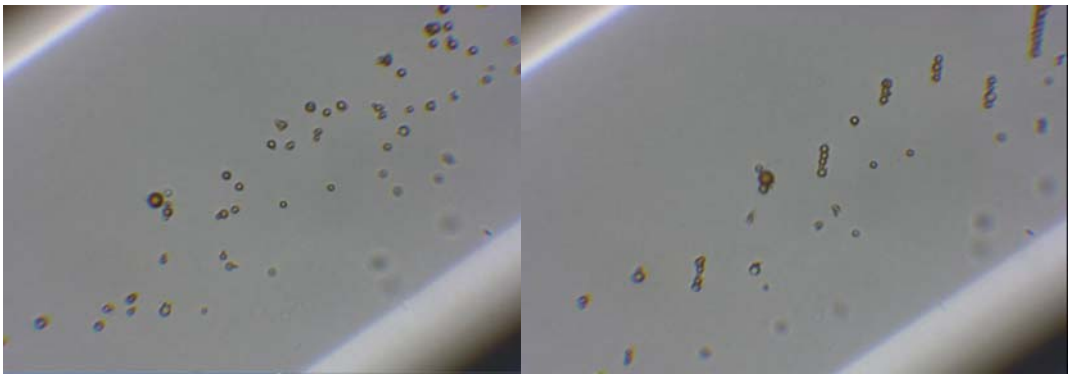

Figure 2: Flow of magnetic microbubbles in a capillary tube before (left) and after (right) application of a magnetic field.

The different suspensions tested included a mixture of magnetic micelles and non-magnetic microbubbles, which had previously been shown to be highly effective for gene transfection *in vitro* [2]. This study revealed that the two types of particle do not in fact remain separate but instead combine to form magneticmicrobubbles producing a high yield. This was confirmed by mixing fluorescent micelles with non-fluorescent bubbles. Subsequent imaging demonstrated that the microbubbles developed a fluorescent coating after mixing which was retained following centrifugation (Fig.3). Further comparison of the response of the different types of microbubble to both magnetic field exposure and acoustic excitation will also be discussed.

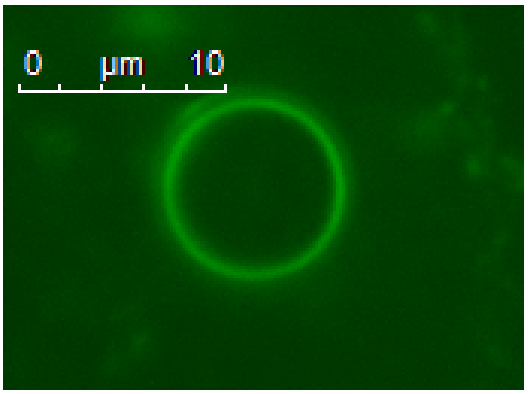

Figure 3: Magnetic microbubble prepared by mixing non-magnetic microbubbleswith fluorescently labelled magnetic micelles.

References

1. Soetanto, K. and H. Watarai, Development of magnetic microbubbles for drug delivery system (DDS). Japanese Journal of Applied Physics, Part 1: Regular Papers and Short Notes and Review Papers, 2000. 39(5 B): p. 3230-3232
2. Stride, E., et al., Enhancement of Microbubble Mediated Gene Delivery by Simultaneous Exposure to Ultrasonic and Magnetic Fields. Ultrasound in Medicine & Biology, 2009. 35(5): p. 861-868
3. Vlaskou, D., et al., Magnetic and Acoustically Active Lipospheres for Magnetically Targeted Nucleic Acid Delivery. Advanced Functional Materials, 2010. 20(22): p. 3881-3894

High speed imaging of vaporization of submicron perfluorocarbon droplets on the microsecond timescale

Nikita Reznik[1], Erik Gelderblom[2], Ross Williams[3], Oleksandr Shpak[2], Nico de Jong[2], Michel Versluis[2], Peter N. Burns[1,3]

[1]University of Toronto, Toronto, Ontario, Canada
[2]University of Twente, Enschede, the Netherlands
[3]Sunnybrook Research Institute, Toronto, Ontario, Canada

Liquid perfluorocarbon (PFC) droplets have been investigated, for a number of years, as a new generation of ultrasound contrast agents. Droplets filled with a low-boiling point PFC, such as perfluoropentane, stay in their liquid form at 37° C until exposed to ultrasound at sufficiently high rarefactional pressures [1]. At that point, droplets vaporize and convert into acoustically active bubbles of gas. This unique property of selective acoustic activation renders the droplets as a useful tool for both diagnostic imaging and therapy. Submicron perfluorocarbon droplets can be vaporized to produce micron-sized gas bubbles [2] [3]. These bubbles were shown to be stable for at least 1 s after vaporization, and respond non-linearly to ultrasound, rendering them suitable for use as ultrasound contrast agents for both B-mode and contrast-specific imaging, such as pulse-inversion [4].

Although recent studies have shown the potential for applicability of vaporized PFC droplets as ultrasound contrast agents for diagnostic purposes, little is known about the process of bubble formation and the immediate behaviour of the bubbles following vaporization, at the relevant, nanoseconds time scale. Furthermore, stability of vaporized droplets is of utmost importance for successful application of the newly created bubbles for ultrasound imaging, and ways of maximizing bubble stability are to be carefully studied.

In this work, we use ultra-high-speed optical imaging in order to study, for the first time, the vaporization of submicron droplets and observe the newly created microbubbles in the first microseconds after vaporization. We examine the initial vaporization-induced growth of the bubbles and the possibility of bubble recondensation back into the initial liquid form. Furthermore, we investigate the stability of the newly created bubbles, and the potential of retention of bubble shells following vaporization.

Methods

PFC droplet emulsions were prepared by a combination of water, 5% v/v perfluoropentane, 0.8% v/v negatively charged fluorinated surfactant Zonyl FSP, and subsequent emulsification with a tip-sonicator.

PFC droplets were vaporized by an in-house made PZT5H transducer (10 MHz, 1.4 cm diameter, f/# 1.0), driven by a Tabor Electronics arbitrary waveform generator amplified by an ENI 350L power amplifier. The transducer was focused on an Opticell containing highly diluted droplet sample. The Opticell was placed under a 100X water immersion objective (N.A. = 1.00) of an Olympus BX-FM microscope, coupled to the Brandaris 128 ultra-high-speed imaging facility [5]. The microscope objective was co-aligned with the transducer focus. The setup was placed in a tank of deionized water, kept at a temperature of 37 ± 2 °C. Droplet samples were vaporized with single ultrasound pulses, ranging from 5 to 10 cycles in length and at peak negative pressures (PNP) ranging from 2300 to 3500 kPa. The camera recorded sets of 128 images at either 10 or 15 million frames per second triggered to begin recording at the arrival of the ultrasound pulse. Optical images from the Brandaris camera were analysed with MATLAB.

Results

Submicron droplets, ranging in size from 100 nm to 1 μm were successfully vaporized with single pulses of ultrasound, as shown in Fig. 1. Following vaporization, the bubbles undergo transient oscillations, during which they could coalesce or fragment (as shown in Fig. 2 and Fig. 3 respectively). Following the transient oscillations, the bubbles were shown to shrink to radii of approximately 1 μm. In approximately 50% of the cases, the bubbles disappeared within a few μs after vaporization.

Bubble disappearance rate was strongly dependent on prior bubble coalescence, with coalesced bubbles showing significantly higher probability of survival. Furthermore, increase in ultrasound excitation pressure decreases the probability of bubble survival following vaporization.

Discussion and Conclusions

Submicron PFC droplet vaporization was observed, for the first time, on a nanoseconds scale. Bubble behaviour immediately following vaporization is significantly different than that observed in the case of micron sized droplet vaporization [6] [7].

Following initial nucleation and vaporization, the bubbles undergo transient oscillations, and may completely disappear within a few μs. Such a rapid disappearance of bubbles may be attributed to their recondensation back into the submicron liquid droplet form. Recondensation is energetically favourable for small bubbles due to the high Laplace pressure experienced. Presence of shell material around the newly created bubbles can significantly reduce the surface tension on the bubble and the associated Laplace pressure, increasing the chances of bubble survival in its gas form. Bubble coalescence during vaporization may serve to increase the surfactant concentration on the bubble surface, which would, in turn, reduce surface tension. This may explain the positive effect of coalescence on bubble survival rate.

This study shows that initial nucleation of droplets is necessary for production of echogenic bubbles. However, additional factors, such as bubble coalescence and bubble shell properties, affect the probability of inception of bubbles that are stable over extended periods of time and can therefore serve as ultrasound contrast agents.

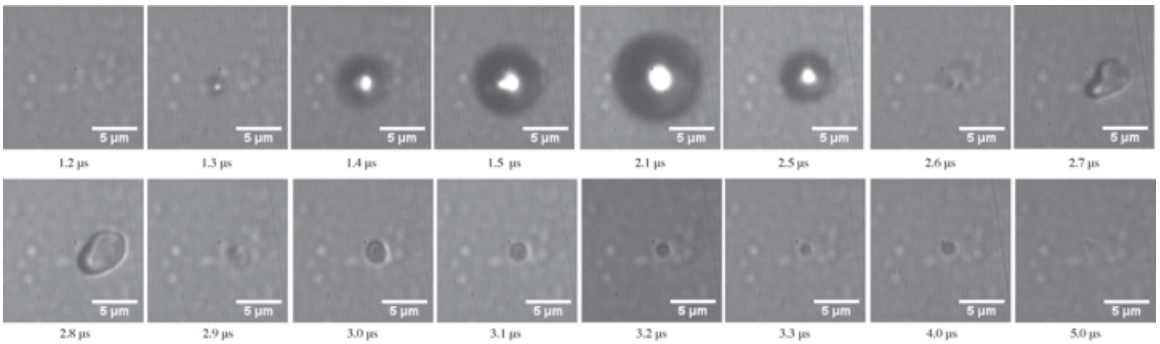

Figure 1. Typical image sequence of vaporization of a single submicron PFC droplet by a 10 cycle ultrasound pulse. Images were taken at 10 million frames per second. The images depict the initial growth and subsequent collapse and disappearance of the vaporized droplet.

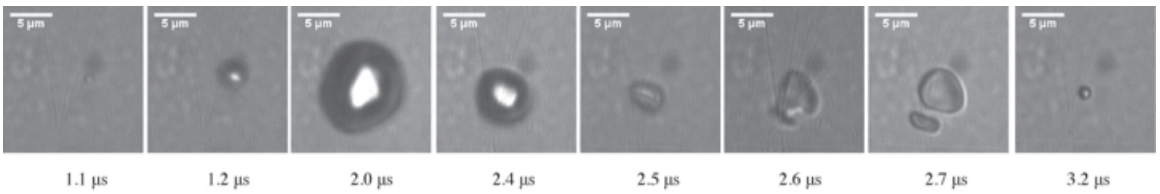

Figure 2. Droplet vaporization with subsequent fragmentation during the bubble collapse stage.

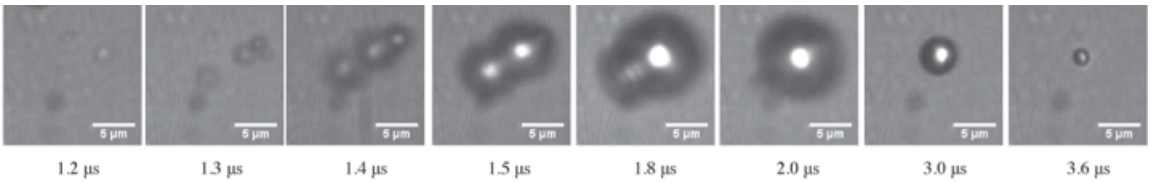

Figure 3. Example of multiple droplet coalescence. The images depict 4 droplets vaporizing in near proximity to each other. Upon physical contact, the vaporized droplets coalesce, followed by the collapse of the single combined bubble.

Acknowledgements
We would like to thank Mike Lee and Dr. Stuart Foster for the preparation of the transducer used for the droplet vaporization experiments.

References

1. O. D. Kripfgans, J. Brian Fowlkes, D. L. Miller, O. P. Eldevik, and P. L. Carson, Ultrasound Med Biol 26, 1177–1189 (2000)
2. N. Reznik, R. Williams, and P. N. Burns, Ultrasound Med Biol 37, 1271–1279 (2011)
3. P. S. Sheeran, V. P. Wong, S. Luois, R. J. McFarland, W. D. Ross, S. Feingold, T. O. Matsunaga, and P. A. Dayton, Ultrasound Med Biol 37, 1518–1530 (2011)
4. D. Simpson, C. T. Chin, and P. N. Burns, in Ultrasonics, Ferroelectrics and Frequency Control, IEEE Transactions on (1999), pp. 372–382
5. C. Chin, C. Lancée, J. Borsboom, and F. Mastik, Review of Scientific … (2003)
6. O. D. Kripfgans, M. L. Fabiilli, P. L. Carson, and J. Brian Fowlkes, J Acoust Soc Am 116, 272–281 (2004)
7. Z. Z. Wong, O. D. Kripfgans, A. Qamar, J. Brian Fowlkes, and J. L. Bull, Soft Matter 7, 4009 (2011)

The “quasi-stable” lipid shelled microbubble in response to consecutive ultrasound pulses

D. H. Thomas[1], P. Looney[1], M. Butler[1], T. Anderson[1], M. Emmer[3], H. Vos[3], N. de Jong[3], M. Borden[4], E. Stride[5], N. Pelekasis[2], V. Sboros[1]

[1]Medical Physics, the University of Edinburgh, Edinburgh, United Kingdom
[2]Department of Mechanical Engineering, University of Thessally, Volos, Greece
[3]Thoraxcenter, Biomedical Engineering, Erasmus Medical Center, Rotterdam, the Netherlands
[4]Department of Mechanical Engineering, University of Colorado, Boulder, CO, USA
[5]Department of Mechanical Engineering, University College London, London, UK

Contrast enhanced ultrasonography offers improved diagnostic imaging and potential therapeutic applications of targeted gene and drug delivery, as a transient increase in porosity and permeability of a cell membrane occurs when in the locality of ultrasound induced microbubble disruption. However, the mechanism of microbubble disruption remains unclear.

The oscillations of single Definity® microbubbles 2-6μm in radius have been measured using the Brandaris ultra high-speed camera and separately using a calibrated microacoustic system, in response to consecutive incident ultrasound pulses. Results show a gradual reduction in microbubble size and predictable changes in acoustic response. Based on comparisons with a Keller–Miksis model, both high-speed optical and acoustical experiments on single microbubbles show that the amplitude of oscillation and acoustic scatter vary depending on size in relation to resonance over consecutive pulses. The data suggest that this size and scatter evolution cannot be described by gas diffusion alone, and that lipid shedding plays an important role in the significant change of surface tension and subsequent size reduction of microbubbles. A correlation between the amount of compression a bubble undergoes and the subsequent amount of shell material shedding was found, with a minimum amount of compression required in order to see any significant reduction in area, suggesting a compression threshold below which the lipid shell is able to resist monolayer collapse. Furthermore, we found a narrower dispersion of responses after disruption, suggesting shell material may organise more optimally following loss of material.

We suggest that the mechanism of lipid shedding is dominant in incident acoustic pressures below the microbubble fragmentation threshold. This controlled mechanism may be deployed by new signal processing for the improvement of image sensitivity, and present novel manipulation for localised drug release.

An optimal instrument to evaluate the best method for ultrasound contrast imaging

F. Guidi[1], R. Mori[1], J. Viti[1,2] and P. Tortoli[1]

[1]Università di Firenze, Electronics and Telecomm. Dept, Firenze, Italy
[2]Biomedical Engineering, Erasmus Medical Centre Rotterdam, the Netherlands

Background

Advanced contrast imaging techniques make use of specific pulsing schemes, consisting in the transmission of sequences of tone bursts [1][2] or of suitable coded signals [3][4], with varying amplitude and/or phase. Combinations of tones in the same pulse repetition interval (PRI) can also be adopted [5][6]. In all cases, extracting the contrast-related information from the echoes obtained in different PRIs, requires appropriate signal processing to be performed by the ultrasound receiver.

Although simulations are always useful to evaluate a new method, experimental testing is a mandatory step to clarify pros and cons of any approach. However, the implementation of a new contrast imaging technique on a pre-existing ultrasound apparatus is in general quite demanding, since the "host" imaging system must be flexible enough to transmit sequences of arbitrary waveforms and must be capable to properly combine the received echoes. Furthermore, the receiver must be low-noise and linear over a wide dynamic range to suitably handle the weak harmonic components of echo signals.

In this work we propose the **UL**trasound **A**dvanced **O**pen **P**latform (ULA-OP) [7] as flexible, sensitive and high performance development tool suitable to implement a large class of methods for ultrasound contrast imaging.

System description

ULA-OP is a compact imaging system entirely developed in the MSDLab of the University of Florence. The transducer front-end manages up to 192 transducer elements by dynamically mapping 64 transmit/receive (TX/RX) channels. Each TX channel is developed around an arbitrary waveform generator, while each RX channel is based on a very low-noise preamplifier, a programmable gain amplifier and a 12 bit, 50 MHz sampling, A/D converter.

Raw data can be acquired on a PC before or after beamforming, as well as after coherent demodulation. ULA-OP is in fact connected to a PC where a real-time software manages all communications and display activities. The software is completed by add-on modules, each implementing specific real-time functions as B-mode, Color Flow Mode, elastography etc. Notably, a special Contrast Pulse Sequence

(CPS) function has been recently developed. This function allows the user to transmit arbitrary sequences of arbitrary waveforms from each TX channel, while the RX echoes are beamformed and stored in a large buffer. Different CPS modules can be simultaneously activated: for each module the user can program an independent set of weights, which are applied to the echoes received in consecutive PRIs, before adding them together. Real-time images obtained through the different CPS modules can be simultaneously displayed to compare the respective performance.

Experiments

The following concurrent functions were implemented: a) standard B-Mode imaging; b) pulse inversion (PI); c) power modulation (PM); d) combined PMPI.

This was obtained through the transmission of a periodic sequence of Hanning weighted bursts with normalised amplitude and phase equal to (0.5,0°), (1,0°), (1, 180°) respectively. The echo-data received over subsequent PRIs were multiplied by the following coefficient sets: [0,1,1], [2,-1,0] and [2,0,1], in the three concurrent modules, to produce PI, PM and PMPI images, respectively.

By transmitting the sequence toward a test object (eg, a wire) acting as reflector, the overall linearity of the system can be evaluated. We measured a first-to-second harmonic ratio of about 50 dB for the echo signal obtained with any of the above pulses. Combination of echoes in both PI and PM modes produced a rejection of the fundamental component by more than 40 dB.

Examples of images obtained by using of BR14 (Bracco Research, Geneve, CH) microbubbles diluted in water will be presented. In particular, the simultaneous display of results obtained in PI, PM and PMPI Modes gives evidence to the corresponding contrast differences.

Conclusion

ULA-OP offers the TX/RX, real-time processing and data storage flexibility needed for the test of new ultrasound contrast imaging methods. The capability of transmitting arbitrary waveforms could be exploited to try arbitrary phase or power modulation schemes as well as more demanding methods (e.g. chirp reversal[4], radial modulation[5]). If the available real-time CPS function does not directly match the processing requirements of a new approach, the latter could be preliminarily tested off-line by exploiting the system capability of storing both the pre- and post-beamforming RF data.

ULA-OP is thus proposed as an ideal instrument for the evaluation of arbitrary methods for US contrast imaging.

References

1. P.J. Phillips, “Contrast pulse sequences (CPS): imaging nonlinear microbubbles”, *2001 IEEE Ultrasonics Symposium*, vol. 2, pp. 1739-1745, 2001
2. R. J. Eckersley, C. T. Chin, and P. N. Burns, “Optimising phase and amplitude modulation schemes for imaging microbubble contrast agents at low acoustic power,” *Ultrasound in Medicine & Biology*, vol. 31, no. 2, pp. 213–219, 2005
3. J. M. G. Borsboom, C. T. Chin, A. Bouakaz, M. Versluis, and N. De Jong, “Harmonic chirp imaging method for ultrasound contrast agent”, *IEEE Trans. UFFC*, vol. 52, no. 2, pp 241–249, 2005
4. A. Novell and A. Bouakaz, “Chirp reversal power modulation contrast imaging,” 16th European symposium on Ultrasound Contrast Imaging, 2011
5. A. Bouakaz, M. Versluis, J. Borsboom, and N. de Jong, “Radial modulation of microbubbles for ultrasound contrast imaging,” *IEEE Trans. UFFC*, vol. 54(11), pp. 2283–2290, 2007
6. R. Hansen and B. Angelsen, “Contrast imaging by non-overlapping dual frequency band transmit pulse complexes,” *IEEE Trans. UFFC*, vol. 58(2), pp. 290–7, 2011
7. E.Boni *et al.* "A Reconfigurable and programmable FPGA based system for non-standard ultrasound methods", accepted for publication in *IEEE Trans. UFFC*

Ultrasound improved distribution of liposomal drug in tumour tissue and enhanced uptake in cells

Catharina de Lange Davies[1], Siv Eggen[1], Mercy Afadzi[1], Esben A. Nilssen[3], Rune Hansen[4], Bjørn Angelsen[2]

[1]Dept of Physics and [2]Dept of Circulation and Medical Imaging, The Norwegian University of Science and Technology
[3]Epitarget AS
[4]Dept of Medical Technology, SINTEF

A major obstacle in delivery of encapsulated drug to tumour cells is the low uptake and heterogeneous distribution of the drug in tumour tissue. Ultrasound may improve the delivery of encapsulated drug in various ways depending on the frequency and intensities applied, by inducing radiation force, heating or cavitation. The aim of the present work was to study the microdistribution in tumour tissue of doxorubicin encapsulated in sonosensitive liposomes injected intravenously in athymic mice bearing prostate tumour, and compare the uptake and micro-distribution in ultrasound-exposed and non-exposed tumours. Furthermore the effect of ultrasound and microbubbles on cellular uptake of liposomal doxorubicin was studied *in vitro*.

Prostate cancer xenografts were grown subcutaneously on the leg of athymic mice. Sonosensitive liposomes based on dierucoyol-phosphatidylcholine (DEPC) without non-dissolved gasses and containing doxorubicin were labelled with the lipophilic dye DiD and injected intravenously in mice. The liposomes were allowed to circulate for 24 hr, before ultrasound exposure of the tumours. The leg was placed in a tank with degassed water and the tumours were exposed to a focused ultrasound beam at frequency 300 kHz or 1 MHz and intensities corresponding to mechanical index (MI) of 2.4 or 2.2, respectively, for 10 min and 5% duty cycle. Frozen tumour sections were imaged along a radial track from the periphery of the tumour sections. The blood vessels were visualized by immunostaining the endothelial cells on frozen sections or by intravenous injection of FITC-lectin 5 min before sacrificing the mice. The distribution of DiD labelled liposomes and released doxorubicin were studied by confocal laser scanning microscopy. Cells growing in culture were incubated with the same DiD labelled liposomes and exposed to 300 kHz ultrasound either without or in the presence of microbubbles. Without microbubbles, MI up to 2.7 was applied for 180 s and 20% duty cycle. In the presence of microbubbles lower exposure had to be used to avoid too much cell death, and MI up to 1.05 for 120 s and duty cycle of 10% was applied. The cellular uptake of liposomes and doxorubicin was studied by flow cytometry.

Ultrasound enhanced the uptake of doxorubicin and improved the distribution of the drug throughout the extracellular matrix. In untreated tumours only small amounts of doxorubicin were observed and the drug was located close to the blood vessels. In the ultrasound-exposed tumours the uptake was enhanced significantly and doxorubicin had penetrated further away from the blood vessels. 300 kHz ultrasound was more efficient than 1 MHz.

Ultrasound exposure without microbubbles did not enhance the cellular uptake of neither the liposomes nor doxorubicin. However, in the presence of microbubbles, ultrasound treatment increased the percentage of cells with doxorubicin, but the amount of internalized doxorubicin was low, and no increase in the percentage of cells with DiD labelled liposomes or fragments of liposomes was found. These results indicate that doxorubicin had been released from the liposomes extracellularly before being internalized.

A prerequisite for successful cancer therapy is that the cytotoxic drugs reach all the cancer cells. The present results demonstrate that low frequency ultrasound improved the delivery of doxorubicin encapsulated in sonosensitive liposomes both by improving the cellular and tumour uptake, and by improving the distribution of the drug throughout the tumour tissue. Thus, combining ultrasound treatment and delivery of liposomal drug may improve the cancer therapeutic outcome.

High frequency ultrasound contrast imaging of transgenic mouse embryos

J. Denbeigh, M. Puri, F. S. Foster

It is believed that genetic mouse modeling can yield insights into the gene functions that control key processes in both mice and humans.[1] A concerted effort to examine phenotypic outcomes in transgenic and gene-targeted mice (including morphological changes as well as modifications in development, biochemistry, and behavior) is underway in order to advance our understanding of the influence these various gene products have on both disease and development.[1] While sophisticated methods for imaging morphological changes in mice have already been achieved using magnetic resonance imaging (MRI) and ultrasound in *in vivo* applications, there are few imaging applications which are currently able to assess the molecular landscape in a living mouse embryo. This is unfortunate, since this period of growth is crucial not only for studying the function of genes that cause congenital diseases and/or embryonic or neonatal lethality, but also presents an opportunity to study a regulated model of angiogenesis.

The strategy of performing functional and molecular imaging of biological pathways using targeted microbubbles has already been employed by a number of groups to demonstrate the ability of targeted ultrasound contrast imaging to monitor molecular expression in a variety of tumour models.[2-3] We report here on the development of techniques to infuse targeted microbubble contrast agents into whole living embryos in the interest of performing real time molecular imaging within transgenic murine embryos. Endoglin is a transmembrane receptor whose expression is up-regulated in actively proliferating cells and is highly expressed in tumour associated endothelium.[4] It has therefore been suggested as an appropriate marker and target for tumour related angiogenesis therapies. In the knockdown mouse model, heterogyzous embryos (+/-) exhibit 50% reduced expression of endoglin compared to their wild type (+/+) counterparts,[5] while complete deficiency in endoglin (-/-) is embryonic lethal. Using litters of wild type and knockdown (Eng +/-) embryos, our goal was to investigate whether we could differentiate between phenotypes by quantifying endoglin targeted microbubble binding.

Preliminary experiments were performed on litters of E15.5- E18.5 mice. Mouse embryos were removed from the mother, dissected out of the uterus, and placed in chilled fortified DMEM media. Prior to injection, each embryo was dissected from the yolk sac and revived. 20 uL of microbubble solution was then infused at a rate of 0.02 mL/min using a perfusion pump and trimmed glass needle. A 21 MHz linear array transducer (VisualSonics) was then positioned over the embryo. See Figure 1 for a depiction of the technical set-up.

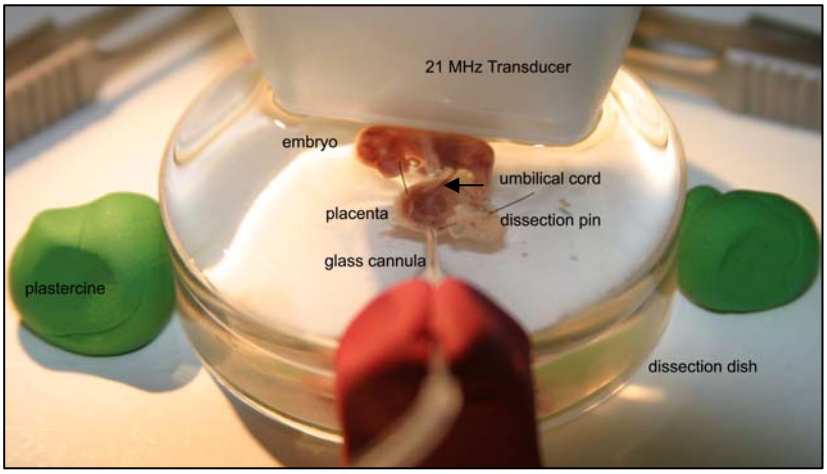

Figure 1. Experimental Set-up.
Arrangement of cannula, embryo and transducer positioned in ultrasound gel for microbubble injections.

These studies involved the injection of endoglin targeted microbubbles (TargetReady MicroMarker) in litters of endoglin wild type (Eng +/+) and heterozygous (Eng +/-) embryos (ICR background). The binding ability of two different sources of biotinylated CD105 (Endoglin) from clone MJ7/18 was assessed (eBioscience and in-house). The roles of antibody concentration (20, 40 or 80 ug antibody/vial) and microbubble concentration (dilute: $1.75x10^7$MB/mL or concentrated: $2.51x10^7$MB/mL) were also examined (see Table 1 for summary of injection parameters).

Antibody Source	Endoglin MJ7/18	
	In house	**eBioscience (13-1051)**
Antibody Concentration	40 ug [$1.75x10^7$MB/mL] 80 ug [$1.75x10^7$MB/mL]	20 ug [$1.75x10^7$MB/mL] 80 ug [$1.75x10^7$MB/mL] 80 ug [$2.51x10^7$MB/mL]

Table 1. Experimental Injection Conditions

For our molecular ultrasound imaging studies, a burst pulse was used to disrupt all bubbles in the plane of view and a sequence of nonlinear contrast image frames including both pre and post bubble disruption were obtained after permitting the microbubbles to circulate for 4 minutes. Imaging was conducted at 18 MHz (MS250S linear array transducer) using 4% power, with a 0.1 s burst pulse and a contrast gain of 30dB. After injection of each embryo, the tail was cut and placed in phosphate buffer. Once all tails were collected, they were stained for LacZ expression. Tails were scored for phenotype the next day. Contrast mean power ratios (CMPR) indicating relative microbubble binding within the brains of each embryo were attained and plotted according to their phenotype and experimental conditions (see Figure 2 below). Independent sample t-tests were performed for each set of injection parameters, assuming normal distribution (skewness < |1|), equal variances (Levene's test), and α=0.05. T-tests failed to reveal a statistically reliable difference between the CMPR means of the heterozygous (Eng +/-) phenotypes and the wild type (Eng +/+), except in the case of 80 ug Endoglin (in house) microbubbles ($1.75x10^7$MB/mL), where t(19) = -2.53, p = 0.02, α=0.05 (see table 2 below).

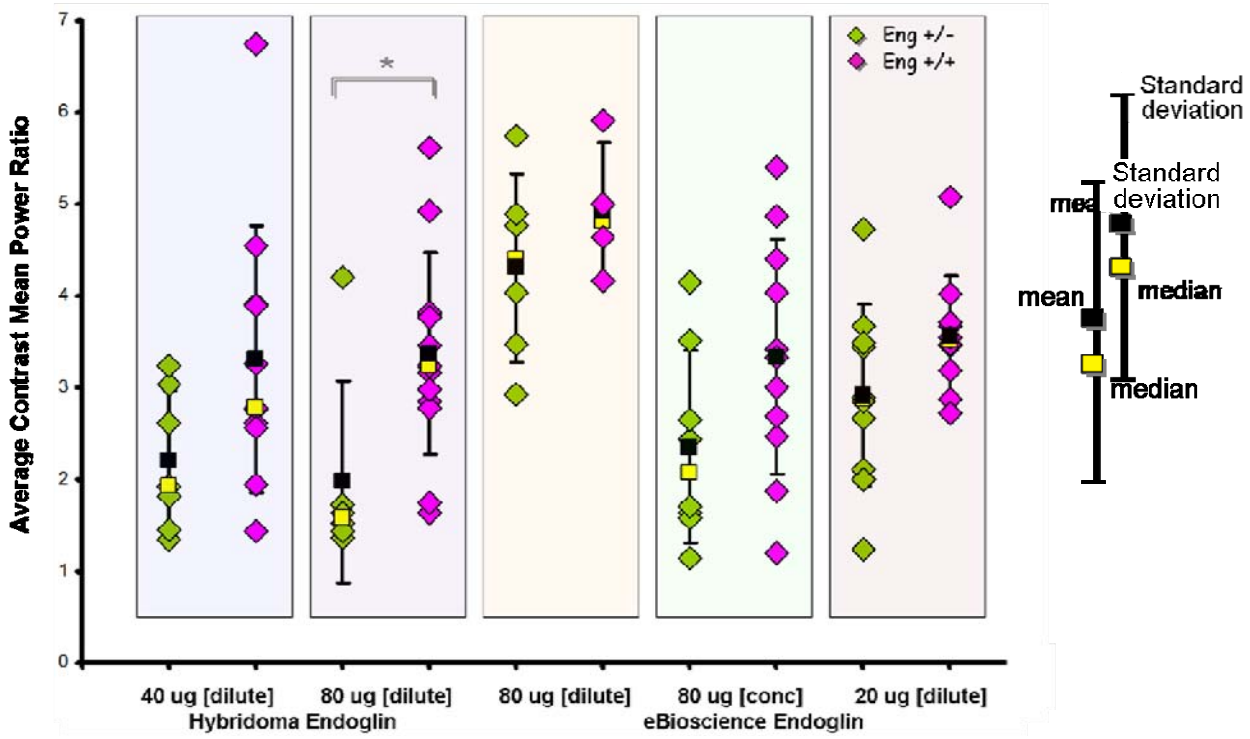

Figure 2. Experimental Injection Conditions
A significant difference (α=0.05, p<0.05) in the Average Contrast Mean Power Ratios was found between the binding of endoglin targeted microbubbles within the wild type (Endoglin +/+) and knockdown (Endoglin +/-) embryos for the litters injected with dilute concentrations ($1.75x10^7$ MB/mL) of 80 ug in-house endoglin targeted microbubbles. No significant difference was observed between the means of the other CMPRs.

Experimental Conditions	Eng +/-		Eng +/+		t	p
	Mean	SD	Mean	SD		
In-house						
40 ug [$1.75x10^7$MB/mL]	2.21	0.75	3.32	1.47	-1.84	0.09
80 ug [$1.75x10^7$MB/mL]	1.99	1.04	3.35	1.09	-2.53	*0.02
eBioScience						
20 ug [$1.75x10^7$MB/mL]	4.31	1.03	4.93	0.74	-1.03	0.33
80 ug [$1.75x10^7$MB/mL]	2.44	1.09	3.39	1.32	-1.55	0.14
80 ug [$2.51x10^7$MB/mL]	3.82	1.81	4.26	1.20	-1.55	0.14

Table 2. Statistical Analysis
Independent sample t-tests were used to compare the means of the CMPRs for each phenotype (+/-, +/+) according to experimental conditions. The means were statistically significantly different when $p<0.05$, indicated by *, where $\alpha=0.05$.

Initial results show that endoglin targeted microbubble binding within mouse embryos is achievable. Our ability to differentiate between different molecular phenotypes, however, seems to be dependent on both the type of targeting antibody used, as well as the concentration of antibody used per vial of microbubbles. Microbubbles targeted with the eBioscience antibody demonstrate a wide range of contrast mean power ratios in both phenotypic groups, suggesting that this antibody may not be as specific to the endoglin receptor as the in-house antibody. We also observe that increasing the amount of antibody added to the surface of the bubbles or increasing the microbubble concentration injected does not necessarily produce a statistically significant difference in the mean CMPRs of the embryo brains between the two phenotypic groups (+/-, +/+). In the single case with significantly different means ($p<0.05$ for 80ug in-house antibody), wild type embryos exhibit a 1.7 fold increase in their CMPRs, less that one might expect for a 50% difference in endoglin expression. Nevertheless, we may use these parameters to predict and categorize the phenotype of each embryo by quantifying endoglin targeted microbubble binding. These studies are limited by their small sample numbers however this preliminary work suggests that the antibody conditions may dramatically influence the targeting ability of these bubbles, thus playing a significant role in our capacity to differentiate between various molecular landscapes. Ultimately, the importance of antibody selection must be addressed by groups hoping to provide quantitative molecular ultrasound imaging, as some microbubble-antibody combinations may be able to provide better 'quantitative' information than others.

In summary, the development of contrast imaging methods for mouse embryos may provide a useful model for exploring the molecular landscape of angiogenic and developmental endothelial markers in transgenic mouse models at high ultrasound frequencies. This study demonstrates that reduced expression arising from the knockdown of endoglin is detectable with the right combination of microbubble and antibody.

References

1. Kulandavelu S. et al. ILAR journal, 2006
2. Rychack et al., Molecular Imaging, 2007
3. Willmann, J.K., et al., Radiology, 2011
4. ten Dijke P. et al., Angiogenesis, 2008
5. Jerkic, M., et al. Cardiovascular Research, 2006

The acoustic properties of microbubbles and their concentration dependence at 12 - 45 MHz

Chao Sun, V. Sboros, M.B. Butler, CM Moran

Medical Physics, Centre for Cardiovascular Research, University of Edinburgh, Edinburgh, UK

Introduction

High frequency ultrasound (>20MHz) is utilized to obtain high spatial resolution (<100 microns) images for intravascular, superficial tissue and pre-clinical ultrasound imaging applications. Ultrasound contrast agents (UCAs) are gas-filled microbubbles used to significantly enhance scatter of ultrasound. This study investigated the acoustic properties of solutions of Definity (Lantheus Medical Imaging, USA), SonoVue (Bracco Group, Italy) and a pre-clinical contrast agent MicroMarker (Bracco Group, Italy) microbubbles at a series of concentrations over the frequency range from 12 to 45 MHz at $20^{o}C \pm 1^{o}C$.

Method

Experiments were performed based on a broadband substitution technique using the Vevo770 pre-clinical ultrasound scanner (VisualSonics Inc., Toronto) and four transducers (nominal centre frequency and focal length bracketed): 710B (25 MHz, 15mm), 707B (30 MHz, 12.7mm), 704 (40 MHz, 6mm), 711 (55 MHz, 6mm). The output power at 10% and 100% for each of the transducers was measured using a Polyvinylidene Fluoride (PVDF) membrane hydrophone with an active element of 0.2 mm. For all the experiments 3 lines of radio-frequency (RF) data (digitised at 420 MHz) were collected over 100 consecutive frames from a region-of-interest (ROI) centred at the focal position. Contrasts agents were reconstituted as the manufacturer's instructions. A series of concentrations were chosen based on the practical application and doubling relationship. The concentrations of Definity used were 0.01×10^{6}, 0.075×10^{6}, 0.15×10^{6}, 0.3×10^{6}, 0.6×10^{6}, 1.2×10^{6} and 2.4×10^{6} microbubbles/ml. The microbubbles were diluted in air saturated distilled water. Experiments were repeated three times for each concentration. The attenuation ($dB\bullet cm^{-1}$) of the contrast agent solutions were calculated over the 3dB bandwidth of the transducers and normalised to the echo received from a TPX reflector based at the focus. Normalized backscattered power was calculated by normalizing the mean squared acoustic pressure of backcattered signal to the signal from the reflector at the transducer focus in the microbubble solution.

Result and discussion

From the Definity results, Figure 1 shows the attenuation decreases with the increasing frequency over the range 12 - 45 MHz at the concentration 1.2×10^6 microbubbles/ml. Both the normalized backscattered power and attenuation increase with increasing concentration (Figure 2). The transducer 711, which transmits the highest frequency ultrasound (furthest from the resonance frequency), shows the lowest backscattered power and attenuation. There is no significant difference of normalised backscattered power between the two power settings at 10% and 100%.

After understanding the acoustic characterizations of the microbubbles, nonlinear effects can be studied by analyzing the harmonic components. Similar experiments on SonoVue and MicroMarker are in process. Comparison of the acoustic properties, both at fundamental and harmonic frequencies, of the contrast agents when insonated at high frequencies will enable us to determine their potential use for pre-clinical animal studies.

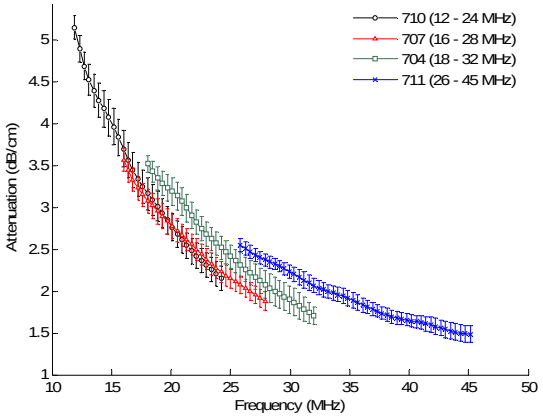

Fig1. The frequency dependence of the attenuation of Definity at the concentration 1.2×10^6 microbubbles/ml measured by four transducers

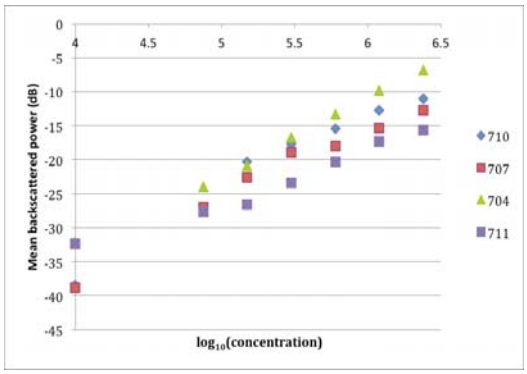

Fig2.a

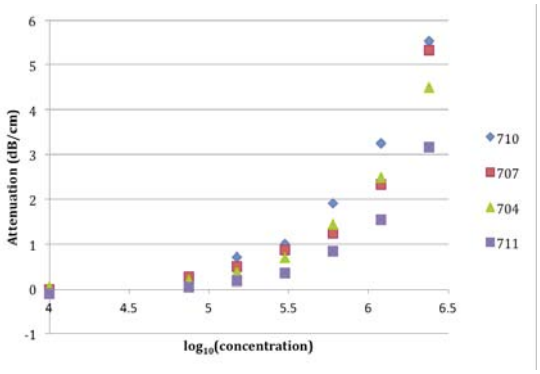

Fig2.b

Fig2. Mean backscattered power (a) and attenuation (b) as a function of the logarithm of concentration

What determines softening or hardening spring effect appearing in nonlinear resonance of a shell-coated microbubble?

Hiroki Kubo, Akihiro Sato, Toshihiko Sugiura

Mechanical Engineering, Faculty of Science and Technology, Keio University, Japan

Introduction

By irradiating ultrasound, microbubbles (MBs) reflect superharmonics or subharmonic signals. By receiving these nonlinear signals, shell-coated MBs can be used as ultrasound contrast agents (UCA) for medical imaging, drug delivery for ultrasound therapy, and so on. Thus, it is significant to understand their nonlinear oscillations for development of UCA.

It is known that the shell of UCA has a great influence on the behavior of nonlinear oscillations. The most widely used dominant equation for shell-coated microbubbles is the one by Marmottant, et al. [1]. However, numerical results based on that equation show two different nonlinear effects depending on conditions; softening spring effect in which the resonance frequency tends to decrease with the excitation amplitude increment and hardening effect in which the resonance frequency tends to increase with the excitation amplitude increment. Thus, the aim of this study is to investigate in what conditions which shift the resonance frequency of shell-coated MBs shows.

Method

The Marmottant model was used to investigate influence of the change of the acoustic pressure and the excitation frequency on the fundamental and subharmonic responses. This governing equation was non-dimensionalized to become generalized and analyzable. The non-dimensional equation was simulated by using the Runge-Kutta method, and the time histories of the oscillation and the frequency response curves were obtained. Furthermore, the non-dimensional parameters in the governing equation were evaluated to clarify the dominant terms among them. Here, assuming that the shell-coated bubble is BR14, its physical property was used.

Results

By numerical simulations, we obtained the solution of the amplitude-dependent natural frequency, which is characteristic of nonlinear oscillation. In contrast to the response of a gas MB without shell showing only softening effect, that of a shell bubble in this model has both hardening and softening effects depending on the excitation amplitude: the natural frequency tends to decrease with the excitation amplitude below some critical value, but increase beyond that critical amplitude as shown in Fig.1.

Furthermore, it was revealed by the numerical analysis that the most dominant term in the equation was the shell elasticity, which appears as the surface tension, and that the shell elasticity depends on the initial radius of the bubble, as found in Fig.2. This shell elasticity that gas MBs do not have makes the shift of the resonance frequency complex.

Fig.3 shows frequency response curves corresponding to several initial radii under the constant non-dimensional excitation amplitude. It can be found that a bubble with larger initial radius can show the hardening spring effect more easily in the frequency response. Fig.4 shows frequency response curves for different initial radii and different excitation amplitudes (acoustic pressures). Only the result of the case (a) in the condition of smaller radius and lower acoustic pressure shows the softening effect among them.

Conclusion

The shell elasticity, depending on the initial radius, is the dominant parameter on nonlinear oscillation of shell-coated MBs. Their frequency response curves show complicated softening-hardening spring effect, corresponding to negative shift or positive shift of the natural frequency. The condition that determines hardening or softening depends both on the initial radius and on the acoustic pressure amplitude. Specifically, a bigger MB tends to show the hardening effect, and a MB under higher acoustic pressure also tends to show hardening, while a smaller MB under lower pressure can show softening. Contrast imaging often uses subharmonic resonance of acoustic echoes. Subharmonic resonance arises only when the excitation frequency is equal to the integral multiple of the natural frequency, so it is better to understand such complex shift of the natural frequency during contrast imaging.

Reference

Marmottant et al, JASA 118:3499, 2005

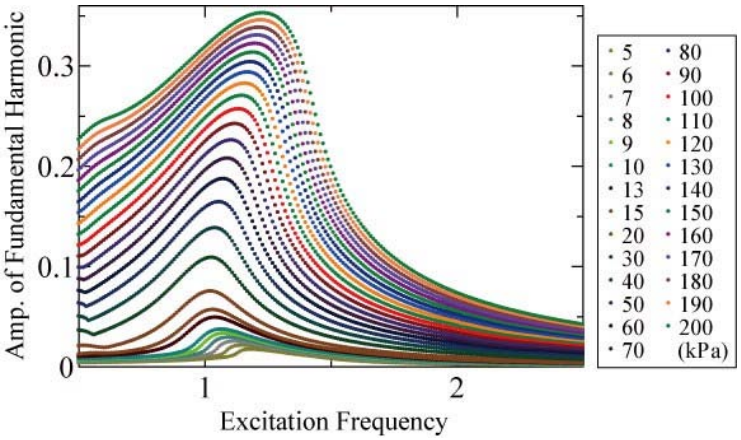

Fig.1 Primary resonance curves for different ultrasonic amplitudes.

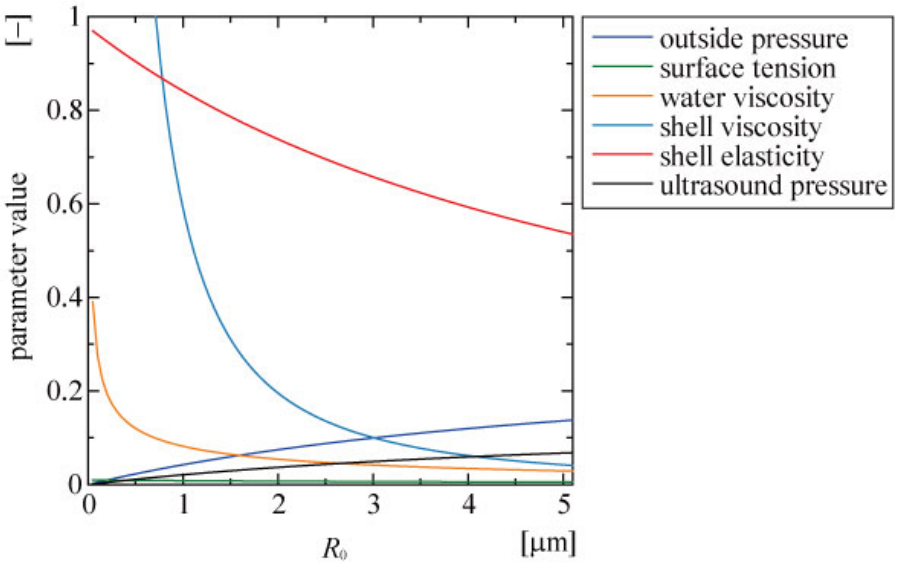

Fig.2 Relationship between initial radius and non-dimensional parameter value.

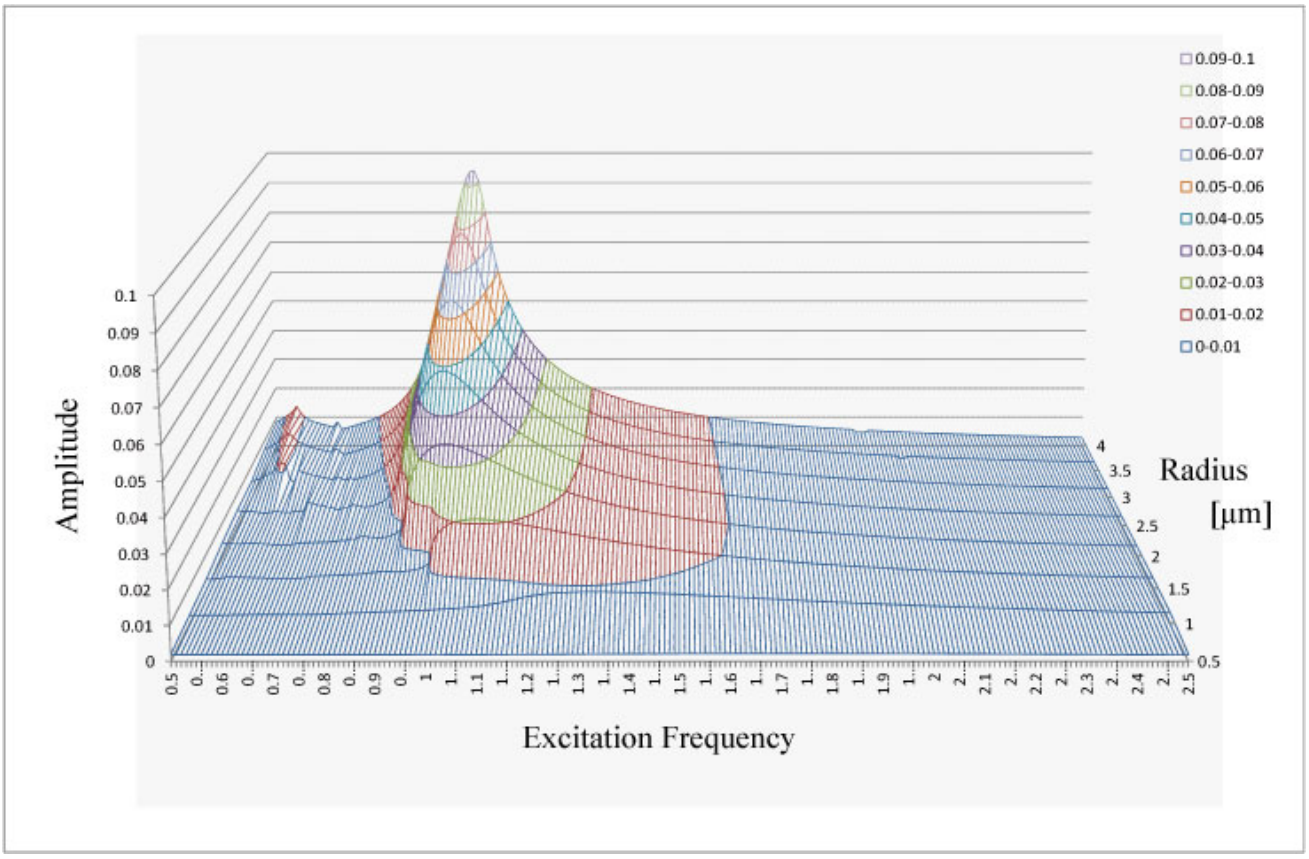

Fig.3 Primary resonance curves for different initial radii (non-dimensional excitation amplitude is const.).

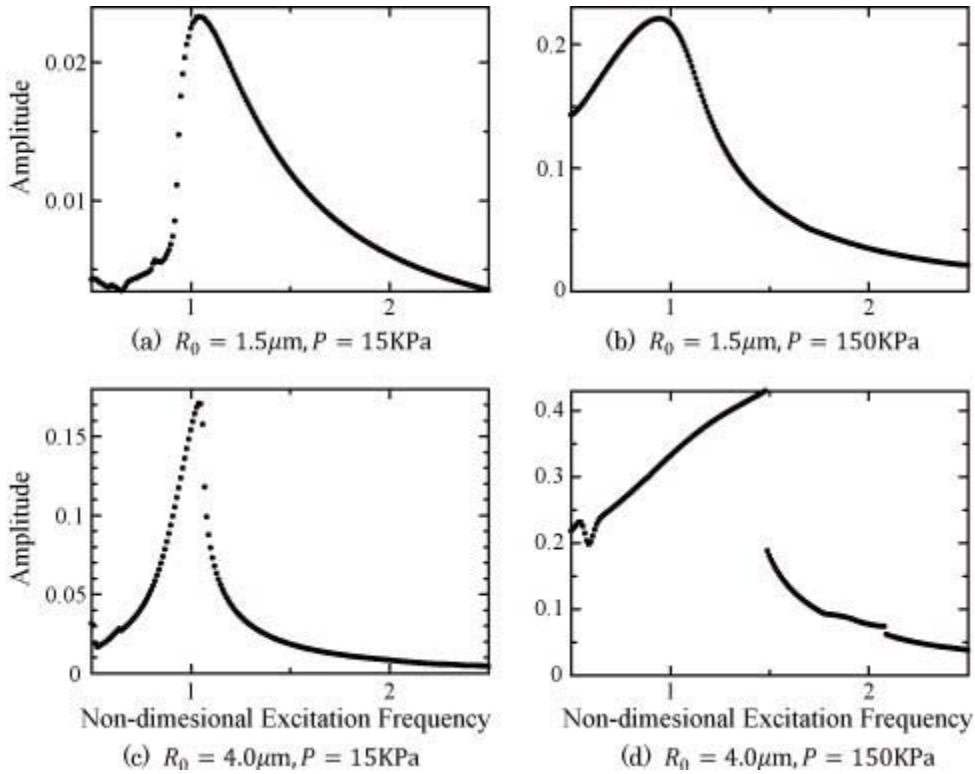

Fig.4 Primary resonance curves for different ultrasound pressure (P) and different initial radii (R_0).

Differential effects of microbubble adhesion on activated versus non-activated endothelium

Fairuzeta Ja'Afar†, John M Seddon†, Edward Leen‡, Charles A. Sennoga*

Department of Chemistry†, Department of Bioengineering and Department of Experimental Medicine‡, Imperial College London, South Kensington Campus, London SW7 2AZ, UK*

Microbubbles (MBs) are employed as contrast agents in ultrasound diagnostic imaging and therapeutic guidance. Although designed to pass freely through the vasculature, the microcirculatory transition of MBs has been found to be abnormally prolonged in inflamed tissues (see e.g., Lindner et al 2000; Owen et al, 2010; Shalhoub et al, 2011), suggesting that the surface composition of non-targeted MB encapsulations can influence their vascular rheology.

Whereas previous studies suggest albumin-shelled MBs adhere primarily through the leukocyte β_2-integrin Mac 1 and lipid-shelled MBs adhere through opsonisation by serum complement (Lindner et al 2000; Anderson et al, 2010; Villanueva et al, 1997), the differential binding effects of various MBs both on activated and non-activated endothelium, remains largely unknown.

In this study, our primary objective was to examine the adhesion of MBs to activated or non-activated endothelium and assess whether MB shell composition influenced their adhesion. We further explored whether charge-specific interactions with the endothelium in regions where the glycocalyx is compromised, would reflect the level of adhesion observed.
Video microscopy was used to determine these interactions. Human umbilical endothelial cells (HUVECs) were cultured in petri dishes; activated with TNF-α; loaded into flow phantoms and infused with the commercial agents Optison™, SonoVue™, Definity™ and the experimental agent BR38. The former is an albumin-shelled agent while the others are lipid-shelled. The role of surface charge was examined using laser Doppler velocimetry and phase analysis light scattering.

Adherence of Optison™ and SonoVue™ onto activated was significant ($p<0.05$) compared with non-activated HUVECs. In contrast, the adhesion of BR38 and Definity™ was not significant ($p>0.05$). There was no correlation between MB surface charge and adhesion. A comprehensive measure of MB surface charge is required to ascertain the role of charge in MB adhesion.

Enhanced gene and drug delivery with ultrasound and microbubbles

Ayache Bouakaz, J.M. Escoffre, A. Novell, A. Zeghimi

UMR INSERM U930, Université François Rabelais, Tours, France

In this present experimental study, we investigated the use of new generation of microbubbles, Vevo-Micromarker®, for gene transfer and we compared to BR14® and SonoVue®.

Among the non-viral methods for the *in-vitro* gene delivery, sonoporation is a simple, inexpensive and a safe technology[1]. This approach provides a transient increase in the membrane permeability and hence the plasmid DNA entry into cells. In this context, the application of ultrasound with the new generation of contrast microbubbles, Vevo Micromarker®, has been first investigated *in-vitro* and compared to BR14® and SonoVue® microbubbles. Moreover, the acoustical properties of the microbubbles were measured to gain an insight into the biophysical mechanism involved in the transfection process. Our results show that the transfection efficiency of glioblastoma cells achieved with the Vevo Micromarker® microbubbles and ultrasound is approximately 1.5 times higher than given by the BR14® and SonoVue® microbubbles. To our knowledge, it is for the first time that a transfection rate of almost 70% is reported using the combination of ultrasound and gas microbubbles. Furthermore, it has been found that the persistence of the microbubbles to insonation is directly correlated to the induced transfection efficiency. Indeed, our study shows findings indicate that the attenuation and the destruction of microbubbles are two key parameters in the sonoporation efficiency. This approach has been extended to deliver anti-cancer drugs. The co-administration of microbubbles and doxorubicin[2] or irinotecan showed to provide synergetic therapeutic efficacy.

References

1. J.M. Escoffre, A. Novell, A. Zeghimi, A. Bouakaz (2010) Ultrasound & microbubbles for in vitro gene delivey. *Drug Development & Delivery,* **11**: 42-47
2. J.M. Escoffre, J. Piron, A. Novell and A. Bouakaz (2011) Doxorubicin delivery into tumor cells with ultrasound and microbubbles. *Molecular Pharmaceutics,* **8**:799-806

Acknowledgement
The authors acknowledge Bracco Research Geneva for supplying the microbubbles. This study is partly funded by the EU Project SONODRUGS (NMP4-LA-2008-213706).

Gd-lipid microbubbles as theranostic agents for MRI-guided focused ultrasound therapy

Mark Borden[1], Jameel Feshitan[1,2], Mike Boss[3]

[1]Mechanical Engineering, University of Colorado, Boulder, CO 80309, USA
[2]Chemical Engineering, Columbia University, New York, NY 10027, USA
[3]National Institute of Standards, Magnetics Group, Boulder, CO 80302, USA

We have synthesized a novel class of theranostic agents consisting of Gd(III) ions chelated to lipid-coated, size-selected microbubbles for utility in both magnetic resonance and ultrasound imaging. The macrocyclic ligand DOTA-NHS was bound to PE headgroupsor primary amines tethered to PEG groups on the lipid shell of pre-synthesized microbubbles. Gd(III) was then chelated to the DOTA on the microbubble shell. The reaction temperature and pH were optimized to increase the rate of Gd(III) chelation while maintaining microbubble stability. ICP-OES analysis of the microbubbles provided measurement of the Gd(III) surface density. The Gd(III)-bound microbubbles were found to be echogenic *in vivo* during high-frequency ultrasound imaging of the mouse kidney. The Gd(III)-bound microbubbles also were characterized by MRI at 9.4 T using a spin-echo technique and by NMR at 1.5 T using the CPMG sequence. A fascinating interplay was found between water access and susceptibility effects, providing drastic changes in both the longitudinal and transverse proton relaxation rates before and after microbubble cavitation. We believe that the Gd(III)-bound microbubbles will find application in the measurement of cavitation events and sonoporation during MRI-guided focused ultrasound therapy and to track the biodistribution of shell remnants.

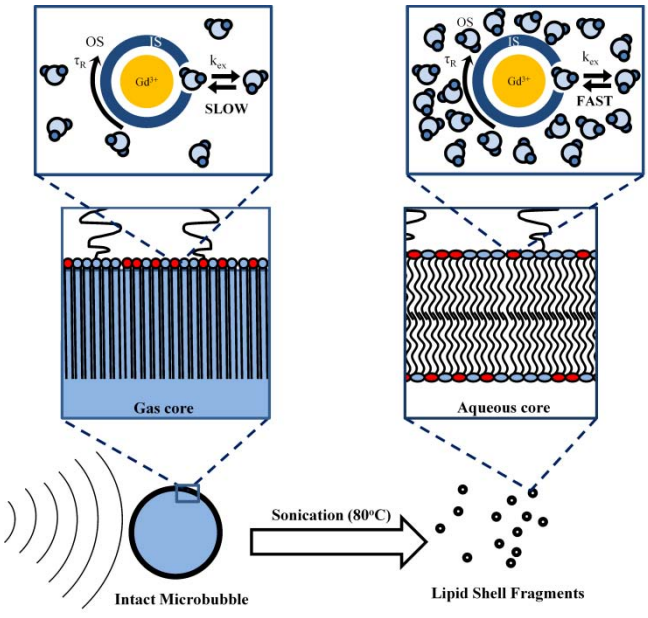

Ultrasound-enhanced drug delivery with a diagnostic scanner?

Michalakis Averkiou

University of Cyprus, Nicosia, Cyprus

Ultrasound-enhanced drug delivery has received a lot of attention in the recent years. In combination with developments in nanomedicine and nanomaterials it now is possible to deliver drugs to specific sites and often under imaging guidance for a more efficient treatment and fewer adverse side effects [1, 2]. In most of the published works in this area, microbubbles are used together with ultrasound and drugs. The term sonoporation has been coined to indicate various phenomena which result in the cellular uptake of drugs while ultrasound (and microbubbles) is applied [3]. With somewhat similar physical mechanisms to sonoporation other applications such sonothrombolysis [4], opening of the blood brain barrier to enable drug transport [5], and gene transfection [6] have recently evolved in a parallel fashion.

The exact mechanism of sonoporation (and the other mentioned processes) is still not fully understood and under heavy investigation. Often the "optimal" ultrasound parameters are simply derived by trial and error. After an extensive literature review in this topic certain prevalent ultrasound parameters in terms of frequency (0.2-2 MHz), amplitude (0.1-2 MPa), number of cycles (4-10K), and duty cycle (1-50%) are found [7, 8]. Most published research was done with experimental ultrasound transducers, however, a few works with HIFU/MRI systems, and diagnostic ultrasound scanners have been reported [1, 9]. The underlying hypothesis is that ultrasound induces a form of cavitation (low and stable in one end and violent inertial cavitation at the other) that presumably leads to sonoporation.

The use of custom made (single or multi- element) transducers with all the necessary instrumentation might bring all the needed flexibility to induce efficient cavitation but it may be close to impossible to apply in-vivo without real-time imaging. Clinically available and experimental HIFU/MRI systems have the flexibility to produce the required conditions but are unable to image the microbubble activity in real time. The use of an ultrasound scanner to interleave therapy and real-time imaging would be the obvious choice if the optimal ultrasound sonoporation conditions could be achieved. Nonlinear low mechanical index (MI) methods are now fully developed and able to image the flow of microbubble drug carriers in-vivo and high MI bubble destruction imaging modes from the past could be re-visited to image the therapy process. Forgotten modes like SAE (stimulated acoustic emission), ADI (agent detection imaging) together with intermittent/triggered imaging can be further explored for therapy.

Undoubtedly, if an ultrasound scanner can produce the sonoporation conditions while offering high resolution bubble imaging it would be the perfect drug delivery system for the same reasons that make ultrasound a popular imaging modality today: ease of use, mobility, real-time, bedside availability, and low cost.

References

1. S. Chen, R. V. Shohet, R. Bekeredjian, P. Frenkel, P. A. Grayburn, “Optimization of ultrasound parameters for cardiac gene delivery of adenoviral or plasmid deoxyribonucleic acid by ultrasound-targeted microbubble destruction,” Journal of the American College of Cardiology, Volume: 42, Issue: 2, Pages: 301-308, 2003
2. J. H. Hwang, et al., "Correlation between inertial cavitation dose and endothelial cell damage in vivo," Ultrasound in Medicine and Biology, vol. 32, pp. 1611-1619, 2006
3. A. van Wamel, et al., "Vibrating microbubbles poking individual cells: Drug transfer into cells via sonoporation," Journal of Controlled Release, vol. 112, pp. 149-155, 2006
4. Feng Xie, John Lof, Carr Everbach, Anming He, Richard M. Bennett, Terry Matsunaga, Jason Johanning, Thomas R. Porter, “Treatment of Acute Intravascular Thrombi With Diagnostic Ultrasound and Intravenous Microbubbles,” JACC : Cardiovascular Imaging, vol. 2 , No. 4, 2009
5. Alexandrov, A.V., Demchuk, A.M., Burgin, W.S., Robinson, D.J., Grotta, J.C., “Ultrasound-Enhanced Thrombolysis for Acute Ischemic Stroke: Phase I. Findings of the CLOTBUST Trial,” Journal of Neuroimaging 14 (2), pp. 113-117, 2004
6. Leong-Poi, H., Kuliszewski, M.A., Lekas, M., Sibbald, M., Teichert-Kuliszewska, K., Klibanov, A.L., Stewart, D.J., Lindner, J.R., “Therapeutic arteriogenesis by ultrasound-mediated VEGF165 plasmid gene delivery to chronically ischemic skeletal muscle,” Circulation Research 101 (3), pp. 295-303, 2007
7. A. Rahim, et al., "Physical parameters affecting ultrasound/microbubble-mediated gene delivery efficiency in vitro," Ultrasound in Medicine and Biology, vol. 32, pp. 1269-1279, 2006
8. R. Karshafian, et al., "Sonoporation by Ultrasound-Activated Microbubble Contrast Agents: Effect of Acoustic Exposure Parameters on Cell Membrane Permeability and Cell Viability," Ultrasound in Medicine and Biology, vol. 35, pp. 847-860, 2009
9. R. Bekeredjian, et al., "Augmentation of cardiac protein delivery using ultrasound targeted microbubble destruction," Ultrasound in Medicine and Biology, vol. 31, pp. 687-691, 2005

Ultra fast brightfield and fluorescence imaging

Xucai Chen, Jianjun Wang, Flordeliza S. Villanueva

Center for Ultrasound Molecular Imaging and Therapeutics, University of Pittsburgh, Pittsburgh, PA, USA

Background

Ultrasound (US)-assisted therapies such as US-induced microbubble (MB) destruction have potential to enhance thrombolysis and drug or gene delivery for cardiovascular disease. Visualization of US-MB-cell interactions, which occur in nano-second time scale due to the physics of US, should yield insights into therapeutically relevant MB dynamics, and improve design of new US-MB-mediated therapies. We present a high speed brightfield and fluorescence imaging system that allows unique *in vitro* and *in vivo* microscopic observations of MB acoustic behavior.

Methods

Our integrated system includes a custom multi-frame camera and software control (Cordin Company), customized modular microscope and laser delivery system, US generator, and combined US and optical imaging chamber for *in vitro* and *in vivo* MB observations. The camera system, based on a rotating mirror design, contains 64 digital CCD cameras (1392 x 1040 pixels) and acquires 2 image frames per CCD via a pair of mirrors. A strobe light triggered from the timing board is used for the brightfield light source. A fast pulse capable Cyan-488 optically pumped semiconductor laser system is used for fluorescence imaging. A custom fiber optics alignment system delivers laser light through the microscope.

Results

The system images at up to 25 million frames per second (Mfps) for 128 frames for both brightfield and fluorescence imaging. Figure 1(A) shows selected frames of fluorescent beads (1, 2, 4 μm), proving the concept of ultra-fast fluorescent imaging, and demonstrating the potential for *in vivo* intravital microscopy of vibrating fluorescent MBs in the microcirculation. Figure 1(B) shows selected brightfield frames of US-induced MB vibration, jet formation, and breaking. Comparison of high speed brightfield and fluorescence movies of polymer MB under identical ultrasound condition revealed that gas has escaped from the polymer shell and oscillates at large amplitude while the shell membrane oscillates at much smaller amplitude. This observation may have implications for US mediated therapy such as drug and gene delivery.

Conclusion

We have developed a high speed camera system for fluorescence and brightfield imaging at 25 Mfps. This system should enable unique visualization of interactions between US, MB, and cells *in vitro* and *in vivo*, and ultimately help to optimize novel US-MB mediated therapies for cardiac disease and molecular imaging.

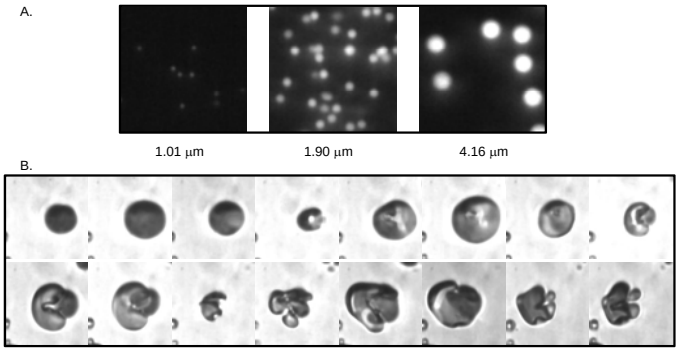

Figure 1. Selected frames from (A) fluorescence movies of reference beads at 25 Mfps; (B) a brightfield movie of microbubbles excited with 1 MHz ultrasound at 25 Mfps.

High-speed fluorescence imaging of the US-triggered release from liposome-loaded microbubbles

Erik Gelderblom[1], Ying Luan[2], Heleen Dewitte[3], Bart Geers[3], Ine Lentacker[3], Ton van der Steen[2], Nico de Jong[2], Michel Versluis[1]

[1]Physics of Fluids, University of Twente, Enschede, the Netherlands
[2]Biomedical Engineering, Erasmus MC, Rotterdam, the Netherlands
[3]Ghent Research Group on Nanomedicine, Ghent University, Ghent, Belgium

Introduction

Many examples of the therapeutic application of ultrasound contrast agents microbubbles have emerged in the last couple of years [1]. Various microbubble designs have been shown to be capable of carrying drugs to a specific region in the body and enhancing the uptake or delivery efficacy, in particular when drugs are loaded into liposomes and attached to the surface of the microbubbles [2]. Although the therapeutic effect has been shown, the physical mechanism behind it has not been fully clarified.

An essential step in the process of triggered drug delivery is the release of a drug from the bubble surface. The release takes place at a microseconds timescale and the drugs or drug-carrying vesicles (~200 nm) are too small to resolve with a standard microscope. Thus, it is an extremely challenging task to visualize these processes. Here we use high-speed fluorescence imaging to visualize the ultrasound-triggered release from fluorescently labeled liposome-loaded microbubbles at a frame rate of 100,000 frames per second.

Materials and methods

Liposome-loaded microbubbles were prepared using the method described by Geers et. al. [2]. Three types of samples were made: I) fluorescently labeled unloaded bubbles, II) fluorescently labeled bubbles loaded with non-fluorescent liposomes, and III) non-fluorescent bubbles loaded with fluorescently labeled liposomes. Vials containing perfluorbutane and a solution of DPPC and DSPE-PEG-SPDP were mechanically activated using a Capmix™ device to create the microbubbles. Liposomes were added before activation to produce loaded microbubbles. The liposomes were coupled to the microbubble surface through covalent thiol-maleimide linkages. The lipophilic fluorescent marker DiI was incorporated into the phospholipid monolayer or liposome bilayer, located in between the DSPE-PEG molecules. The absorption spectrum of the dye matches the wavelength of the laser used for fluorescence excitation in the experimental setup.

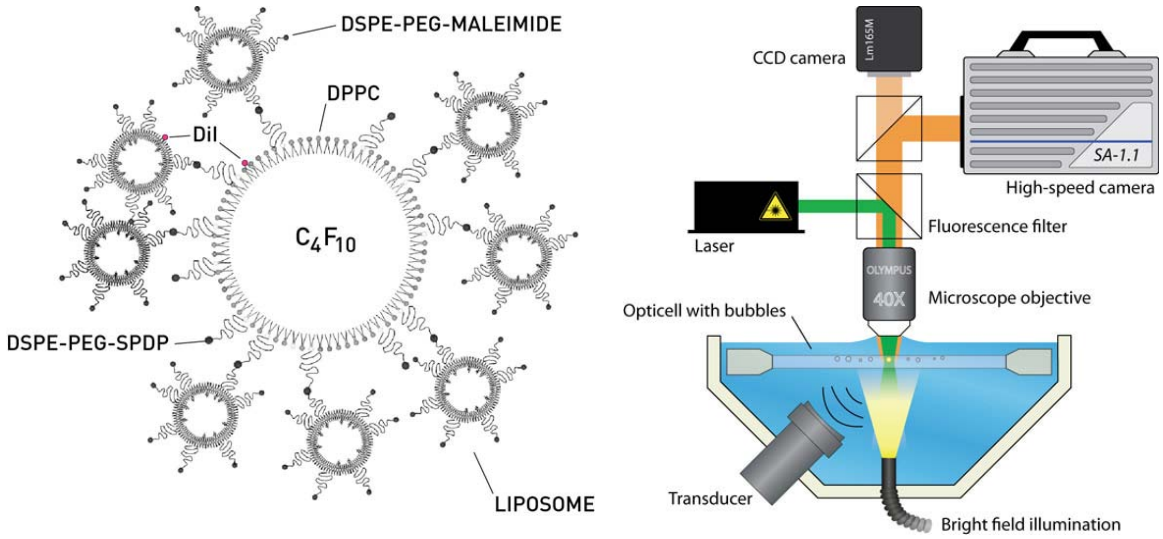

Figure 1 – Schematic of a liposome-loaded bubble and the experimental setup.

The bubble samples were diluted and injected into an optically and acoustically transparent culture chamber Opticell™. The Opticell™ was placed in a water bath containing a 1 MHz focused ultrasound transducer at the bottom, connected to an arbitrary waveform generator. The water bath was located underneath an upright fluorescence microscope, incorporating a 40X water-immersion objective for imaging and for focusing of the laser light. Two cameras were coupled to the microscope: a Photron SA-1.1 high-speed camera for fluorescence imaging at 100 kfps and a Lumenera Lm165M CCD camera recording high-resolution bright-field images at 15 fps simultaneously. The bubbles were insonified by single ultrasound pulses containing 10, 100 or 1000 cycles at 1 MHz and a peak-negative pressure ranging from 20 to 100 kPa.

Results

Various release phenomena were observed, depending on the bubble type and ultrasound parameters. For all three bubble types, low acoustic pressures (20-40 kPa) and a high number of cycles resulted in the release of small fluorescent particles, most likely to be islands of phospholipids detached from the bubble shell. An example is given in figure 2A.

Unlike the 'slow' release of particles at low pressures, applying high pressures (80-100 kPa) resulted in the instantaneous release of most of the bubble's fluorescent shell material, as depicted in figure 2B.

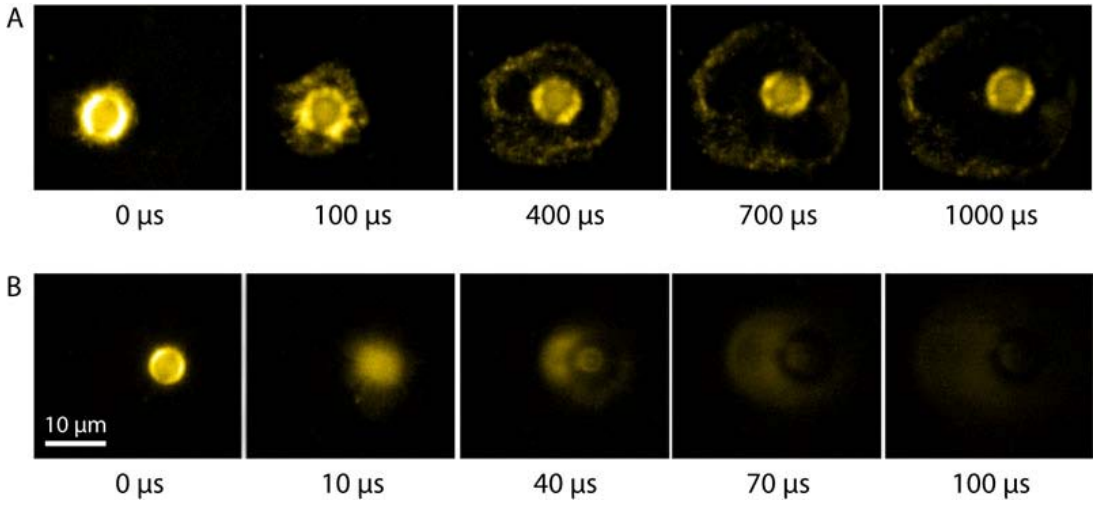

Figure 2 – Release from liposome-loaded microbubbles: A) Slow release of particles at low pressure; B) Fast release at high pressure.

Furthermore, the measurements revealed the dynamical redistribution of fluorescent material over the bubble shell during oscillations and other effects, such as budding and deformation of both liposome-loaded and unloaded microbubbles [3].

Outlook

High-speed fluorescence imaging provides detailed, time-resolved information about the ultrasound-triggered release of phospholipids and liposomes from microbubbles. It gives valuable insight into the ultrasound parameters required for ultrasound-triggered drug-delivery. When studying the effect of shedding on the dynamics of phospholipid-coated bubbles, this method offers a tool to monitor lipid-shedding at a relevant timescale.

References

1. M.R. Böhmer, A.L. Klibanov, K. Tiemann, C.S. Hall, H.Gruell & O.C. Steinbach, Ultrasound triggered image-guided drug delivery, European Journal of Radiology 70 (2009)
2. B. Geers, I. Lentacker, N.N. Sanders, J. Demeester, S. Meairs & S.C. De Smedt, Self-assembled liposome-loaded microbubbles: The missing link for safe and efficiënt ultrasound triggered drug-delivery, Journal of Controlled Release 152 (2011)
3. G. Pu, M.A. Borden, M.L. Longo, Collapse and shedding transitions in binary lipid monolayers coating microbubbles, Langmuir 22 (2006)

Molecular imaging – The near future

Beat A. Kaufmann

University Hospital Basel, Switzerland

The term molecular imaging has been coined for methods that non-invasively detect the expression of relevant, disease specific molecules. For ultrasound molecular imaging, microbubbles are targeted to disease markers by using one of two strategies. The first strategy takes advantage of modificatons of the microbubble shell surface for attachment of microbubbles to activated leukocytes that reside in inflamed blood vessels. The second and more versatile strategy uses surface conjugation of specific disease ligands to the microbubble surface for targeting. In recent years, these novel applications have been tested in several animal models of relevant cardiovascular disease. Detection of vascular inflammation in atherosclerosis both in very early disease stages and in established atherosclerosis is feasible using these techniques. Also, the detection of microvascular inflammation in the myocardium is promising for the diagnosis of transplant rejection and recent myocardial ischemia (ischemic memory imaging). Assesment of markers of angiogenesis using ultrasound molecular imaging both in health and disease states such as diabetes mellitus have recently allowed for unique insights into the regulation of the growth of new blood vessels. Together with the inherent advantages of ultrasound imaging, which include availability, fast scanning protocols, and low cost, these preclinical data make ultrasound molecular imaging an interesting candidate for disease screening.

In the near future, further preclinical developments will be the testing of the feasibility of ultrasound molecular imaging for the assessment of treatment effects, in particular of treatments aimed at reducing vascular inflammation in atherosclerosis. Also, better characterization of the interaction of targeted microbubbles with the endothelium could result in improved microbubble design. For clinical translation, developments in conjugation chemistry for ligand attachment, and development of non-immunogenic, safe and affordable ligands will be necessary.

Finally, the costs for development of agents for use in humans and for toxicology studies will be an obstacle that has to be overcome for conducting first trials in humans.

Molecular imaging of small animals: which modality to use?

Marion de Jong

Departments of Nuclear Medicine and Radiology, Erasmus MC Rotterdam, the Netherlands

Looking at the number of citations in PubMed including the word “translational research”, the average yearly number of cumulative citations is about 37%. This fact stresses the importance of preclinical research that is conducted in close collaboration with the clinic in order to provide research data applicable in the clinic. As such, methods developed in the preclinical research should be able to be translated into the clinic and molecular imaging techniques play an increasingly important role in this respect.

In this presentation, different imaging modalities will be presented, including CT, MRI, PET(/MRI), SPECT(/CT), Optical imaging, and Ultrasound, that can all be used in both the clinic and in preclinical research. All techniques have their specific pros and cons as exemplified in the table below.

	Target	**Contrast needed**	**3D**	**Resolution**	**Sensitivity**	**Radiation**
µCT	Bone Anatomy	No Can	Yes	0.1 µm	Low	Yes
MRI	Perfusion Anatomy Function	Yes Can Can	Yes	0.1 mm	Medium	No
PET	Function	Yes	Yes	1.0 mm	High	Yes
SPECT	Function	Yes	Yes	0.3 mm	High	Yes
OI	Location Function	Can Yes	Yes	1.0 mm	High	No
US	Flow Function Anatomy	No Can	Yes		Medium	No

In conclusion, there is no “golden” image modality that can “do it all”; fusion of imaging modalities is increasingly being used to obtain both high-sensitivity and high-resolution multimodality images.

The utility of molecular imaging techniques in drug development

Eugenii A. Rabiner, FCPsych SA

Imanova Centre for Imaging Sciences, Hammersmith Hospital, London, UK

The unrivalled sensitivity and specificity of positron emission tomography (PET) have made it an essential tool in the drug development process. PET enablesthe robust quantification of a molecular targetwith PET is ideally suited to provide information for go-no-go decisions during drug development.However, PET is expensive and requires large multi-disciplinary teams to execute optimally, which limits its use. Thus the challenge for drug developers wishing to use PET is two-fold. The first is to identify the points in the drug development process where the information provided by PET studies has the potential to lead to a change in the development plan – with consequent saving of time and resource. The second is to ensure that the PET studies conducted are optimally designed, to produce the essential information with the minimal study size, cost and duration.

To date, the greatest impact for PET in drug development has been in the early phases, leading up to proof-of-concept (POC) studies. There are several reasons for this. The cost of drug development increases exponentially with the progress of a novel molecule through the process, hence decisions to progress or terminate a drug early on in the process will have the greatest impact. PET is particularly suited to determine the access of a novel drug to its target, and to quantify the relationship between the administered dose and occupancy of the target. This information can be used to significantly reduce the dose range tested, saving time and money. And lastly, the cost and complexity of PET make the case for its inclusion in large, multi-site, Phase III trials, difficult to formulate.

Nuselect an optimal molecule to progress, refine the dose range of a compound to be taken into human, and optimise the dose to be examined in a proof-of-concept study. The use of PET studies to answer specific questions within the development process will be reviewed.

The experience of the past 20 years has provided some valuable lessons for drug developers using molecular imaging.

1. PET ligand development should be viewed as a specialised process, distinct from the development of a novel drug, and can be optimised by the use of appropriatebiomathematical models.
2. The frequent need to develop novel PET ligands for novel targets, means that the imaging strategy should be articulated very early in the development process, with preparatory work starting 1-2 years prior to projected first study in humans.
3. Where PET ligand development is not feasible, some valuable information may be obtained by labelling the drug candidate and evaluating its kinetics in tissue.
4. Judicious studies in pre-clinical species will provide valuable information on the dose range to be tested in humans, while very early human studies will confirm tissue pharmacokinetics and refine the dose range for POC studies.
5. Refined experimental designs, combining molecular imaging with classical pharmacokinetic analyses, enable the estimation of target occupancy following repeat dosing in the clinic, to be estimated from single dose occupancy data in healthy volunteers.
6. A multi-modal approach, incorporating other imaging modalities may provide added benefits.

PET techniques have providedvaluable input into the development of novel pharmaceuticals, and can provide useful lessons to the growing field of ultrasound contrast imaging.

Nanobody-coupled microbubbles as novel molecular tracer

Sophie Hernot, PhD[1], Sunil Unnikrishnan, MSc[2], Zhongmin Du, PhD[2], Talent Shevchenko, PhD[2], Bernard Cosyns, MD, PhD[1,3], Alexis Broisat, PhD[4], JakubToczek, MSc[4], Vicky Caveliers, PhD[1,5], Serge Muyldermans, PhD[6,7], Tony Lahoutte, MD, PhD[1,5], Alexander L. Klibanov, PhD[2], Nick Devoogdt, PhD[1]

[1]In vivo Cellular and Molecular Imaging, Vrije Universiteit Brussel, Belgium
[2]Cardiovascular Division University of Virginia School of Medicine, VA, USA
[3]Department of Cardiology, UZBrussel, Belgium
[4]Radiopharmaceutiques Biocliniques, INSERM, U1039, Faculté de Médecine de Grenoble, France
[5]Department of Nuclear Medicine, UZBrussel, Belgium
[6]Laboratory of Cellular and Molecular Immunology, Vrije Universiteit Brussel, Belgium
[7]Department of Structural Biology, Vlaams Instituut voor Biotechnologie, Belgium

Camelid-derived single-domain antibody-fragments (~15kDa), called nanobodies, are a new class of molecular tracers that are routinely identified with nanomolar affinity for their target and that are easily tailored for molecular imaging and drug delivery applications. We hypothesized that they are well-suited for the design of targeted microbubbles (μBs) and aimed to develop and characterize eGFP- and VCAM-1-targeted μBs. Anti-eGFP (cAbGFP4) and anti-VCAM-1 (cAbVCAM1-5) nanobodies were site-specifically biotinylated in bacteria. This metabolic biotinylation method yielded functional nanobodies with one biotin located at a distant site of the antigen-binding region of the molecule. The biotinylatednanobodies were coupled to biotinylated lipid μBs via streptavidin-biotin bridging. The ability of μB-cAbGFP4 to recognize eGFP was tested as proof-of-principle by fluorescent microscopy and confirmed the specific binding of eGFP to μB-cAbGFP4. Dynamic flow chamber studies demonstrated the ability of μB-cAbVCAM1-5 to bind VCAM-1 in fast flow (up to 5 dynes/cm^2). *In vivo*targeting studies were performed in MC38 tumor-bearing mice (n=4) (Figure). μB-cAbVCAM1-5 or control μB-cAbGFP4 were injected intravenously and imaged using a contrast-specific ultrasound imaging mode. The echo intensity in the tumor was measured 10 minutes post-injection. μB-cAbVCAM1-5 showed an enhanced signal compared to control μBs ($p<0.05$). Using metabolic and site-specific biotinylation of nanobodies, a method to develop nanobody-coupled μBs was described. The application of VCAM-1-targeted μBs as novel molecular ultrasound contrast agent was demonstrated both *in vitro*and *in vivo*.

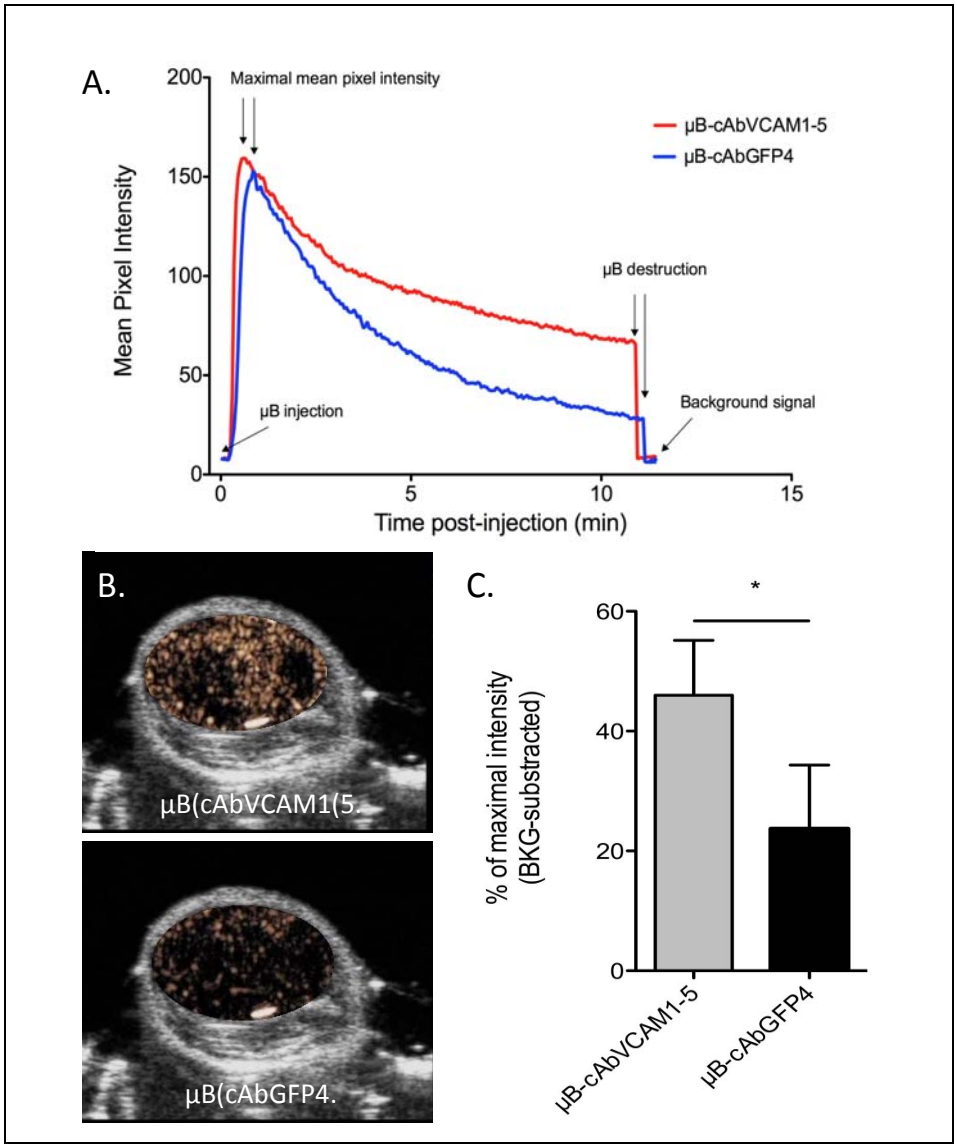

Figure: (A) Representative time-course curves of contrast-enhancement in tumor following injection of μB-cAbVCAM1-5 and μB-cAbGFP4 (control). (B) Transverse B-mode images of MC38 tumors overlaid with a ROI showing contrast-specific signal in tumor 10 minutes after intravenous injection of either μB-cAbVCAM1-5 (upper image) or μB-cAbGFP4 (lower image) in the same mouse. (C) Quantification of μB adherence in tumor, *p<0.05 for comparison of contrast-specific signal in tumor after injection of μB-cAbVCAM1-5 and control μBs. Signal at 10 min post-injection was expressed as % of the maximal intensity reached ~ 20 s after injection, and corrected for background.

Mapping microbubble viscosity using fluorescence lifetime imaging microscopy (FLIM)

N. A. Hosny[a], Grace Mohamedi[b], Yilei Wu[a], Tang Mengxing[c], Robert J. Eckersley[d], Marina Kuimova[a], Eleanor Stride[b]

[a]Department of Chemistry, Imperial College London, UK
[b]Institute of Biomedical Engineering, University of Oxford, UK
[c]Department of Bioengineering, Imperial College London, UK
[d]Imaging Sciences Department, Imperial College London, UK

Over the past 3 decades, encapsulated microbubbles have become well established as the most effective type of contrast agent for ultrasound imaging. However there remain some significant challenges which must be overcome in order to fully realise the potential of microbubbles in advanced applications such as perfusion mapping, targeted drug delivery and gene therapy. These are largely related to the poor characterisation of the relationship between the ultrasound parameters and the dynamic response of the microbubbles. Quantifying this relationship is crucial because it is this which determines both the imaging signal and microbubble destruction in therapeutic applications. A key requirement is accurate measurement of the surface properties of the microbubbles, in particular, the viscoelastic response. Estimates have been successfully obtained through fitting theoretical models to acoustic and/or high speed camera measurements. However, methods for independent characterisation of surface properties have been largely lacking. Whilst the effective elasticity can be determined with reasonable accuracy via quasi-static measurements, currently there are limited direct measurement techniques that are able to non-destructively quantify and map the viscosity within a lipid membrane structure.

The aim of the proposed research is to investigate a new strategy for performing these measurements based on fluorescence detection from small fluorophores termed ‘molecular rotors’. When these molecules are situated in a viscous environment, e.g. by incorporation into a microbubble coating, rotation is slowed down and this strongly affects fluorescence parameters, such as intensity, decay time and spectral profile. Viscosity thus can be measured directly by detecting the change in either the fluorescence spectra or lifetimes of the rotor. Importantly, the rate of rotation of the rotors correspondsto bubble oscillations at MHz frequencies.

Measurements were performed on air-filled 1,2-distearoyl-sn-glycero-3-phosphocholine (DSPC)coated microbubbles prepared withmeso-substituted boron-dipyrromethene (BODIPY-C_{10}) integrated into the lipid membrane. Using the Förster-Hoffmann equation a direct relationship between lifetime and viscosity was determined and the results indicate that microbubbles with diameters<50 μmare characterised by coatingviscositiesin the range 600-1000 cP. In addition, investigation was made of the spatial variation across the bubble surface for different bubble compositions, the effect of bubble size, preparation method and time and temperature dependence and the results of these studies will be discussed.

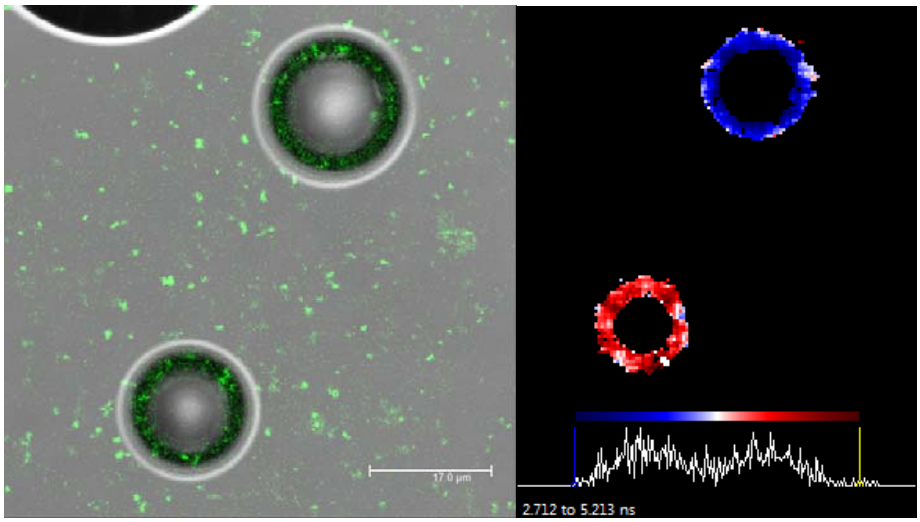

Figure 1 – Left: Overlaid brightfield transmitted and multi-photon confocal image of two DSPC coatedmicrobubbles loaded with BODIPY-C_{10} represented as green fluorescent intensity (scale bar 17 µm). Right: FLIM image of the same microbubbles with clear differences in lifetime.

Prospective randomized comparison of long versus short pulse duration therapeutic impulses in improving epicardial and microvascular recanalization during a continuous microbubble infusion in acute myocardial infarction

***FengXie*, ShunjiGao, Juefei Wu, Evan Unger, Jinjin Liu, William T. Shi, Francois Vignon, Jeffry Powers, John Lof, Shelby Kutty, Jia Liu, Thomas Porter**

University of Nebraska Medical Center, Omaha, NE, USA

Background

In vitro studies have demonstrated that cavitation of microbubbles (MB) within a thrombus can be sustained by prolonging the ultrasound pulse duration (PD). Since the shear stress induced by this cavitation may be responsible for thrombus dissolution, we prospectively tested whether guided high mechanical index (MI) impulses with a longer PD could improve epicardial and microvascular recanalization in acute myocardial infarction (AMI).

Methods

In 36 atherosclerotic pigs, a coronary thrombotic occlusion in the left anterior descending was induced, followed by randomization to A) diagnostic ultrasound (DUS) guided high MI impulses with longer 20 usec PD during a lipid MB infusion; B) DUS guided high MI impulses with a 5 μsec PD during MB infusion; or C) control (no DUS or MB). All pigs received 1/2 dose tissue plasminogen activator (TPA), heparin, and aspirin. The guided high MI impulses were applied only when low MI imaging detected MB within the risk area (RA). Angiographic recanalization rates (ARR), ST segment resolution, and wall thickening (WT) recovery within the RA were compared.

Results

ST segment resolution and WT improved with both guided 20 usec and 5 usec impulses
($p<0.05$ compared to TPA alone). However, ARR at 30 minutes into treatment improved only in pigs treated with guided 20 usecimpulses (10/12 versus 5/12 control; $p<0.05$; Figure).

Conclusions

Microvascular and epicardial recanalization can be achieved rapidly in AMI with a systemic MB infusion and DUS-guided long PD impulses.

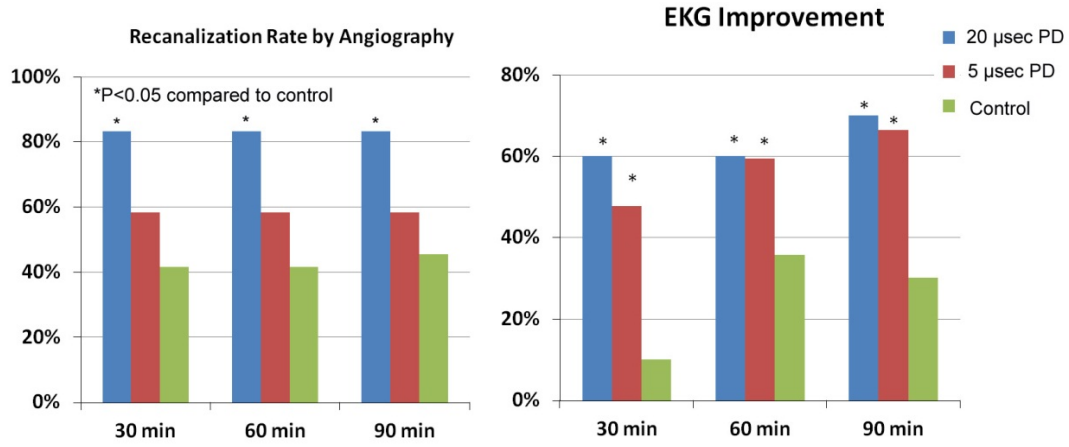

Phase shift variance imaging

Monica Siepmann[1], Stanley Fokong[2], Jessica Bzyl[2], Martin P. Mienkina[1], Mara Novak[2], Wiltrud Lederle[2], Fabian Kiessling[2], Georg Schmitz[1]

[1]Department of Medical Engineering, Ruhr-University Bochum, Bochum, Germany
[2]Department of Experimental Molecular Imaging (ExMI), Medical Faculty, RWTH Aachen University, Aachen, Germany

Most ultrasound contrast detection techniques exploit the non-linear response of the oscillating microbubbles (MB). The performance of these techniques is however affected by non-linear sound propagation, making tissue suppression amplitude and echogenicity, as well as depth dependent. An alternative presents the detection of microbubble destruction based on the changes in the acoustic response. In this work we propose a novel criterion for microbubble destruction detection which allows uniform background suppression.

The microbubble detection technique presented here is based on the variance of the phase shift of consecutive echoes. Unlike pulse inversion and amplitude modulation schemes, we analyse the changes in response to a sequence of identical pulses. The advantage of such a sequence is also that it can be acquired with any system capable of Doppler imaging without hardware modification. Beneath tissue rejection we hypothesize that the proposed criterion also permits the distinction of flow from agent disruption.

A statistical model of the Phase Shift Variance (PSV) was derived that describes stationary background and linear motion. Deviations from this model are used to detect MB destruction. The discrimination of contrast agent disruption from background by the PSV was evaluated in experiments. The technique was first implemented on the freely programmable Sonix RP ultrasound system (Ultrasonix). A detection series consisting of 20 identical three cycle sine pulses at 9.5 MHz (4.5 MPa peak negative pressure) was transmitted at a pulse repetition frequency of 5 kHz. To test the homogenous suppression of tissue with different echogenicity, a standardized phantom (CIRS Model 050) with different inclusions (hyperechoic lesion, wire targets) was imaged. The flow suppression was analyzed in a phantom with blood mimicking fluid flowing at 1cm/s. To demonstrate the detection of bound contrast agent, cyanoacrylate encapsulated airfilled microbubbles were targeted to VEGFR2 by coupling with streptavidin and incubation with biotinylated goat anti-mouse VEGFR2. Subsequently they were added to Human Umbilar Vein Cells disseminated in culture chambers (Ibidi µ-slide). The slides were imaged in the focus of the transducer with the same sequence as described above. Figure 1 shows the histograms obtained from the experiments. It can be seen that the PSV allows a good separation of bubbles from tissue and flow. Results for the stationary materials are independent of their echogenicity.

The phase shift of the flowing scatterers is slightly enhanced, however it is still well separable from the bubbles. Receiver Operating Characteristic (ROC) curves obtained from background and targeted MB yielded an area under curve (AUC) of 100%. The comparison to flow still yields 99.90% AUC of the ROC.

The method was transferred to the high frequency imaging system Vevo2100 (VisualSonics) to test its sensitivity for single bubble quantification. The concentration of the MB suspension was quantified with a Coulter counter. Gelatine phantoms containing MB with concentrations ranging from 10^3 to 10^4 MB/ml and silica gel as background scatterers were prepared. The Sensitive Particle Acoustic Quantification (SPAQ) technique was employed to quantify destroyed bubbles. This method works by moving the transducer stepwise in elevational direction, destroying bubbles in small, defined slices and counting the destruction events. As the slice volume is known, this allows an absolute quantification of the number of bubbles. Destruction events were detected with the proposed PSV method. Therefore IQ data of 3D Power Doppler acquisitions were recorded in the systems digital RF mode, from which PSV images were calculated. Figure 2 shows an image obtained from one of the gelatine phantoms with embedded MB (concentration $c=5*10^3$ MB/ml, SPAQ step size 100µm) and a reference image containing only silica gel. No differences in the B-Mode intensity of the two phantoms could be observed. The number of bubbles in 150 images per phantom was counted. The absolute counts obtained deviated less than 10% from their nominal value according to the dilution. Thus we could prove the high sensitivity of the method to the destruction of single bubbles. A future study will evaluate the method for the quantitative assessment of tumor progression. Figure 3 shows the result of an initial in vivo experiment with VEGFR2 targeted microbubbles (10^7 MB bolus injection) in a nude mouse with a human breast cancer xenograft.

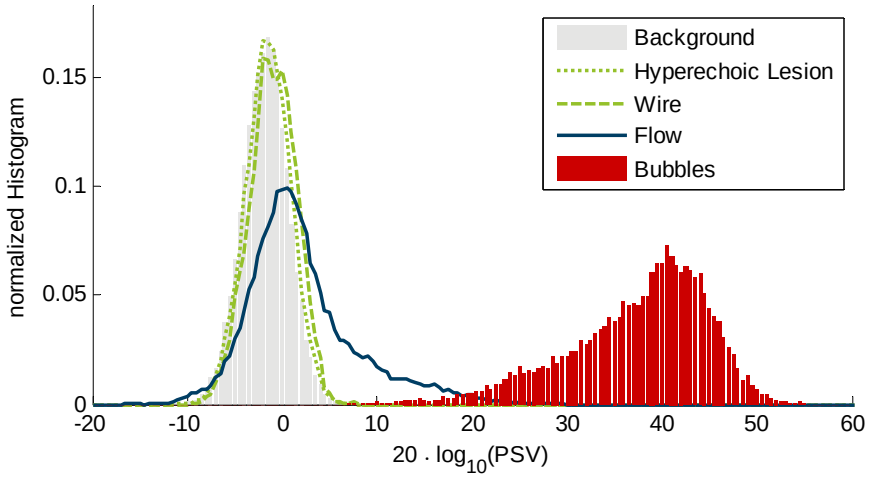

Figure 1: Histograms of microbubbles in vitro and different regions of a tissue mimicking phantom. The area under the ROC curve is 100% for bubbles compared to the CIRS phantom background and 99.90% compared to the flowing scatterers.

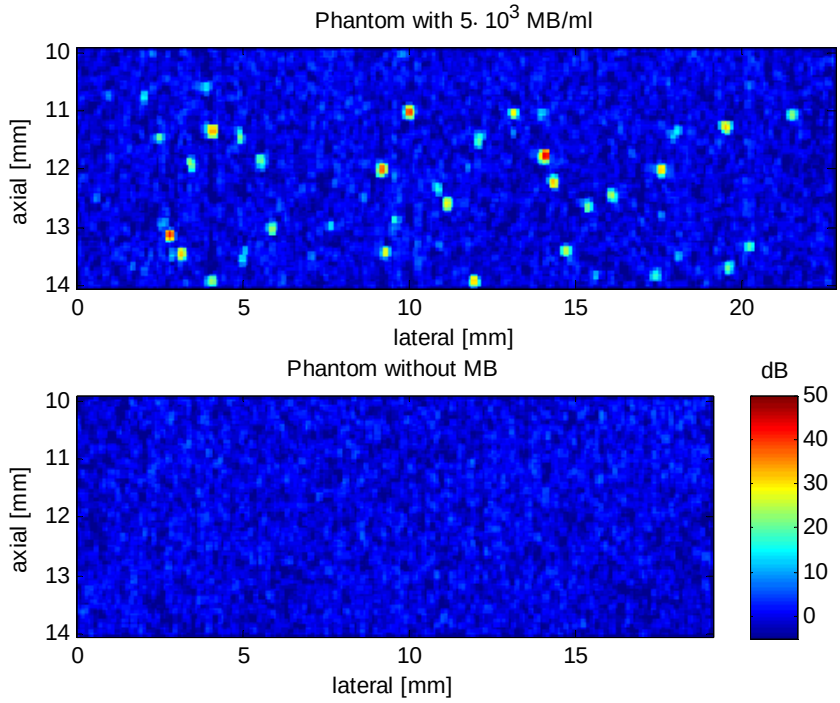

Figure 2: 5*10^3 MB/ml embedded in gelatine imaged with the Phase Shift Variance technique compared to silica gel phantom without agent.

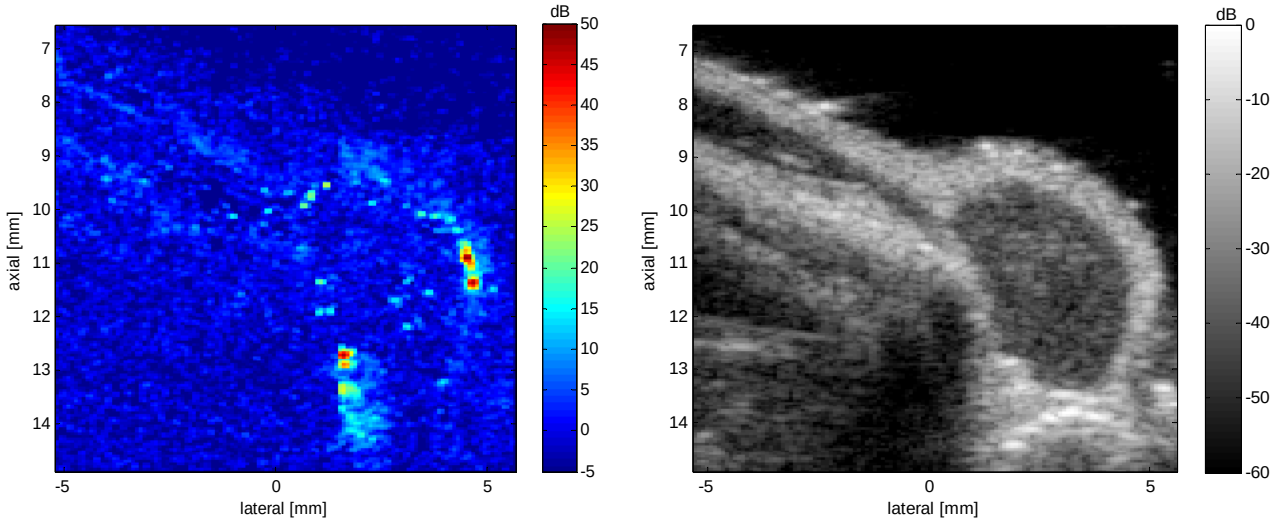

Figure 3: In vivo image of a tumor xenograft with microbubbles targeted to VEGFR2. Left: PSV image. Right: B-mode image

Counter-propagation contrast-enhanced ultrasound imaging: a new detection strategy free from nonlinear propagation artifacts

G. Renaud*, J.G. Bosch*, V. Shamdasani[$], R. Entrekin[$], N. de Jong*[#], A.F.W. van der Steen*[#]

**Biomedical Engineering, Thoraxcenter, Erasmus MC, Rotterdam, the Netherlands*
[#]Interuniversity Cardiology Institute of the Netherlands, Utrecht, the Netherlands
[$]Philips Healthcare, Bothell, WA, USA

In the PARISk CTMM project, contrast-enhanced ultrasound imaging is performed on non-symptomatic patients to investigate the role of intra-plaque vasa vasorum in the mechanisms leading to the rupture of atherosclerotic plaques in the carotid artery. A pseudo-enhancement, termed far wall artifact, was identified behind the distal wall of the carotid artery in contrast images for all of the 140 patients examined so far [1]. The presence of neo-vascularization can not be assessed in all plaques situated on the distal wall because contrast images are polluted by this pseudo-enhancement (Fig. 1).
It turns out that the creation of this pseudo-enhancement is inherent to the pulse sequence employed to perform contrast imaging, in this case amplitude modulation (or power modulation) [1]. A large majority of methods (including amplitude modulation, pulse inversion and combinations of these) currently implemented in ultrasound scanners require linear wave propagation in order to reveal nonlinear scattering produced by contrast microbubbles [2]. Nonlinear propagation through contrast agent dramatically distorts the waveforms transmitted in the contrast-mode pulse sequence, even at low mechanical index (Fig. 1). Therefore present detection techniques generate pseudo-enhancement at the location of echogenic tissue situated behind any vessel or blood pool containing contrast agent. All perfusion-like analyses are expected to be impaired by this artifact.

In order to overcome nonlinear propagation artifacts, a new artifact-free pulse sequence called counter-propagation contrast imaging was developed. A patent has being filed and the technique is being implemented in an ultrasound scanner in collaboration with Philips Healthcare to be tested *in vivo* within the framework of PARISk CTMM project. Counter-propagation contrast imaging uses a 2-waveform pulse sequence. The sequence consists in transmitting first an imaging wave. Secondly a waveform containing the same imaging wave and a manipulation wave, fired after the imaging wave with no overlap in time, are transmitted (Fig. 2). It exploits the fact that the nonlinear interaction between two acoustic waves propagating in opposite directions (counter propagation) is not efficient in soft tissue. Nonetheless a gas microbubble in a liquid constitutes a large and localized contrast in compressibility. Such a localized source of acoustic nonlinearity allows nonlinear interaction between two counter-propagating waves. After scattering or reflection of the imaging wave in the medium, the resulting back-propagating wave crosses the manipulation wave, since they propagate in opposite

directions. The presence of a microbubble at the location where the two waves cross each other allows the manipulation wave to modulate the local acoustic properties. In such a case, the manipulation wave will affect the propagation of waves backscattered in response to the imaging wave. Emitting the imaging wave without transmitting the manipulation wave provides a reference. Thus comparing the echoes received in the two situations (with and without transmission of the manipulation wave) allows us to retrieve the effect of the manipulation wave and localize contrast microbubbles. In practice, the frequency contents of the imaging wave and the manipulation wave must not overlap significantly in the frequency domain so that signals received in response to the imaging wave can be isolated by means of frequency filtering. However we prove here that the technique can be implemented with a single ultrasound transducer having a typical -6 dB frequency bandwidth of 70%.

An *in vitro* validation of the new method in a tissue-mimicking phantom is presented (Fig. 3). A single RF line is acquired with a 5 MHz mono-element transducer. For comparison, amplitude modulation is performed within the same pulse sequence using the same waveform as the imaging wave of the new method, with identical amplitude and half amplitude. As expected, counter-propagation contrast imaging does not produce any nonlinear propagation artifact whereas amplitude modulation does (Fig. 3).

The development of artifact-free contrast detection strategies can considerably improve contrast-enhanced ultrasound imaging of micro-vascularization for diagnosis of atherosclerosis as well as blood perfusion analyses in organs.

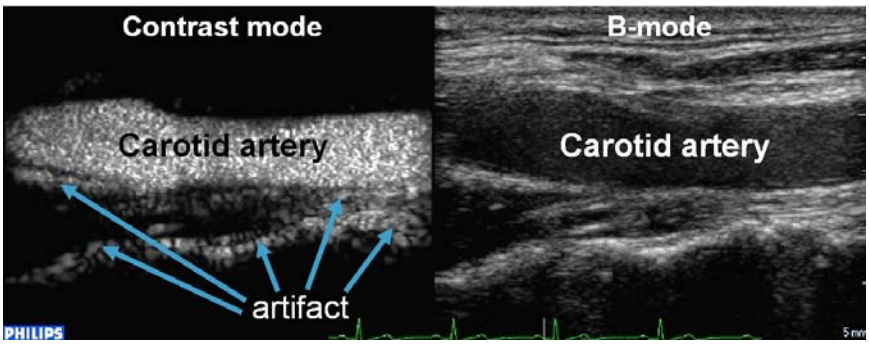

Fig. 1. *In vivo* appearance of the far wall pseudo-enhancement in a longitudinal view of a human carotid artery acquired by a Philips iU22 scanner with a L9-3 probe (contrast mode is performed by amplitude modulation). The mechanical index is 0.06.

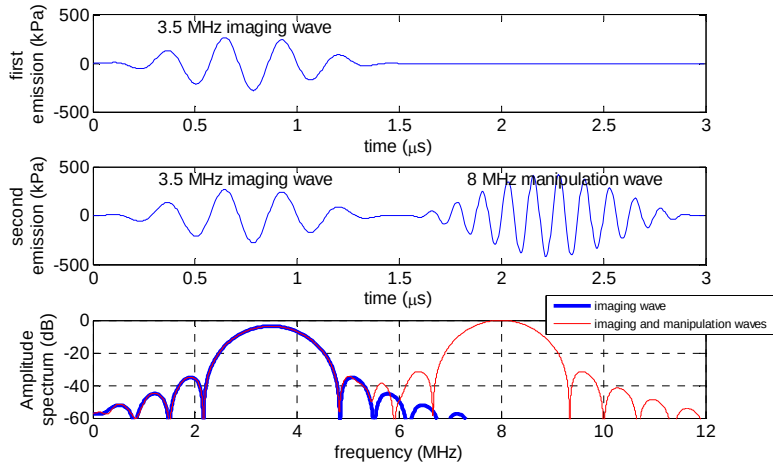

Fig. 2. Pulse sequence of the new artifact-free method, called counter-propagation contrast imaging, for a mechanical index of 0.15, used for the *in vitro* validation.

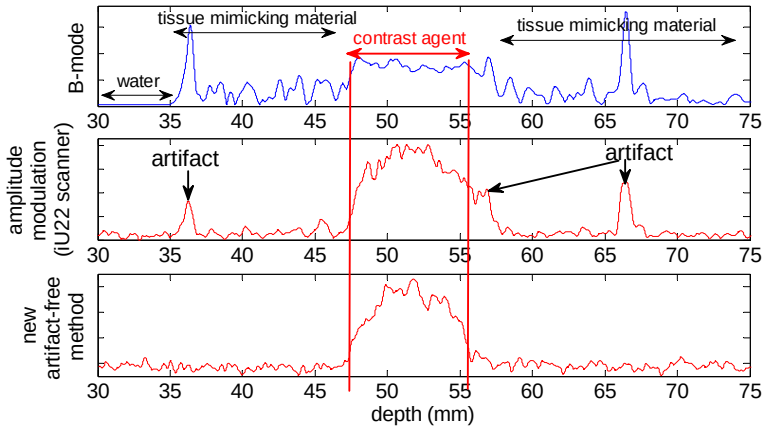

Fig. 3. *In vitro* validation of the new artifact-free contrast detection method and comparison with amplitude modulation. A single RF line is acquired with a single element transducer in a tissue-mimicking phantom containing a 9 mm diameter cavity filled with a 1:2000 diluted suspension of BR14 (Bracco) contrast

References

1. "Far-Wall Pseudoenhancement During Contrast-Enhanced Ultrasound of the Carotid Arteries: Clinical Description and in Vitro Reproduction", Gerrit L. ten Kate, Guillaume G.J. Renaud, Zeynettin Akkus, Stijn C.H. van den Oord, Folkert J. ten Cate, Vijay Shamdasani, Rob R Entrekin, Eric J.G. Sijbrands, Nico de Jong, Johan G. Bosch, Arend F.L. Schinkel, Antonius F.W. van der Steen, accepted in Ultrasound in Medicine and Biology
2. "In vitro comparative study of the performance of pulse sequences for ultrasound contrast imaging of the carotid artery", G. Renaud, J.G. Bosch, N. de Jong and A.F.W. van der Steen, proceeding of IEEE International Ultrasonics Symposium, Orlando, 2011

This research was supported by the Center for Translational Molecular Medicine and the Netherlands Heart Foundation (PARISk).

Dual frequency excitation for broad band nonlinear imaging

M. A. Averkiou, C. Keravnou, C. Mannaris

Department of Mechanical and Manufacturing Engineering, University of Cyprus, Nicosia, Cyprus

Introduction

Nonlinear imaging relies on pulsing schemes like pulse inversion, power modulated pulse inversion, and power modulation (PI, PMPI, and PM), to extract certain harmonic components. These schemes normally use monofrequency pulses (tone bursts). More elaborate approaches use FM chirps and other codes, or dual frequency pulses, e.g., radial modulation. It has been shown in the past that the same nonlinear techniques that are used for microbubbles can also be used with higher amplitudes in nonlinear tissue imaging. The most important aspects of nonlinear bubble techniques are bubble sensitivity, tissue suppression, and image resolution. A new method is proposed where it uses dual frequency pulses at frequencies f and 2f. The new technique offers improved bubble sensitivity and image esthetics while still fully eliminating tissue signals.

Description of new method

The proposed method is a 2 (or more) pulse scheme where pulses with two frequencies are used. The two primary frequencies are a mixture of *f* and 2*f*, according to

$$y = [a * \sin(\omega t) + b * \sin(2\omega t + \phi)] * \exp[-(\frac{\omega t}{N_{cyc}\pi})^{2m}],$$

where $\omega=2\pi f$, *a* and *b* are the coefficients (weights) of *f* and 2*f*, and Ø is a phase component that moves the second harmonic to a precise location on the pulse in relation to the fundamental.

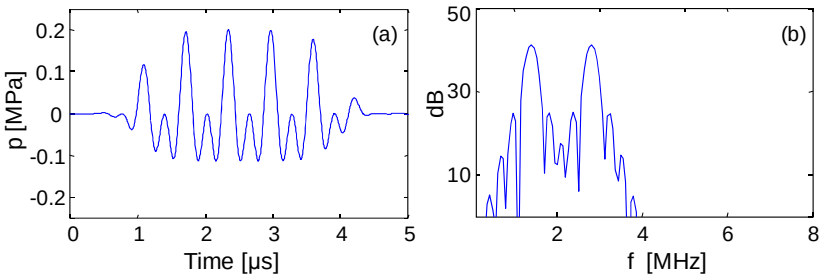

Figure 1: A typical dual frequency pulse where the second harmonic component was placed at the negative portion of the pulse.

Since the two frequency components have different focusing gains and different attenuations, we can design for a specific pulse at the focus by changing the coefficients *a* and *b* of the source function. All the nonlinear combinations (harmonics, sum frequencies, difference frequencies, etc.) are multiples of *f*. The harmonics of *f* are 2*f*, 3*f*, 4*f*, …, and of 2*f* are 4*f*, 6*f*, … The sum frequency components are *f*+2*f*=3*f*, 2*f*+2*f*=4*f*, *f*+3*f*=4*f*, *f*+4*f*=5*f*, …, and the difference frequency components are 2*f*-*f*=*f*, 3*f*-*f*=2*f*, … The end result is a nonlinear signal with *f*, 2*f*, 3*f*, 4*f*, …, where all components come from *multiple level nonlinear interactions*. The use of pulsing schemes (PI, PMPI, PM, etc.) extracts harmonics everywhere in the bandwidth of the transducer.

The proposed method has the following advantages:

- Uses all transducer bandwidth.
- Creates efficiently harmonics both at low and high frequencies—low frequencies are useful for penetration, high frequencies are useful for resolution.
- Use of multi-band frequency compounding schemes enhances image esthetics.
- No new hardware for the diagnostic scanner is needed for its implementation.
- It gives the highest amount of nonlinear fundamental.
- It offers the ability to design bubble specific pulses with the weights *a*, *b* and the phase (for example, the left pulse below in Fig. 2 would have a dramatically different response on a bubble from the right pulse).
- Since it works best with PI, it will increase the frame rate as compared to other schemes that use more than 2 pulses.

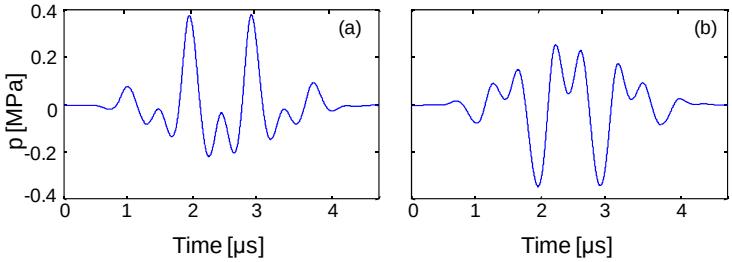

Figure 2: A pair of 2 pulses where they would produce different nonlinear bubble responses.

Theoretical and experimental results

The proposed pulsing scheme was investigated for nonlinear tissue imaging and for contrast imaging. Despite the fact that the source of nonlinearity is different in these two cases, previous work has shown that the harmonic trends between nonlinear propagation and nonlinear scattering are very similar. The main discriminating factor between the two is the degree of nonlinearity at a given acoustic pressure. We have considered a pulse with f =1.4 MHz, $2f$=2.8 MHz, m=3, N_{cyc}=5, a=0.5, b=0.25.

Nonlinear propagation in tissue

We have assumed nonlinear propagation in a tissue like medium. To form the pulsing schemes (PI, PMPI, PM) we use the pulses in Fig. 3, where a dual frequency pulse, its inverse, and its half are shown together with their respective spectra.

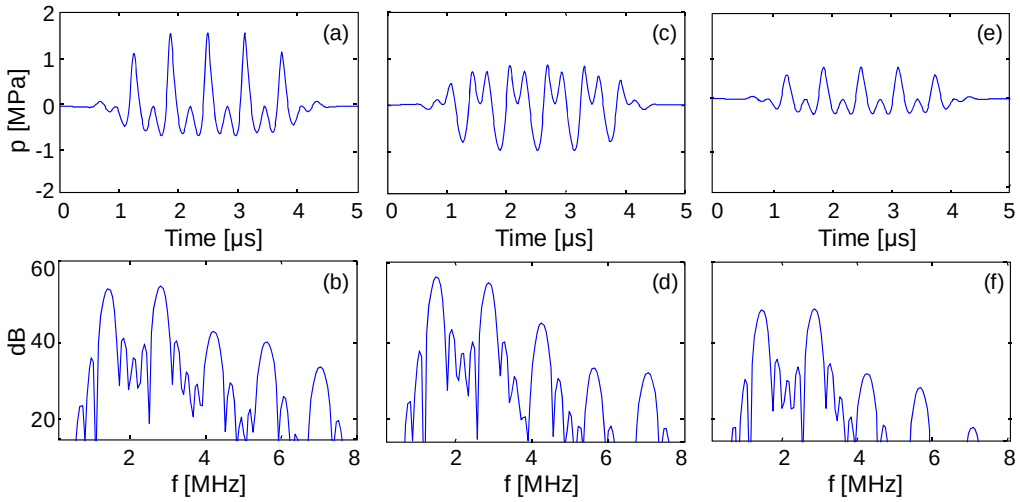

Figure 3: Three dual frequency pulses used for forming pulsing schemes. A normal pulse (a)-(b), an inverted pulse (c)-(d), and a pulse at half amplitude (e)-(f).

It is seen that nonlinear propagation is causing the generation of all harmonic components including the nonlinear fundamental which we can not distinguish from its linear counterpart. Pulsing schemes are formed with the pulses of Fig. 3 and are shown in Fig. 4. All schemes produce all the possible harmonic components but at different levels. Table 1 below shows the harmonic levels for 3 different pulsing schemes, namely, PI, PMPI, and PM for the example shown above in Fig. 4, where everything has been normalized with respect to the highest harmonic level which for this example was the 3rd harmonic. It is demonstrated that PI has 6 or more dB gain at all harmonic components over the other two schemes.

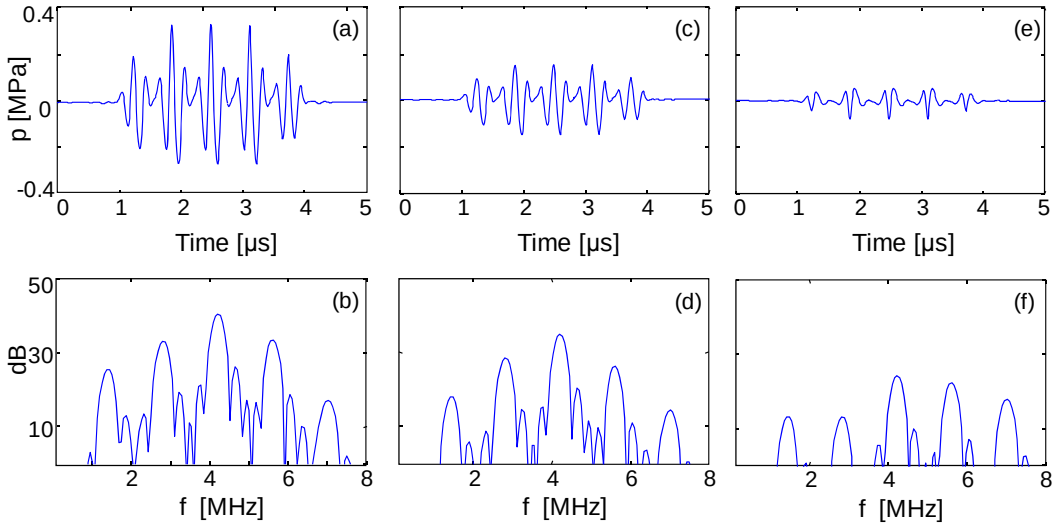

Figure 4: Pulsing schemes for nonlinear propagation in tissue with the dual frequency pulses of Fig. 3. PI (a)-(b), PMPI (c)-(d), and PM (e)-(f).

	1.4 MHz	2.8 MHz	4.2 MHz	5.6 MHz
PI	-16	-8	0	-7
PMPI	-23	-13	-6	-15
PM	-28	-28	-17	-19

Table 1: Normalized harmonic levels of PI, PMPI, and PM for the proposed dual frequency pulse in nonlinear tissue imaging.

Nonlinear scattering from microbubbles

The same trends have been observed with nonlinear scattering from microbubbles in numerical simulations of bubble oscillations and experiments (see Figure 5). The resonance frequency/radius of the microbubble controls the content of the produced harmonics. In this case too the scattered acoustic pressure with PI has 5 or more dB more signal than the other schemes (see Table 2). However, the main advantage of the method is the full extraction of bubble signals at *all* harmonics.

Conclusion

A new nonlinear detection method has been proposed that uses a dual frequency pulse consisting of a frequency and its weighted and phase shifted 2nd harmonic. This method relies on multi-pulse schemes to isolate *all* harmonic components. In the case of PI where it is the cyclic variation of phase between the two pulses, now with the "cyclic variation" of frequency within a pulse *all nonlinear components are fully extracted.*

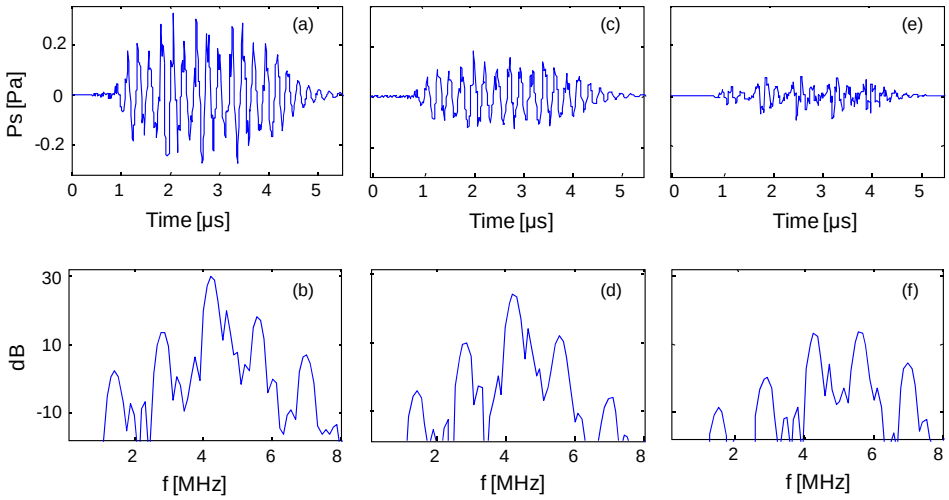

Figure 5: Pulsing schemes for nonlinear scattering from a 2 μm diameter microbubble with a pulse with *a*=0.667, *b*=0.33, at *MI*=0.06. PI (a)-(b), PMPI (c)-(d), PM (e)-(f).

	1.4 MHz	2.8 MHz	4.2 MHz	5.6 MHz
PI	-28	-17	0	-12
PMPI	-34	-20	-6	-18
PM	-38	-30	-17	-16

Table 2: Normalized harmonic levels of PI, PMPI, and PM for the proposed dual frequency pulse in nonlinear bubble imaging.

Contrast-enhanced intravascular ultrasound chirp imaging

D. Maresca[1], K. Jansen[1,2], G. Renaud[1], G. van Soest[1], X. Li[3], Q. Zhou[3], N. de Jong[1,2,4], K. K. Shung[3], A. F.W. van der Steen[1,2]

[1]Biomedical Engineering, Thoraxcenter, Erasmus MC, Rotterdam, the Netherlands
[2]Interuniversity Cardiology Institute of the Netherlands, the Netherlands
[3]Department of Biomedical Engineering, University of Southern California, Los Angeles, USA
[4]Imaging Science and Technology, Delft University of Technology, Delft, the Netherlands

Atherosclerosis is a disease of the arterial wall and one of the major causes of death worldwide. Cardiac adverse events result frequently from the rupture of a vulnerable atherosclerotic plaque in the coronary vasculature. It is recognized that the development of new microvessels in the arterial wall is critical to plaque progression and constitutes a marker of plaque vulnerability. However, these networks of microvessels, referred to as vasa vasorum (VV), are below the detection limit of clinically available intravascular imaging techniques.

Intravascular ultrasound contrast imaging of VV was demonstrated in 2006 by Goertz et al. In this work, we investigate the feasibility of contrast-enhanced intravascular ultrasound chirp imaging. The transient resonant response of a microbubble close to resonance differs for an up or down frequency sweep insonification. By relying on this asymmetry, we present a contrast imaging mode that provides a good contrast to tissue ratio (CTR) at a clinically approved UCA concentration.

The UCA used in this study was Definity®. The pressure scattered by a 1 μm diameter bubble in response to an up and down sweep chirp (duration 0.5 μs, frequency sweep 22 to 46 MHz, MI 0.19) was simulated with a viscoelastic shell model that used as an input Definity® high frequency shell parameters. Experimentally, the UCA was activated and decanted for 15 to 30 minutes to extract contrast bubbles inferior to 2 microns in diameter which resonate at IVUS frequencies. A 1:1000 dilution was prepared and chirp reversal contrast measurements were performed by filling the lumen and the first two channels of a tissue mimicking phantom with the UCA while the third channel was filled with water.

The simulation results displayed clearly the dissymmetry of up and down sweep chirp bubble echoes. Consequently, the subtraction of the compressed bubble echoes gave a residual contrast signal. Experimentally, the chirp reversal contrast image had a CTR of 12 dB (see Figure). Bubbles could be detected up to a depth of 5 mm. Moreover, the results were obtained at a clinically approved concentration of this UCA.

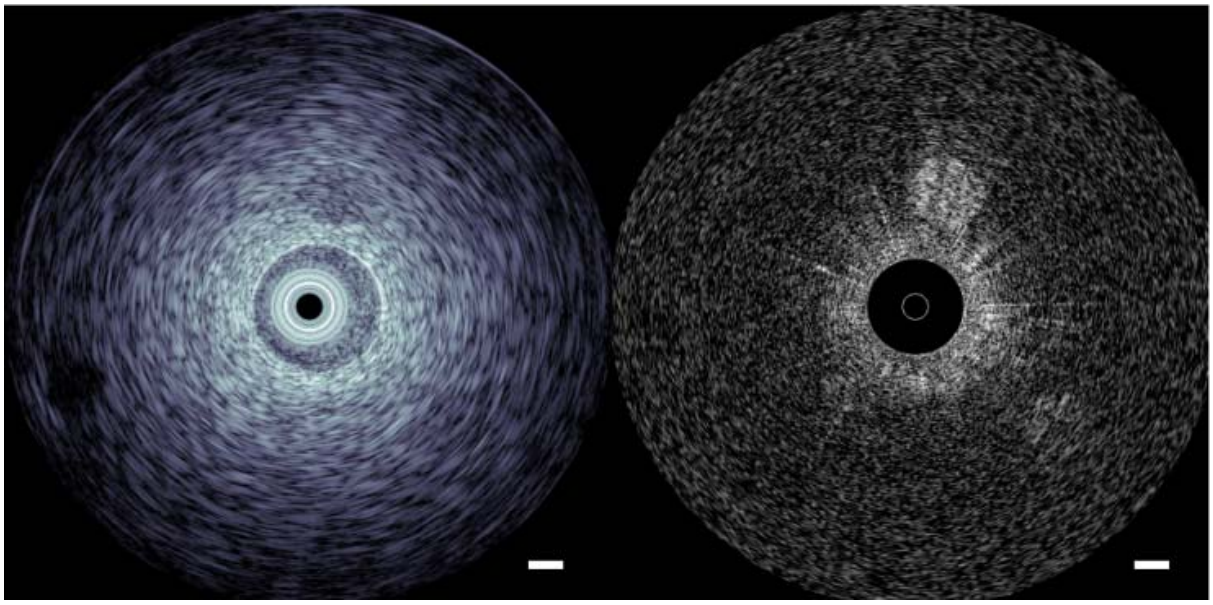

Down sweep chirp image (left) and contrast image (right) of the channel phantom perfused with the UCA. The dynamic range is 54 dB for the left image and 21 dB for the contrast image. The scalebar represents 1 mm.

Real time high frequency subharmonic imaging using self-demodulation

V. Daeichin[1], A. Needles[2], I. Skachkov[1], T. Faez[1], G. Renaud[1], J.G. Bosch[1], A.F.W. van der Steen[1,3], N. de Jong[1,3]

[1]Biomedical Engineering, Thoraxcenter, Erasmus MC, Rotterdam, the Netherlands
[2]VisualSonics Inc, Toronto, Canada
[3]Interuniversity Cardiology Institute of the Netherlands, Utrecht, the Netherlands

The main goal of this study is to optimize a real-time nonlinear contrast mode for small-animal imaging at high frequencies (15-40 MHz), on a array-based micro-ultrasound system. Harmonic imaging modes for ultrasound contrast agent (UCA) detection at frequencies above 15 MHz are hampered by nonlinearity produced by the tissue. Also techniques relied on subtraction schemes involving B-mode image does do not provide enough contrast to tissue ratios (CTR) under many imaging conditions. Subharmonic (SH) emission from ultrasound contrast agent (UCA) is of interest for cardiovascular imaging since it is produced only by the UCA and not by tissue and it is free from the distal wall artifact. Thus, SH imaging (transmitting at f0 and receiving at f0/2) provides improved visualization of UCA within the vasculature while suppressing the scattered signals from the surrounding tissue. However suppression of surrounding tissue, potentially landmarks for sonographic navigation, in the SH imaging limits its use as a primary imaging modality in clinical applications. We showed in our previous study that a suitable design of the excitation pulse envelope to generate a self-demodulation (S-D) signal at the SH frequency can enhance the SH emission of UCA up to 20 dB. In this paper we present results of using excitation pulses with rectangular envelopes in a commercial ultrasound scanner modified to allow real time imaging in both grayscale and SH imaging modes. Pulse inversion, amplitude modulation, subtraction pulse inversion together with the effect of the S-D signal were systematically investigated for the detection of nonlinear fundamental and SH signal components to maximize the CTR in the 15-50 MHz range. Commercially available UCA, MicroMarker, was investigated in vitro over an acoustic output range of 200 kPa to 1.5 MPa. In vivo the SH response of MicroMarker was investigated in the chicken embryo model. Results of our study demonstrate the feasibility of real-time dual grayscale and SH imaging at high frequency on a modified commercial scanner. The ability to simultaneously visualize both imaging modes in real time should improve the applicability of SH imaging as a future primary preclinical high frequency imaging modality.

Intravascular ultrasound contrast imaging on a commercial catheter using radial modulation

Francois T.H. Yu, Flordeliza Villanueva, Xucai Chen

Center for Ultrasound Molecular Imaging and Therapeutics University of Pittsburgh, Pittsburgh, PA, USA

Introduction

Sub-harmonic and harmonic based approaches for contrast imaging are difficult to implement on a commercial IVUS catheter, mostly because of limited transducer bandwidth and microbubble resonance frequency being lower than transducer frequency.In this study, we characterized a radial modulation (RM) intravascular ultrasound (IVUS) system, implemented using a 20 MHz commercial catheter, intended for contrast enhanced vasa vasorum imaging. RM is a dual band approach applicable for high frequency microbubble (MB) imaging, where a low frequency (LF) ultrasound pulse is used to manipulate the MB radius while a synchronized high frequency (HF) pulse successively measures MB backscatter in expanded and compressed states. Subtracting the two HF signals yields high resolution imaging with contrast enhancement and tissue suppression.

Materials and methods

Lipid-encapsulated perfluorocarbon MBs were circulated in hollow agar-based (2% w/w) tissue mimicking phantoms doped with sigmacell(0.5% w/w). The IVUS catheter was housed against the wall of the tube and rotated at 2.6 and/or 30 frames per second, allowing simultaneous imaging of MB and tissue scattering. RM and B-mode images were analyzed at increasing depths to determine contrast to tissue ratio (CTR) and contrast to tissue ratio improvement (CTRI) relative to the same image in B-mode.

Results

The effects of phase synchronization, MB concentration and LF pressure amplitude on the CTR and CTRI were measured. Our prototype IVUS system could produce RM images at 30 frames per second that selectively enhanced contrast signal and suppressed tissue and blood signal. Tubes with 200 μm diameter embedded in the tissue phantom to mimic microvessels could be selectively imaged at high resolution and reconstructed in 3D when perfused with microbubbles. The optimal synchronization phase was found to correspond to the oscillation phase of resonant MB. CTR and CTRI decreased from 12 and 14 dB near the catheter to 5 and 3 dB at 5 mm, respectively. This corresponded to LF pressures dropping from 295 kPa at 2 mm down to 105 kPa at 5 mm.

Discussion/conclusions

It was demonstrated that our prototype IVUS system allows microbubble specific imaging at high resolution. Contrast signal could be detected up to a distance of 5 mm, which should be sufficient for coronary imaging. Further improvements couldbe expected by using monodispersed MBs and developing a more efficient LF pressure delivery system.

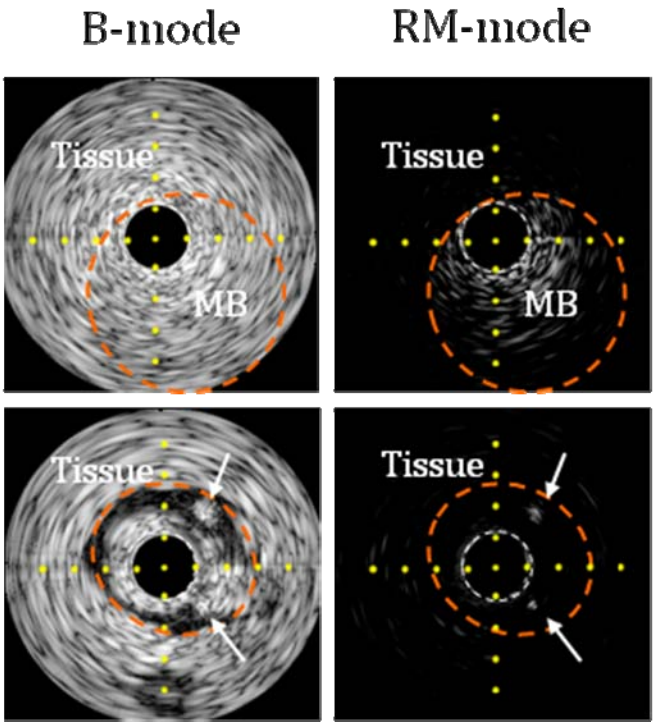

Figure : (TOP) IVUS B-mode and RM images of MBs infused in a 6 mm diameter wall-less 2% (w/w) agar tissue mimicking phantom containing scatterers. The catheter is positioned against the "vessel" wall. (BOTTOM) MBs are infused in two 200 µm tube (indicated by arrows at 1 and 5 o'clock in the B mode image), placed in heterogeneous tissue surrounding the flow phantom, in parallel with the longitudinal axis. Wall-less vessel boundary is drawn in orange. Yellow dots are separated by 1 mm. The dark circle in the center is the space occupied by the transducer. Dynamic ranges are respectively 40 dB and 30 dB for the B-mode and RM-mode images.

The 17th European Symposium on Ultrasound Contrast Imaging Rotterdam is sponsored by:

GE Healthcare - Medical Diagnostics
Mrs. Sarah Bonnett
EMEA MR & Ultrasound Marketing Leader
The Grove Centre
White Lion Road
Amersham, HP7 9LL – UK

BRACCO International BV
Mr. Marco Graf, Congress Manager
GCO Global Strategic Marketing
Centro Galleria 2
Via Cantonale
CH-6928 Manno
Switzerland

SIEMENS AG - Ultrasound Division
Mr. Richard Medley, Product Manager
H WS ES US CRM Operations
Sir William Siemens Square
Newton House
Frimley, Camberley, SY GU16 8QD – UK

KNAW
Mrs. P. Meijman
Manager International Research Grants
P.O. Box 19121
1000 GC Amsterdam
The Netherlands

PHILIPS Medizin Systeme GmbH
Mr. Janusz Bielczynski
CV Ultrasound Marketing Manager
Hewlett Packard Str.2
D-71034 Boeblingen
Germany

MSD Nederland B.V.
Bob Hoogduyn
Rayonmanager Cardiometabool
Waarderweg 39
2031 BN Haarlem
The Netherlands

Oldelft BV
Mr. R. 't Hoen
Elektronicaweg 10
2628 XG Delft
The Netherlands

Visualsonics
Mr. Anil K K Amlani
Acting President and CEO
3080 Yonge Street
Toronto, Ontario
M4N 3N1 – Canada

Hitachi Medical Systems
Ellison Bibby
European Marketing
Sumpfstrasse 24
6300 Zug – Switzerland

Nederlandse Hartstichting
Mw. Dr.ir. K. Eizema
Manager Research Department
P.O. Box 300
2501 CH Den Haag
The Netherlands

Coeur
Mr. J.W. Deckers
Erasmus MC - Thoraxcenter
Dr. Molewaterplein 50
3015 GE Rotterdam
The Netherlands

FIRST ANNOUNCEMENT 2013

18th EUROPEAN SYMPOSIUM ON ULTRASOUND CONTRAST IMAGING

17-18 JANUARY 2013

ROTTERDAM, THE NETHERLANDS

Course Directors: **Folkert ten Cate**
Nico de Jong

Information: **on the 18th EUROPEAN SYMPOSIUM ON ULTRASOUND CONTRAST IMAGING:**

Mieke Pruijsten , m.pruijsten@erasmusmc.nl

Erasmus MC
Universitair Medisch Centrum Rotterdam

sponsors:

The 17th European Symposium of Ultrasound Contrast Imaging, Rotterdam is sponsored by: